AD-756 260

A DYNAMIC PHOTOELASTIC ANALYSIS OF STRESS WAVES FROM INCLINED LINE SOURCES

James W. Dally, et al

Maryland University

Prepared for:

Department of the Interior

15 October 1972

ARPA Order No. 1579, Amend No. 3 Contract No. H0220010

Program Code No. 2F10

Principal Investigator - James W. Dally

Co-principal Investigator - William L. Fourney

Co-principal Investigator - David C. Holloway

Semi-annual Technical Report

A Dynamic Photoelastic Analysis of Stress Waves From Inclined Line Sources

Department of

MECHANICAL ENGINEERING

of

THE UNIVERSITY OF MARYLAND

October 15, 1972

Sponsored by
Advanced Research Project Agency
ARPA Order No. 1579, Amend. No. 3
Program Code 2F10

Contract No. H0220010

Contractor - University of Maryland

College Park Campus

Principal Investigator - James W. Dally (301)454-2410
Co-principal Investigator - William L. Fourney (301)454-2411
Co-principal Investigator - David C. Holloway (301)454-2411

Semi-annual Technical Report

A Dynamic Photoelastic Analysis of Stress Waves From Inclined Line Sources

Prepared for
U.S. Department of the Interior
Bureau of Mines
Twin Cities
Minnesota

October 15, 1972

Contract Expiration Date August 31, 1973
Amount of Contract - $30,500

Abstract

Dynamic Photoelastic methods were employed to analyze the stresses produced in models of a bench face. The dynamic loading was accomplished with a uniformly distributed line charge which was inclined to the vertical face. The angle of inclination of the line charge was selected so that the front of either the S or P wave would be parallel to the vertical boundary of the bench face.

The dynamic event was divided into several phases which included: The incident portion where the strain energy is carried to the bench face by means of the P wave and later by the S wave; the first reflection period where the P wave reflects from the vertical boundary; the interaction period where the reflected PP and PS waves reinforce the incoming S wave; the second reflection period where the S wave reflects from the vertical bench face; and finally the crack propagation period where cracks initiated at the line charge propagate into the field of the model.

The photoelastic data obtained from six different model tests was analyzed to determine attenuation in the stress wave during the incidient period, the distribution of the energy delivered to the bench face and the effectiveness of the reflection and interaction processes. The propagating cracks were observed to establish crack velocity and the nature of the stress field through which the crack was travelling.

Table of Contents

List of Illustrations

1.0 Introduction

It is generally recognized that blasting techniques employed in open-pit mining are extremely important since they effect both the economy and safety of the operation. Improved blasting techniques depend upon a very thorough understanding of the dynamic stresses generated by the explosive at the bore hole, the propagation and reflection of stress waves, the initiation and subsequent propagation of cracks and the interaction of propagating cracks and stress waves. Dynamic photoelasticity provides an experimental approach to study these different phenomena since several features of the dynamic event can be made visible in the whole field fringe patterns.

This report outlines the results of six dynamic photoelastic tests where stress wave propagation occurs due to explosive line charges with uniform packing density. Three models denoted in subsequent sections of this report as the "P wave models" were fabricated with a line charge inclined so as to produce a plane incident dilatational wave with its front parallel to the boundary of the model representing the bench face. Three models termed the "S wave models" were made with a line charge with a smaller inclination so that the plane incident shear wave would be parallel to the boundary.

These models provided a visual display of the stress waves generated by the charge and the delivery of the energy to the face of the bench by means of the incident P wave. The reflection of the P wave was observed followed by the interaction of the reflected PP and PS waves with the incident S wave. It was also possible to observe the propagation of cracks which initiated at the line charge and propagated to the top-horizontal boundary of the model.

The results of this experimental program are covered in 5 different sections of the report. The experimental models are defined in Section 2 together with the procedures employed in conducting the six individual tests. A brief review of elementary stress wave theory has been covered in Section 3. The detailed analysis of the photoelastic results is presented in Section 4 and the general conclusions drawn from these results are given in Section 5.

2.0 Experimental Procedure

2.1 Photoelastic Models

This investigation involves the application of dynamic photoelasticity to the problem of stress wave propagation from a uniformly distributed line charge. The photoelastic model represents a bench face with a vertical wall. Three models were fabricated with an included angle of 38 degrees between the line charge and vertical face of the bench. Three additional models were fabricated with an included angle of 22 degrees. Drawings of the models showing the dimensions and position of the line charge relative to the boundaries of the models are shown in Fig. 2.1. All photoelastic models for the experiments were fabricated from 1/4" thick sheets of Columbia Resin (CR-39). A rectangular array of grid lines on 1" centers were scribed on the models after they had been cut from 24" x 36" sheets. The actual size of each specimen varied slightly and dimensions were selected to prevent extraneous reflections from occuring during the dynamic event. The top and front edges of the models were machines (milled) to provide suitable boundaries for photoelastic determinations.

A groove 6 in. long x 1/32 in. wide x 0.08 in. deep was machined into one face of each model with a small end mill. The groove was then packed with 280 mg of lead azide which was dampened with alcohol to reduce handling hazards. A bridge wire was placed at one end of the groove to serve as the detonator. The lead azide was then permitted to dry. The bridge wires were made of constantan .001 in. in diameter and 1/8 in. long. After drying, shields were attached on both side of the model to prevent smoke from obscuring the dynamic records of the stress patterns. The lead azide was then detonated by igniting the bridge wire using a 2000 VDC - 20 joule firing pulse.

In the design of the models, two geometric parameters were varied - the angle (θ) between the line charge and the vertical face and the distance between the top end point on the line charge and the vertical face (S). The included angles θ were 38 and 22 degrees and the distances S were 3, 4 and 5 inches respectively. With the models, where θ = 38 degrees, detonation of the line charge of Pb N_6 produced a dilatational or P wave with a planar front parallel to the vertical face of the model. Similarly the models with θ = 22 degrees were used in experiments where the detonation produced an S wave with a planar front nearly parallel to the vertical face.

The photoelastic fringe patterns associated with the propagating stress waves were recorded on a high speed multiple spark camera. The initiation of the camera was delayed by 43μ sec to allow the Pb N_6 to burn along the length of the line charge and to permit the P and S wave fronts to form.

2.2 Recording System for Dynamic Photoelasticity

A multiple spark gap camera (2.1, 2.2, 2.3) was used to record the dynamic photoelastic fringe patterns produced in the half-plane models. This camera shown in Fig. 2.2 is capable of 16 frames and can be operated at framing rates which can be varied in discrete steps from 30,000 to 800,000 frames/sec. The resolution of the camera is a function of the fringe gradient and fringe velocity. Experiments indicate that gradients of 20 fringes/in. with velocities of 75,000 in./sec. represent the upper limit of the camera's resolution capability.

The optical system of the camera which is illustrated schematically in Fig. 2.3 performs three basic functions: polarization, image separation and magnification. The optical elements include a field lens (18 in. diameter with a focal length of 30 in.) and sixteen camera lenses each with focal

lengths of 6.4 inches. Image separation is accomplished by positioning the spark-gaps and camera lenses relative to the optical axis of the bench. Magnification of the optical system is determined primarily by the focal lengths of the field and camera lenses and their relative spacing. In this instance the magnification factor was -0.12 which gave a 2.2 in diameter image corresponding to the 18 in. diameter field.

A simple, yet effective, light-field polariscope is incorporated into the system by utilizing two circular polarizers (HNCP-38) between the spark-gap light source and the field lens.

The film selected for recording the image was Kodak Gravure Positive. This film has a relative slow emulsion (ASA Tungsten-8) with a fine grain structure and is used extensively in the graphic arts. As it is sensitive to light between 3500 and 5100 angstroms (i.e., the blue region) and the output of the spark gaps peak in this region, its apparent speed is much higher than the ASA speed rating indicates. The film was employed with a Kodak K-2 filter which absorbs most of the light with wave lengths below 4900 angstroms. The combination of the film and filter yields a band width from 4900 to 5100 angstroms which is sufficiently narrow to approximate monochromatic light in dynamic photoelastic applications.

2.3 Sychronization

The initiation and the recording of the dynamic event was controlled by employing the synchronization circuit presented in Fig. 2.4. The event is initiated when the operator activates switch S on the firing circuit. The firing circuit then simultaneously emits three pulses. The first is a 2KV pulse which

ignites the lead azide, the second, a 20 V pulse, activates a time delay generator and the third, another 20 V pulse, triggers an oscilloscope.

At the end of the pre-selected delay interval the delay generator issues a 50 volt output pulse which is amplified by a trigger module to about 30 KV This amplified pulse is applied to the third electrode of the trigger gap causing it to ionize and initiate the firing sequence in the multiple spark-gap camera.

The light output from the spark-gaps is sensed by a high frequency photocell (EGG-Lite Mike). The voltage output from the photocell is recorded on the sweeping oscilloscope and an intensity-time trace is obtained which established the time during the event when each of the 16 photographs was exposed.

2.4 Photoelastic Records

Sixteen dynamic isochromatic fringe patterns were recorded for each of the six models considered. The complete collection of the data obtained is presented in Figs. A-1 to A-6 of Appendix A.

Typical photoelastic results for the first series of three experiments for the models with $\theta = 38$ are shown in Fig. 2.5. The two fringe patterns correspond to frames 1 and 4 of the sixteen frame sequence and were recorded 66 and 100 μ sec after detonation. The line charge shown in Fig. 2.5 was ignited at the lower right hand end. The lead azide exhibited a detonation velocity C_c of 115,400 in/sec.; thus, a total of 52 μ sec was required to burn the 6 in. line charge. The velocity (C_p) of the dilatational or P wave was 70,200 in/sec. The requirement that the P wave approach the vertical boundary of the model with a planar front parallel to the boundary is:

$$\theta_p = \text{Sin}^{-1} C_p/C_s = \text{Sin}^{-1} (70,200/115,400) = \text{Sin}^{-1} (0.6083)$$

and $$\theta_p = 37.5 \text{ degrees}$$

Inspection of Fig. 2.5 shows a portion of the fringe pattern associated with the P wave is planar and parallel to the boundary. Also evident is the circular character of the fringe pattern at the upper left and lower central region of the photographs. This circular pattern is due to the disturbance produced at the ends of the line charge which appears to propagate radially outward from both ends.

The fringe pattern associated with S wave is also clearly depicted in Fig. 2.5. It is also a planar wave which makes an angle θ_s with the line charge given by:

$$\theta_s = \text{Sin}^{-1} C_s/C_c$$

For this model, the velocity of the shear wave was C_s = 39,000 in/sec; thus, the angle θ_s = 20.8 degrees.

Typical photoelastic results for the second series of three experiments for the models with θ = 22 degrees are shown in Fig. 2.6. The two fringe patterns correspond to frames 1 and 3 of the 16 frames sequence taken 67 and 87 μ sec after ignition of the line charge. In this instance, the front of the P wave is inclined relative to the vertical boundary and the shear wave is nearly parallel to the vertical boundary.

2.5 Interpretation of Fringe Patterns

The isochromatic fringes illustrated in Fig. 2.5 and 2.6 represent topographical maps of the dynamic stress field during the fraction of a μ sec in the event when the photograph is recorded. The stress field parameter

which is mapped is the principal stress difference $(\sigma_1 - \sigma_2)$. The magnitude of $(\sigma_1 - \sigma_2)$ is a function of the fringe order and is represented by the stress optic law as:

$$\sigma_1 - \sigma_2 = N f_\sigma / t \tag{2.1}$$

where

N is the fringe order

f_σ is the material fringe value

t is the model thickness

The orders of the fringes occuring in the patterns must be assigned by the investigator. Since a standard light field polariscope was employed, the sequence of fringe order is 0.5, 1.5, 2.5, ...etc. An example of the ordering of the fringes is illustred in Fig. 2.6 where fringe orders are depicted for both the P and S waves.

The shear or S wave is associated with an equivoluminal displacement field; hence, the first strain invariant vanishes and $\sigma_1 - \sigma_2 = 0$. Substituting this condition into Eq. 2.1 yields

$$\sigma_1 = -\sigma_2 = N f_{\sigma/2t} \tag{2.2}$$

which permits the determination of the individual values of the principal stresses.

On the free boundaries of the model, either the vertical front face or the horizontal top face, the stress normal to boundaries vanishes and either σ_1 or σ_2 goes to zero. In this case, Eq. 2.1 reduces to

$$\begin{aligned} \sigma_1 &= N f_\sigma / t \quad \text{and} \quad \sigma_2 = 0 \\ \sigma_2 &= -N f_\sigma / t \quad \text{and} \quad \sigma_1 = 0 \end{aligned} \tag{2.3}$$

3.0 Theoretical Background

3.1 P Wave - 38 degree - Model

Two types of stress waves can be propagated in an extended elastic medium. The first of these waves commonly termed as the dilatation or P wave propagates with a velocity of $c_1 = \left[(\lambda + 2\mu)/\rho\right]^{/2}$ where λ is Lame's constant, μ is the shear modulus and ρ is the mass density. The second stress wave known as the distortional or shear or S wave propagates with a velocity $c_2 = \left[\mu/\rho\right]^{1/2}$. The disturbance associated with the S wave is equivoluminal and thus it involves distortion without dilatation. The partical motion in the S wave is perpendicular to the direction of propagation. The dilatational or P wave involves a disturbance composed of a combination of both dilatation and distortion. The partical motion in the P wave coincides with the direction of propagation.

Whenever a single P or S wave interacts with a free surface a reflection occurs which involves the production of both dilatational and distortional waves. If the incident wave is of the P type, then the reflected P wave will follow Snell's law with incidence and reflection angles equal. The S wave produced in the reflection process propagates away from the free surface along a line which makes an angle β_r with the normal to the free boundary where

$$\text{Sin } \beta_r = \frac{c_2}{c_1} \text{ Sin } \beta_i \qquad (3.1)$$

where β_i is the angle of incidence of the P wave.

If the incident wave is of the S type, then the reflected S wave will follow Snell's law with equal incidence and reflection angles. The P wave produced in the reflection process propagates away from the free surface along a line which makes an angle ϕ_r with the normal to the free boundary where

$$\text{Sin } \phi_r = c_1/c_2 \text{ Sin } \phi_i \qquad (3.2)$$

where ϕ_i is the angle of incidence of the S wave.

It is possible to construct wave front diagrams which predict the location of the P and S waves at various times during the dynamic event. Consider the specific problem of a distributed line charge at a 38 degree inclination angle as defined in Fig. 2.1. By using the propagation velocities of c_1 = 70,200 ips and c_2 = 39,000 ips and the detonation velocity of c_e = 115,400 ips, the wave front diagrams during the burning period were determined as presented in Fig. 3.1 a,b and c. Reference to this figure shows the development of plane P and S waves adjacent to the line charge with a circular outgoing wave front originating at the initiation point on the line charge.

After the line charge has burned (t = 52 μsec) the P and S wave propagate outward as depicted in Fig. 3.2 a,b, and c. The front of the P wave advances toward the vertical boundary and the P and S waves separate as time increases. The P wave front is nearly parallel to the vertical boundary while the S wave is inclined at an angle of 16 degrees to this boundary. Circular wave fronts are evident having originated at both the initiation and terminal ends of the line charge. This development of the wave fronts will be denoted as the incident phase in the dynamic event t = 70 to 124 μsec. The waves propagate from the line charge to the vertical face and expand in the process. This expansion reduces the level of the stresses associated with both the P and the S waves.

The P wave reaches both the vertical and horizontal boundaries and reflects as illustrated in Fig. 3.3 (t = 140μsec). The reflected dilatational wave has been labled PP and the reflected shear wave has been labled PS. This reflection phase is important since the incoming P wave is reinforced by the reflected PP and PS waves. The combined waves often have large

tensile stress components and can produce spall type fractures in brittle rock materials which contain numerous flaws. The spall mechanism is important in many quarry applications since it strongly influences the fragmentation of the rock removed from the bench face.

The final phase in the dynamic event is the interaction period illustrated in Fig. 3.4. During the interaction period the reflected PP and PS waves overlap with tne incident S wave. Initially the combination of the S and PP waves occurs at the elevation of the upper end of the line charge. With increasing time the S and PP combination divides with one part sweeping upward and the other part sweeping downward. Further increases in time yields an interaction between the PS and S waves. This combination also divides and the area of reinforcement sweeps up and down the S wave. This set of wave front diagrams representing the interaction phase was terminated at t = 180μsec_c when the S wave reached the vertical and horizontal boundaries just before the S wave reflection process as indicated in Fig. 3.4 (b). The interaction of the PP and PS waves with the incident S wave is important since it provides a mechanism for producing reinforcement of stress waves propagating in a region well removed from the face. It should result in fracturing and fragmentation in a region between the face spalling area and the cracked area around the bore holes.

The final wave front diagram is represented in Fig. 3.5 where the SP and SS waves resulting from the reflection of the shear wave from the vertical face are shown. It is in this final reflection phase where the incident S wave is reinforced first by the SP and then by the SS wave. This is a significant reflection in quarry operations since it provides a second opportunity for spallation at the vertical face or an opportunity for further fragmentation by producing multiple spalls.

3.2 S Wave - 22 degree - Model

Wave front diagrams similar to those presented previously are given for the S wave - 22 degree model in Figs. 3.6 to 3.9. The generation of the initial wave fronts by the detonation of the line charge is shown in Fig. 3.6. The development of the plane front P and S waves is illustrated at times of 10, 30 and 50 μ sec. Circular wave fronts for both the P and S waves propagate radially outward from the initiation point.

The first portion of the period for incident wave propagation is illustrated in Fig. 3.7. Both wave fronts are enlarging with the separation distance between the two waves increasing with time. As a consequence of the difference in wave speeds, the P wave reaches the boundary well in advance of the S wave (see Fig. 3.7c). The reflection of the P wave initiates at a point on the bench face horizontally aligned with the initiation point of the line charge.

The first reflection period is represented in Fig. 3.8 where the P wave reflects from the bench face producing a reflected dilatational wave (PP) and a reflected shear wave (PS). These reflected waves propagate back into the region and interact with the oncoming S wave. These interactions occur first at lower levels on the model and sweep upward as time increases.

The final phase of the dynamic event is illustrated in Fig. 3.9 where the interaction of the PS wave with the S wave has been completed (at t = 170 μsec). Next, the incident S wave reaches the boundary and begins to reflect. The reflected waves SP and SS reinforce the tail of the incident S wave.

4.0 Photoelastic Results

4.1 P Wave - 38° Model

The completed representation of the photoelastic data associated with the three 38 degree models is given in Fig. A-1 to A-3 of Appendix A. A total of 48 fringe patterns have been recorded to indicate the space-time relationship of the stress waves generated from an inclined distributed line charge.

The amount of data collected in this type of a dynamic photoelastic analysis is enormous and procedures which tend to oversimplify the dynamic phenomena must be used to reduce the task of data analysis to a manageable size. To simplify the dynamic event for the 38 degree P wave model, it has been subdivided into five different phases which include the incident, reflection, interaction, 2nd reflection, and crack propagation phases. Each of these five phases will be treated separately in subsequent subsections.

4.1.1 Incident Wave Propagation

A typical fringe pattern showing the P wave propagating from the line charge to the vertical bench face is presented in Fig. 4.1. Examination of the fringe pattern shows that a portion of the wave front is plane and parallel to the vertical bench face. Other portions of the wave front are circular with their centers at the initial or termination points on the line charge.

The profile of the incident P wave at location A-A shown in Fig. 4.1 is given in Fig. 4.2. It is evident that this profile resembles a half sine wave with a half-wave length equivalent to 1.45 in. As the profile changes modestly as the wave propagates from the line charge to the boundary the wave length of the predominate or leading pulse will increase. It appears reasonable then to take the wave length $\lambda \approx 3.00$ in to represent the maximum expected value of λ just before reflection.

During the propagation period as the stress wave travels from the bore

hole to the boundary of the model an attenuation of the leading pulse takes place. The characteristics of the attenuation are shown in Fig. 4.3 where it is evident that the maximum fringe order decays as a function of position and the wave length of pulse width increases with time.

The incident P wave exhibits an appreciable variation in magnitude along its length. If the ridge line is defined in the conventional sense, it can be located on the fringe patterns as illustrated in Fig. 4.1. Following the ridge line from the point of intersection with the line of action of the distributed line charge, the fringe order increases sharply to a peak value then decreases monotonically with increasing distance along the ridge line. The distribution of the fringe order along the ridge line is presented in Fig. 4.4 for the four fringe patterns taken during the incident phase for the model with $S/\lambda = 5/3$. The peak fringe order decays as described previously in the discussion of attenuation of the incident P wave. However, the peak also shifts down the ridge line and the strain energy becomes more uniformly distributed along the wave as it propagates away from the line charge. In spite of the smoothing which occurs during the propagation of the incident P wave the energy in the wave is still concentrated over a very small region. Reference to the fringe pattern presented in Fig. 4.5 shows the distribution of the fringes in the neighborhood of the vertical boundary just prior to reflection. Since the strain energy E is proportional to the square of the fringe order (i.e. $E \propto N^2$) the energy contained in the wave is much more concentrated than it appears from a casual examination of the fringe order. To emphasize the concentration of strain energy a graph of N^2 as a function of position along the vertical boundary is also displayed in Fig. 4.5.

These results indicate that the uniformly loaded line charge does not deliver a uniformly distributed P wave to the vertical bench face. It appears that heavier loads on the two ends of the line would improve the distribution of

energy delivered to the face of the bench. This practice should in turn improve the fragmentation of the rock removed from the face by the spalling process.

The final observation regarding the incident P wave again refers to its profile. It was clearly established that the P wave contains a leading pulse which resembles to some degree a half-sine wave. The magnitude of this pulse varies from 9 to about 4 fringes depending upon its position. It is also important to note that the P wave does not exhibit any significant tail. Inspection of Fig. 4.5 shows that the region behind the initial compressive pulse contains only one small region where the fringe order goes to zero. Thus it appears that the tail of the outgoing P wave which usually carries tensile stresses is nearly absent when it is produced by a uniformly distributed line charge.

The incident shear or S wave is also a dominant phenomena during this period. The fringe pattern associated with the S wave early in the incident phase is identified in Fig. 4.1. The fringes representing the S wave are close packed indicating a relatively sharp peak positioned behind and below the peak of the incident P wave. The incident phase for the S wave is relatively long since the wave travels slowly (in comparison to the P wave). The incident phase terminates when the incident S wave begins to interact with the reflected PP wave. The fringe pattern shown in Fig. 4.6 illustrates the character of the S wave just before the interaction process begins.

The profile showing the fringe order as a function of position through the shear pulse is presented in Fig. 4.7. Again it is clear that attenuation is occurring. Initially the peak value of the fringe order drops sharply as the S wave propagates away from the distributed line charge; however, after propagating a short distance the rate of decay of the peak-fringe order is markedly reduced. Associated with the decay of the peak is a

general increase in the width of the pulse. As was the case with the P wave, the incident S wave does not exhibit a trailing pulse of any significance.

The distribution of the fringe order along the ridge line associated with the S wave is presented in Fig. 4.8. It is noted that the distribution peaks sharply after a short distance along the ridge line early in the event. As the S wave propagates away from the line charge, the peak decays due to attenuation and shifts down the ridge line to lower levels in the model. The distribution of N along the ridge line becomes more uniform; however a significant peak still exists and it is positioned well below the peak of the incident P wave (See Fig. 4.5). The location of peak fringe order in the incident S wave is important during the interaction phase when it combines with the reflected PP and PS waves.

The results described here are based on observation of the P wave - 38 degree model with $S/\lambda = 5/3$; however, similar results were observed for the models with $S/\lambda = 4/3$ and $S/\lambda = 1$. The attenuation of the incident P wave is a function of the distance travelled for all models. This fact is clearly established in Fig. 4.9 where the fringe ratio N_{MAX}/N^{o}_{MAX} is presented as a function of distance. The value of N_{MAX} is taken from the peak associated with the P wave as it propagates toward the vertical face of the model. The value of N^{o}_{MAX} is taken from the peak associated with the P wave as it propagates toward the vertical face of the model. The value of N^{o}_{MAX} used to normalize the data was the maximum fringe order at the $x = 1.0$ position.

The degree of attenuation of the incident P wave can be expressed as a function of position by:

$$N_{MAX}/N^{o}_{MAX}\Big|_{P} = 1/(1 + ax)$$

where the selection of $a = 1/3$ produced a very close fit with the observed data for all three models.

A second common feature of the incident P wave was the shift of the maximum fringe order down the wave front as it propagated to the vertical boundary. Reference to Fig. 4.10 indicates that the shift is essentially complete with a movement of about 1.75in. in the y direction after a propagation in the x direction of about 2.5 inches. Since models with S = 3, 4 and 5 in were employed, this fact implies that the maximum energy density was delivered to the vertical face at essentially the same location in all three models. Spacing of the line charge with respect to the vertical boundary, should not markedly affect the vertical positioning of the region where spallation occurs. Due to the attenuation the positions of the line charge will influence the extent of the spallation with reduced amounts associated with large values of s.

The incident S wave in all three of the P wave - 38 degree models attenuates as the S wave propagates toward the vertical boundary. The degree of attenuation was characterized by normalizing the maximum fringe order in the S wave with the maximum fringe order recorded when the wave was at the x = o position. The results for the fringe ratio are shown in Fig. 4.11 and it is notable that the degree of attenuation of the S wave can be written in exactly the same form as the attenuation for the P wave - namely

$$\left[N_{MAX}/N^{o}_{MAX}\right]_{S} = 1/\ 1 + ax$$

with a = 1/3

The location of the peak stress associated with the S wave remained essentially constant with respect to the position parameter y for each model and during the entire initiation phase. This fact is illustrated in Fig. 4.12 where the parameter y locating the vertical level of the peak stress is shown as a function of the horizontal distance propagated (x).

These results show that the positions of the line charge relative to the

vertical face is not critical for either the incident P or S waves. In both cases the decay due to attenuation is affected but in a predictable manner. The locations of the maximum stressed areas appear independent of the choice of s providing $5 \geq s \geq 3$ in.

4.1.2 Reflection Period

The reflection occurs when the incident P waves encounters the vertical boundary and produces reflected PP and PS waves. The reflection period is extremely short since it is controlled by the predominate wave length and the velocity of the P wave according to

$$t_r = \frac{\lambda}{2 c_1}$$

For $\lambda = 3$ in and $c_1 = 70{,}200$ in/sec, the time required to reflect the P wave is 21.3 μ sec.

The reflection process is clearly illustrated by a sequence of four fringe patterns taken over the interval from 84 to 106 μ sec for the P wave model with $s/\lambda = 1$. The first two of these fringe patterns presented in Fig. 4.13 illustrate the first half of the process. The incident P wave is at the boundary at the beginning of the reflection process in Fig. 4.13 (a). The maximum fringe order is 6 and is located at y = 1.81 in and x = 2.2 in. The ridge line associated with the P wave pulse makes a slight angle with the vertical boundary.

The fringe pattern at t = 91 μ sec depicted in Fig. 4.13 (b) shows partial reflection along the upper half of the vertical boundary. The state of stress in the reflected pulse is of opposite sign and thus tends to cancel the stresses associated with the incident P wave. This cancellation accounts for the sharp reduction in the fringe orders along the upper half of the vertical boundary in Fig. 4.13 (b). Along the lower half of this boundary the stress pulse has just begun to reflect and the maximum fringe

order has not been cancelled.

The second half of the reflection process is illustrated by the two fringe patterns presented in Fig. 4.14. Examination of the pattern taken at t = 99 μ sec shows that the incident P wave has been completely reflected along the upper half of the vertical boundary. The reflected PP and PS waves overlap in this time period and produce fringe maxima of 4.5 at two different interior points. As these fringe order peaks indicate stress pulses with significant tensile stresses it is reasonable to anticipate spallation type failures over large portions of the field during this period. The conclusion of the reflection phase is depicted in Fig. 4.14 (b). The incident P wave has completed its reflection with the lower portion of the vertical boundary and a fringe maxima of 3.5 has developed at a location about 0.7 in from the boundary. The reflected PP and PS waves originating from the upper-half of the boundary are interacting with incident S wave. This interaction will be described in more detail in the next subsection of the report.

If the maximum fringe in the reflected and superimposed PP and PS pulses are determined as a function of position it is possible to establish the effectiveness of the uniformly distributed line charge in producing spallation. This distribution of $N_{MAX}\,]_{REFL}$ as a function of position y is shown in Fig. 4.15. These results show that $N_{MAX}]_{REFL}$ decreases for y larger than 2.5; thus, it appears that an increase in the charge density at the initiation end of the charge would provide a more uniformly distributed stress field producing spallation type failures.

4.1.3 Interaction Period

For the P wave - 38 degree model with $S/\lambda = 1$, the interaction begins near the y = o position when the PP wave and then the PS wave interface with the incident S wave. The duration of the interaction period is the time

necessary for the reflected PP and PS waves to sweep through the incident S wave. Since the incident S wave is inclined at an angle of about 16 degrees with respect to the PP wave front, the duration time of the interaction period is extended. Also, the apparent magnitude of the PS wave is quite small since the incident P wave impinged on the vertical boundary at essentially normal incidence.

Evidence of the initiation of interaction period is shown in the fringe pattern presented in Fig. 4.16a recorded at t = 106 μ sec. At the co-ordinated y = 1.2 and x = 2 there is a sudden increase in the fringe order with a new fringe peak with N = 5.5 MAX established in what appears to be the incident shear wave. Eight μ sec later as illustrated in Fig. 4.16b, this fringe peak has moved down the ridge line of the incident S wave and has increased in magnitude with $N_{MAX}\rceil_{INT} = 6$. The fringe peak of 3.5 evident at y = 0.8 and x = 2.4 is apparently due to the interaction of the PS and incident S waves.

The final stage of the interaction phase can be described with the two fringe patt rns presented in Fig. 4.16. The reinforcement of incident S wave with the reflected PP wave continues to move down the ridge line of the S wave producing the fringe order peak with $N_{MAX}\rceil_{INT} = 6.5$ in Fig. 4.17 (a). Further shifting of the interaction region at the lower extremes of the incident S waves produces the marked reduction in the maximum fringe order to 4.5 as illustrated in Fig. 4.17 (b). This reduction is due to the relatively low values of stress associated with the incident S wave in this location.

The interaction of the reflected PP and incident S waves is important because it provides a mechanism for producing interior stress fields with significant tensile stresses. The reflected PP wave will produce spalling but this spalling is confined to the region near the vertical boundary (usually within 1/2 to 1 in of the boundary). The interaction region begins

at a location about 1 inch from the vertical boundary but as it sweeps down it moves into interior regions and covers the area bounded by $1 \leq x \leq 2$.

4.1.4 Reflection Period - S Wave

In the event that fracturing does not take place in the interaction period, the energy associated with the incident S wave will be carried on to the vertical boundary. As most of this energy is concentrated in the lower reaches of the incident S wave, the reflection with the lower half of the vertical boundary is the most significant.

The photoelastic visualization of the reflection of the S wave with the lower half of the vertical boundary is shown in Fig. 4.18 (a) to (d). Inspection of these patterns shows that a fringe peak sweeps down a line parallel to the vertical boundary and decays from about 4 at y = 3.7in to 3 at y = 5.75 in. Its evident that the reflection process does not reinforce or amplify the stresses associated with the S wave.

The S wave reflection period appears to be of relatively minor importance when considered together with the other three periods (i.e. incident wave propagation, reflection, and interaction periods). In the event that fracture does not occur at interior regions due to interaction, it appears that the S wave is capable of delivering energy to the lower reaches of the bench face during this period.

4.1.5 Crack Propagation Period

Although this series of tests were not designed to study stress wave induced fracture, cracks did occur in all of the models and some preliminary observations are possible. While several cracks were formed in the 38 degree model with $S/\lambda = 1$, this discussion will be restricted to that crack identified in Fig. 4.13 (b). The crack initiated at the end point of the line charge and at $t = 91$ μ sec (recall it required 52 μsec to burn the charge) the crack is about 0.75 in long in this fringe pattern. The crack can be

identified in Figs. 4,14, 4.16, 4.17 and Fig. 4.18 as it propagates upward and to the left.

The distance propagated by the crack is shown as a linear function of time in Fig. 4.19. The crack was initiated at t = 52 μ sec when the detonation reached the end of line charge. After initiation, it propagated with a constant velocity of 18,900 in/sec over the time interval from 52 to 178 μ sec. Its propagation continued after the recording of the dynamic event terminated. The fringe patterns shown in Fig. 4.20 illustrate that the cracks are propagating in the very late phase of the dynamic event. The incident P and S waves have passed and the reflected PP and PS waves are no longer distinguishable. The order of the fringes in the patterns shown in Fig. 4.20 are with a few exceptions 0.5. Apparently, the very low level stresses associated with tails of the reflected PP and PS waves provide sufficient energy to keep the cracks moving at a constant velocity. The fact that the crack velocity is 18,900 in/sec in comparison to the theoretical maximum of 0.38 C_1 = 26,600 in/sec indicates that the crack is moving at high speed (71 per cent of maximum possible). Apparently, the energy required to drive the cracks (once formed) is extremely low in the CR-39 material used for the models. It is anticipated that the energy requirement for rock will be even lower.

These results clearly indicate the importance of the later phases in the dynamic event and show the importance of the residual stress fields which remain after the passage of the incident P and S waves and the reflected PP and PS waves.

4.2 S Wave - 22° Model

The completed representation of the photoelastic data associated with the three 22 degree models is given in Fig. A-4 and A-6 of Appendix A. A total of 48 fringe patterns have been recorded to indicate the space-time relationship for the stress waves generated from an inclined distributed line charge. The 22 degree angle of inclination was selected to bring the S wave front parallel to the vertical boundary of the model.

4.2.2 Incident P Wave Propagation

The incident P wave is shown propagating from the line charge to the boundary in Fig. 4.21. The front of the wave is inclined with the vertical boundary and sweeps up the boundary during the reflection period. The profile of incident P wave for the model with $S/\lambda = 5/3$ is presented in Fig. 4.22. The behavior of the incident P wave is identical to that described previously in Section 4.1.2 the maximum fringe order decreases with distance and the pulse width increases with distance propagated.

The attenuation of the maximum fringe order in all three of the S wave models is shown in Fig. 4.23. In this case the decay of the maximum appears to be a linear function of x where

$$\left[N_{MAX}/\ N^{o}_{MAX}\right]_{P} = 1 - ax$$

where $a = 1/6$ and N^{o}_{MAX} is the maximum fringe order at the position $x = 1.0$ The reason for the change in the form of the attenuation ratio between the P-38° and S - 22° models is due to the inclination of the P wave with the x axis in the S models. In this case, the x direction no longer coincides with the direction of propagation of the wave and as a consequence the decay of N_{MAX} with the position parameter x is altered.

The position of the maximum fringe order as represented by the parameter y appears to shift downward (y increasing) as the P wave propagated toward the

4.2 S Wave - 22° Model

The completed representation of the photoelastic data associated with the three 22 degree models is given in Fig. A-4 and A-6 of Appendix A. A total of 48 fringe patterns have been recorded to indicate the space-time relationship for the stress waves generated from an inclined distributed line charge. The 22 degree angle of inclination was selected to bring the S wave front parallel to the vertical boundary of the model.

4.2.2 Incident P Wave Propagation

The incident P wave is shown propagating from the line charge to the boundary in Fig. 4.21. The front of the wave is inclined with the vertical boundary and sweeps up the boundary during the reflection period. The profile of incident P wave for the model with $S/\lambda = 5/3$ is presented in Fig. 4.22. The behavior of the incident P wave is identical to that described previously in Section 4.1.2 the maximum fringe order decreases with distance and the pulse width increases with distance propagated.

The attenuation of the maximum fringe order in all three of the S wave models is shown in Fig. 4.23. In this case the decay of the maximum appears to be a linear function of x where

$$\left[N_{MAX} / N^{o}_{MAX}\right]_{P} = 1 - ax$$

where $a = 1/6$ and N^{o}_{MAX} is the maximum fringe order at the position $x = 1.0$ The reason for the change in the form of the attenuation ratio between the P-38° and S - 22° models is due to the inclination of the P wave with the x axis in the S models. In this case, the x direction no longer coincides with the direction of propagation of the wave and as a consequence the decay of N_{MAX} with the position parameter x is altered.

The position of the maximum fringe order as represented by the parameter y appears to shift downward (y increasing) as the P wave propagated toward the

boundary. This fact is illustrated in Fig. 4.24 which shows the x-y coordinates for N_{MAX} associated with the incident P wave.

The distribution of the fringe order along the ridge line of the incident P wave pulse is shown in Fig. 4.25. Here it is evident that the peak value of N diminishes with increasing time and that this peak value shifts down the ridge line.

The energy delivered to the boundary by the incident P wave is again concentrated over a relatively short length along a line parallel to the boundary. The distribution of N^2 which is proportional to the energy in the wave is shown a function of ξ in Fig. 4.26 (note ξ is a line parallel to the vertical boundary through the peak of the fringe pulse). It is evident that most of the energy is contained along the line segment from y = 0 to y = 3. It is again clear that a better distribution of energy could be delivered to the vertical face if concentrated charges were added at the initiation and terminal points of the line charge.

4.2.3 Incident S Wave Propagation

The fringe patterns associated with the incident S waves are clearly evident in Figs 4.21 and 4.25. The wave exhibits a plane front nearly parallel to the vertical boundary with a transition to a circular front with its center at the termination of the line charge. The profile of the stress pulses are shown for various times in the propagation a period for the model with $S/\lambda = 5/3$ in Fig. 4.27. Inspection of these results show the attenuation characteristics with the decay of the peak fringe order and the widening of the pulses.

The attenuation of the S wave for all three models is defined in Fig. 4.28 where the fringe ratio $\left[N_{MAX} / N^{o}_{MAX}\right]_S$ is shown as a function of position. The form of this fringe ratio can be expressed as:

$$\left[N_{MAX} / N^{o}_{MAX} \right]_{S} = \frac{1}{1 + ax}$$

where a = 1/3 as was the case for the P wave models. Scatters bands have been placed in Fig. 4.28 to show the maximum variation in the experimental data.

The position of the maximum fringe order associated with the incident S wave varies widely from model to model as shown in Fig. 4.29. The magnitude of the S wave pulse is dependent upon the fracturing of the Model in the local area around the line charge. This fracture process is not exactly reproducible and as a consequence the outgoing shear wave varies to some degree from model to model.

The distribution of the fringe orders along the ridge line of the S wave pulse for the $S/\lambda = 5/3$ model is shown in Fig. 4.30 for various times during the propagation interval. The oscillations of the fringe order along the ridge line is evident through most of the period; however at later times $t \geq 113$ μ sec the fringe peak has shifted downward along the ridge line to lower regions in the model.

4.2.4 P Wave Reflection - S Wave Model

The fringe patterns associated with reflected P wave are presented in Fig. 4.31. The peak fringe order in the incident wave is located between $0 < y < 1$ and as a consequence the significant portion of the reflected PP wave is also in this same location although it has shifted up slightly due to angle of incidence of the normal to the P wave front with the vertical boundary. Small fringe peaks due to the PS wave are evident in Fig. 4.31 c above and below the peak due to the PP wave. At the lower regions of the vertical boundary the amplitude of reflected PP wave is very small with fringe order of about 1/2 which is the same as the sensitivity limit of the photoelastic method.

Typical profiles of the fringe order versus position x are shown in Fig. 4.32. Here it is evident that the attenuation of the incident pulse from a fringe order maximum of 4 to a peak value of 3 took place during the reflection process. It is believed that these reflected PP waves contain significant tensile stress components and will produce spallation type failures at the vertical face.

4.2.5 Interaction Period - S Wave Model

The interaction of the reflected PP and PS with the incident S wave in 22^{o} model with $S/\lambda = 5/3$ is presented in Fig. 4.33. The fringe pattern in Fig. 4.33 (a) shows the incident S wave at the beginning of the interaction period. In the next frame, 13 μ sec later (Fig. 4.33 (b)) the PP and PS have produced a cancellation of the stress field and have markedly lowered the magnitude of the associated fringe pattern.

More detail related to this interaction period can be observed in the fringe patterns for the model with $S/\lambda = 3$. In this case, all the waves have higher amplitudes and many of the characteristics of the reflection and interaction period can be more easily distinguished in the fringe patterns. In 4.34 five sequential fringe patterns are presented to illustrate the reflection and interaction process. The reflection of the incident P wave is depicted in Fig. 4.34 (a) and (b). The fringe pattern develops two peaks in this case. The upper peak reflected PS persists and moves out and is reinforced by the incident S wave as indicated in (d). The lower peak appears to vanish in (b) due to cancellation of the incoming and outgoing components of the P and PP waves. The lower peak shows its influence in the reinforcement of the incident S wave in (c) where the fringe order has increased from 4 to 6.

In this case the reinforcement due to interaction was favorable and

stress levels were enhanced when the PP and PS waves overlapped. Unfortunately the region of reinforcement of the waves is too close to the vertical boundary. The close proximity to the vertical boundary indicates that both the reflection and interaction mechanism is being used to fracture the same region of rock.

4.2.6 Reflected Shear Wave

The reflection phase for the shear wave is illustrated by the fringe patterns shown in Fig. 4.35 for the model with $S/\lambda = 1$. The reflected pulse exhibits an energy peak which is concentrated over the region from $1 \leq y \leq 3$. The reflected shear wave is of much less importance than the reflected PP and PS waves. The reasoning is that the incident S wave will exhibit $\sigma_1 = -\sigma_2$ so that it is comprised of both tensile and compressive stresses of equal magnitude. The reflection process does not add new tensile stresses to the field.

4.2.7 Crack Propagation Phase

Again it was possible to observe cracks propagating during the dynamic experiments. The crack initiating at the end point of the line charge in the 22 degree model with $S/\lambda = 1$ was selected for analysis. This crack is shown at the end of the dynamic recording in Fig. 4.36 although it continued to propagate until it reached the top boundary. It is evident that the crack propagation occurs very late in the dynamic event. Stresses are still in the model, however, they are generally considered to be dynamic residuals which are associated with the tails of reflected waves.

The primary P and S waves and the reflected PP and PS waves are important in producing spallation type failures and in producing fragmentation by interaction processes. However, these waves do not directly drive the cracks initiating from the source. These particular cracks move so slowly

that they are controlled by the low order dynamic residuals from a wide variety of waves.

The crack shown in Fig. 4.36 is characteristic of many observed in the experiments. It initiates at the termination of the line charge and propagates up toward the horizontal boundary. The crack length is shown as a function of time in Fig. 4.37. The propagation velocity is essentially constant at 18,200 in/sec over the time interval from 71 to 141 μ sec and the crack propagated along a path with only modest variations in direction. At about 141 π sec the crack turned relatively sharply and in the process its velocity was reduced. After the turn was completed the crack resumed a velocity close to the original velocity.

5.0 Conclusions

The dynamic photoelastic investigations provide a vast amount of data on the stress-time history of wave propagation from line charges. Some overall conclusions can be drawn from tests which should guide the mining engineer in designing inclined line charges. These conclusions are listed below:

(1) The 38 degree P wave Model is more suitable since the incident P wave is delivered to the vertical boundary so that it reflects back with its energy converted into a tensile PP wave. Little energy is converted into the PS wave with this model.

(2) The tests were designed to make the wave front of the P or S wave parallel to the boundary; however, an improved reflection (particularily for the P wave) could be achieved if the ridge line of the P wave were made parallel to the vertical boundary. This would require fabrication of the P wave model with an angle of 33 degrees rather than the 38 degrees used in these experiments.

(3) Delivery of energy to the vertical face could be improved by adding explosive to line at both ends. In particular, spallation could be improved by placing point charges at either end with the larger of the two charges at the initiation end.

(4) The interaction of the reflected PP wave (in the P wave model) with the incident S wave produces a benefical reinforcement that should produce fracture at interior regions in the model thus improving fragmentation. It is clear that positioning the charge line affects the location in the model where the interaction takes place, and that $s/\lambda = 5/3$ should result in internal fractures further removed from the vertical face providing the amplitude of the stress field is sufficient to produce fracture.

(5) The reflected S wave is probably of minor importance since the reflection does not produce new regions of tensile stress necessary to fracture flaw filled brittle materials.

(6) The cracks were initiated at the line source by high intensity pressure normal to the cavity wall containing the explosive. The cracks propagate with a velocity of about 18,000 to 19,000 in/sec and separate from the incident waves which travel at velocities about 2 and 3 times higher. The cracks continue to propagate very late in the dynamic event and are apparently driven by dynamic residuals of very low amplitude.

Bibliography

2.1 C. Cranz and H. Schardin, Kinematographic auf ru hendem Film und mit extremhoher Bildfrequenz, Zeits. f. Phys. 56 147 (1929).

2.2 D. G. Christie, A multiple spark camera for dynamic stress analysis J. Phot. Sci. 3, 153 (1955).

2.3 Dally, J. W., and Brillhart, L.V., 1968, Application of the multiple spark gap camera to dynamic photoelasticity: J. Motion Pict. and Telev. Eng., v. 66, p. 116-120.

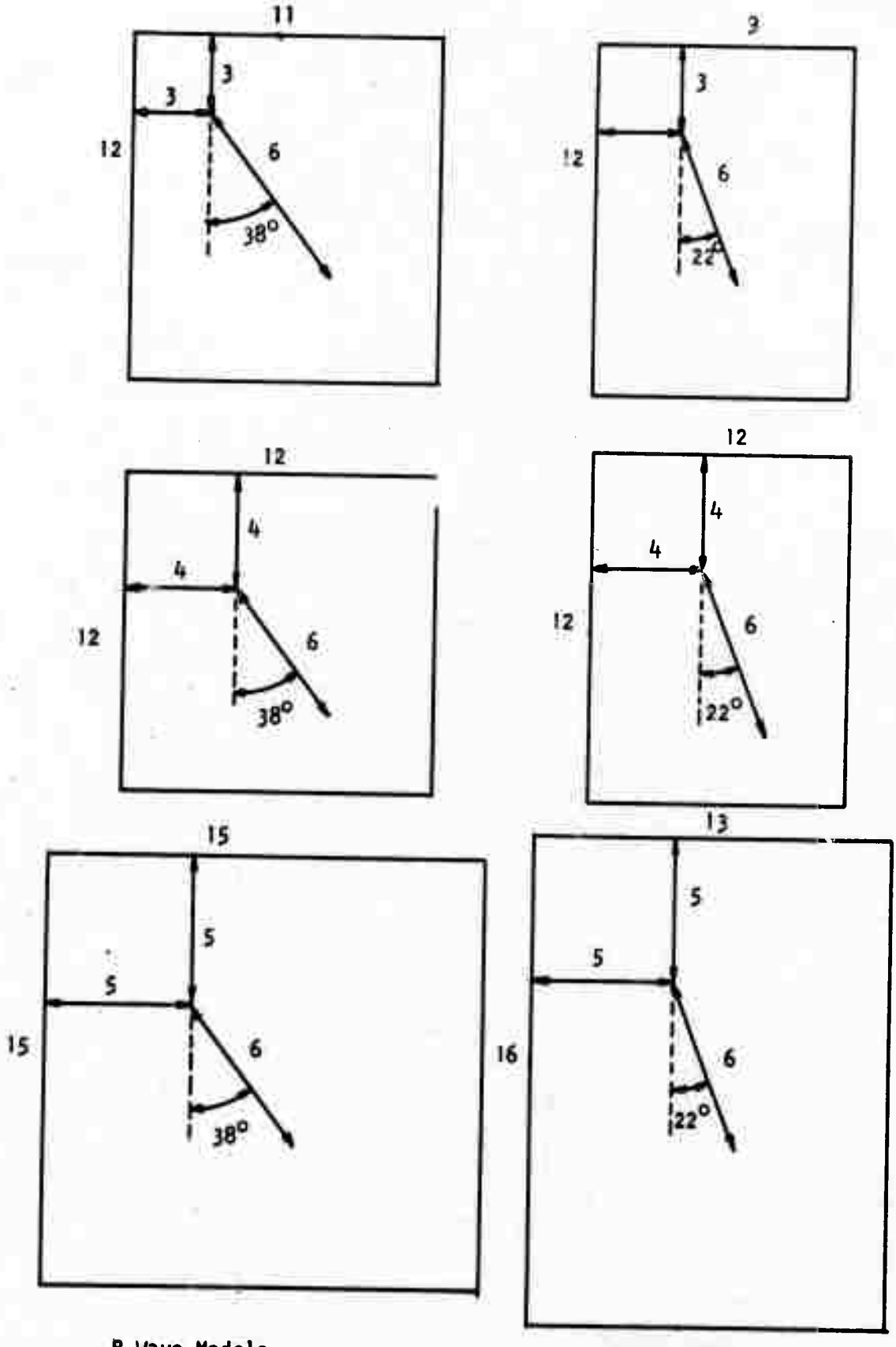

Fig. 2.1 Model Geometry and Line Charge Orientation

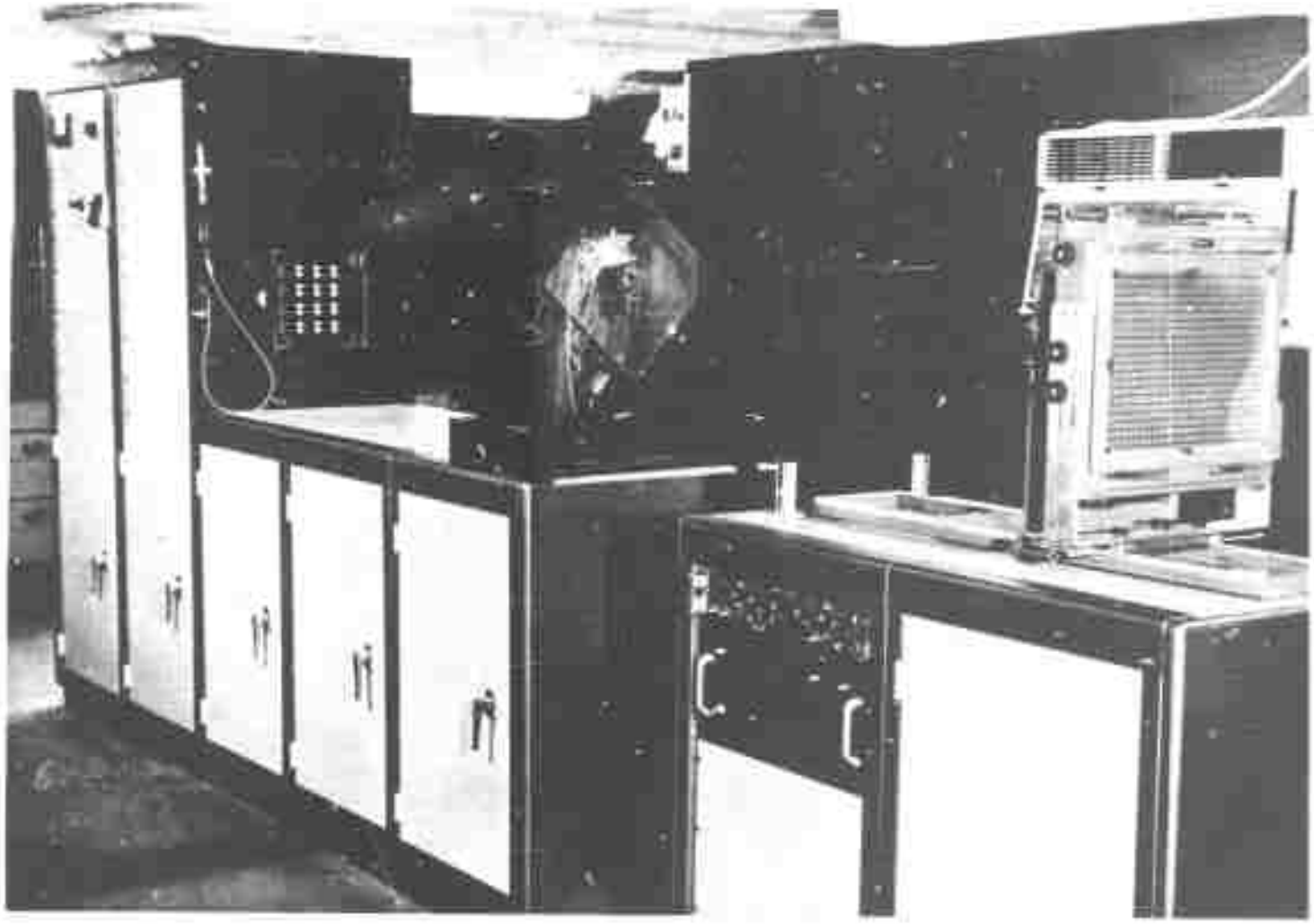

Fig. 2.2 Multiple Spark Camera - Photomechanics Laboratory University of Maryland

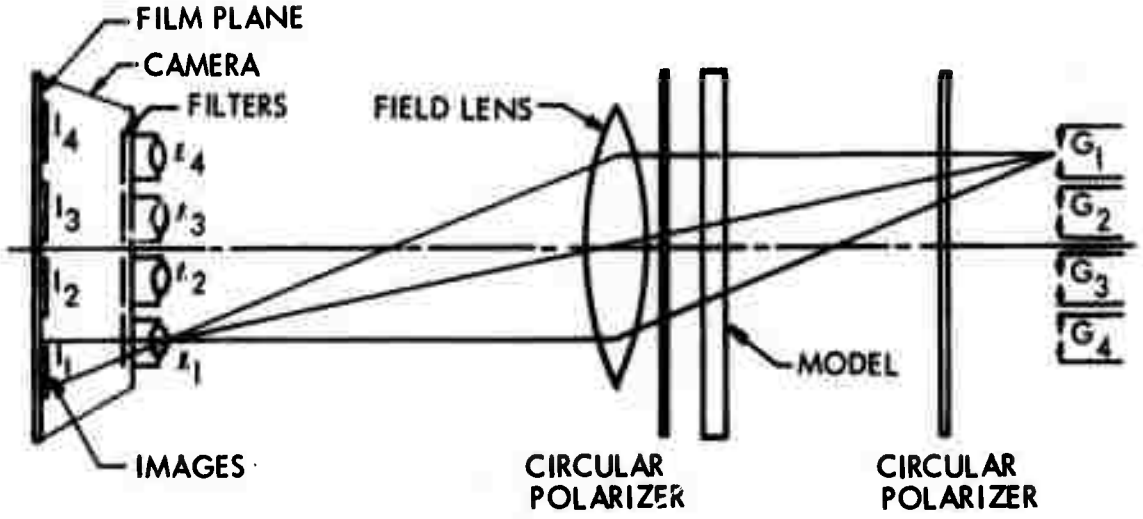

Fig. 2.3 Multiple Spark Camera - Optical

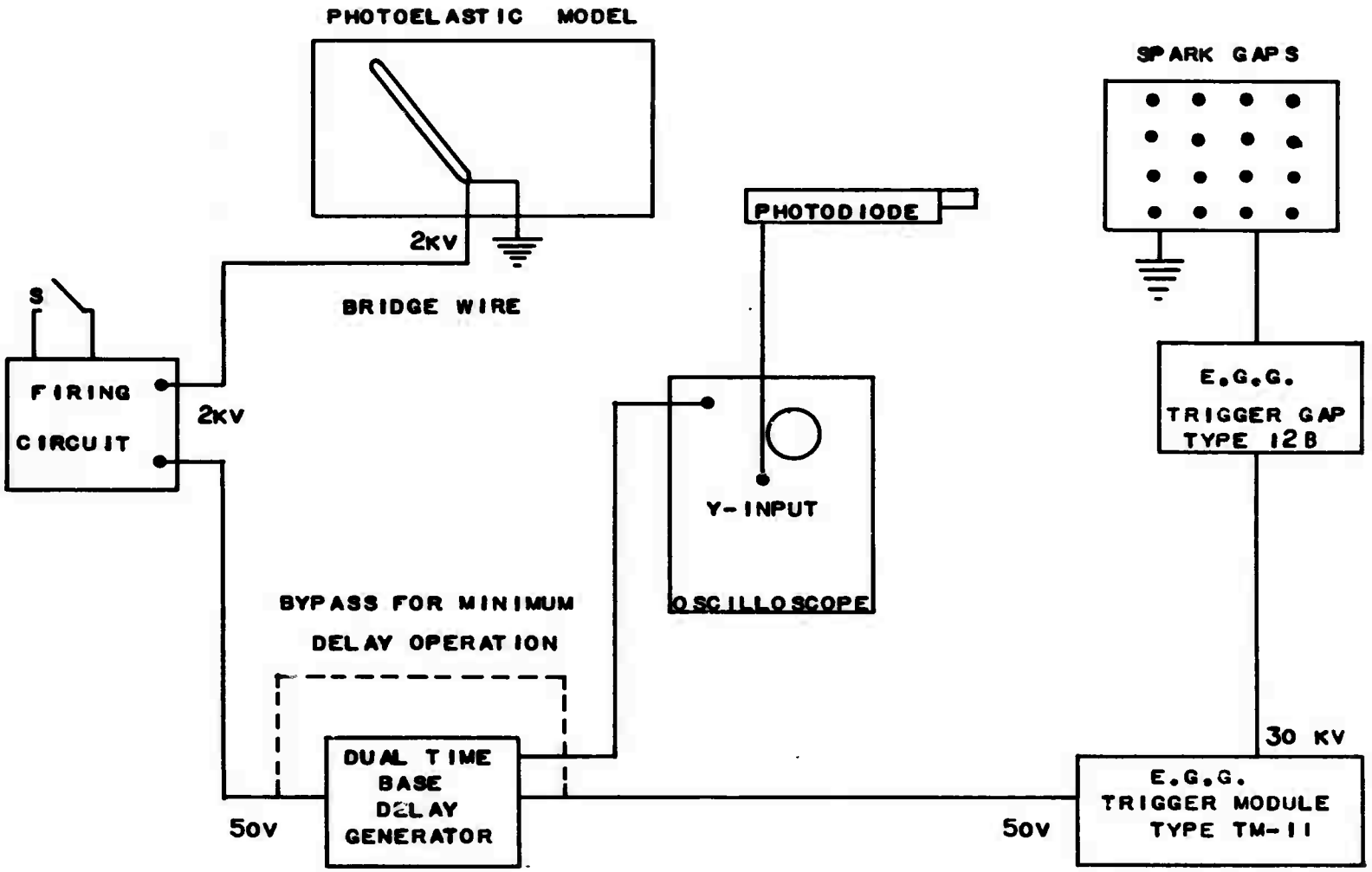

FIG. 2.4 SYNCHRONIZATION CIRCUITS

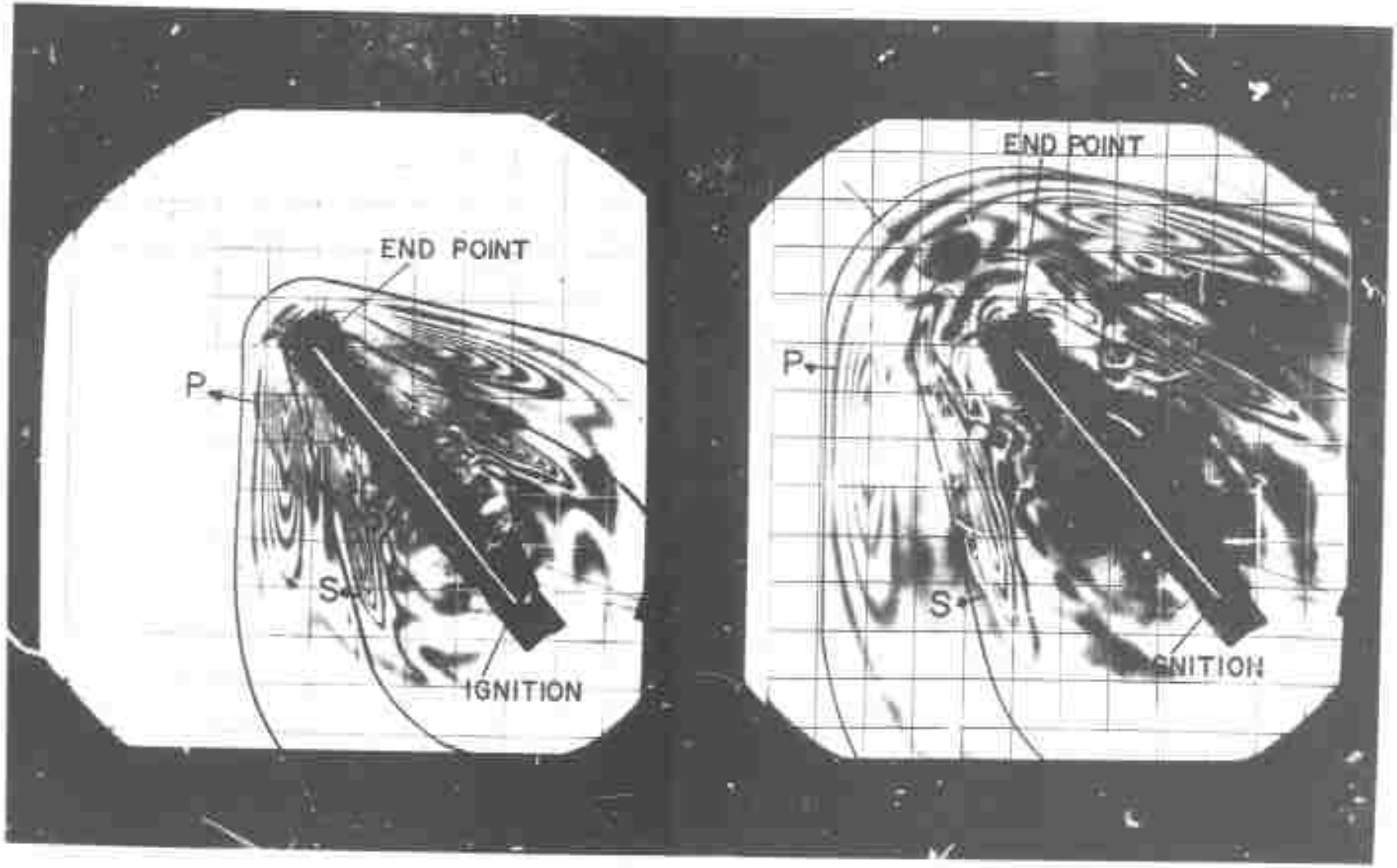

t = 66 μ sec

t = 100 μ sec

Fig. 2.5 Typical Isochromatic Fringe Patterns for Models with θ = 38 degrees

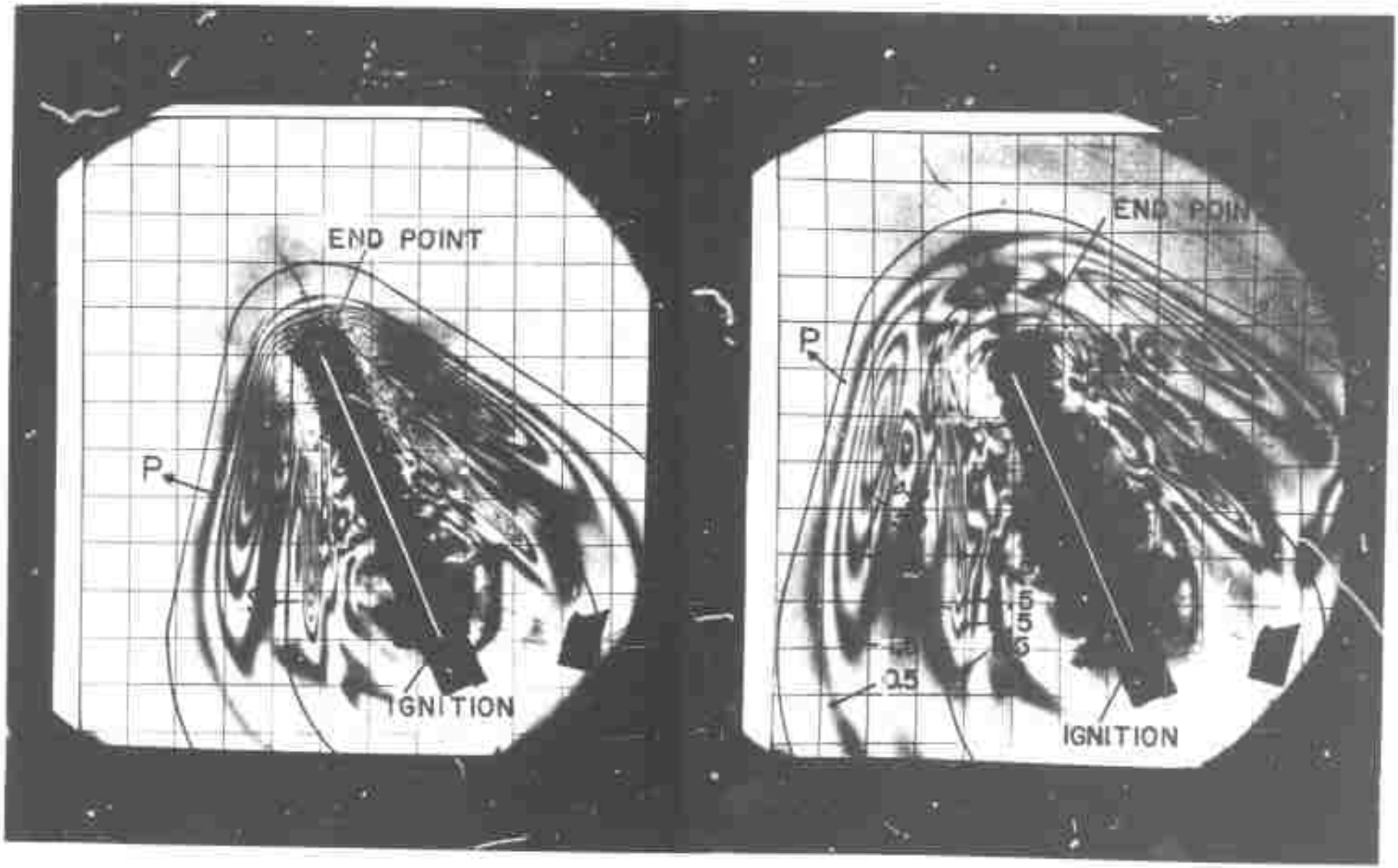

t = 67 μ sec

t = 87 μ sec

Fig. 2.6 Typical Isochromatic Fringe Patterns for Models with θ = 22 degrees

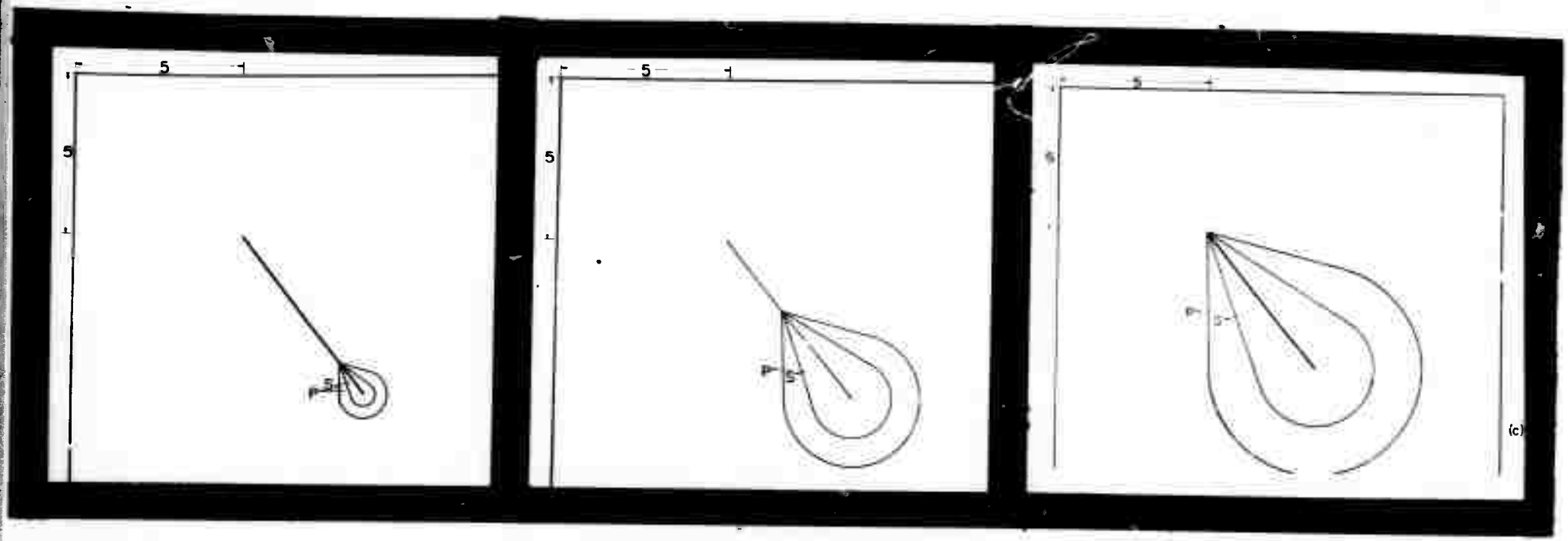

(a) t=10 (b) t=30 (c) t=72

Fig 3.1 Wave Diagram for Burning Period with Distributed Line Charge

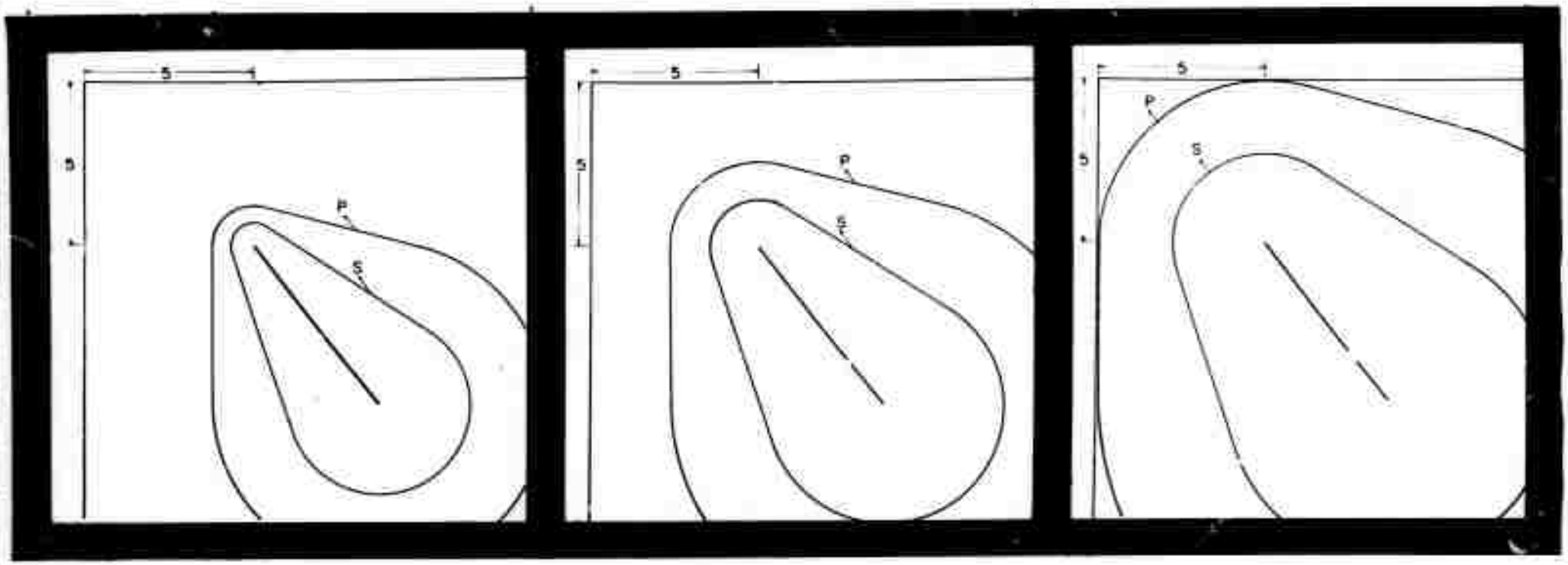

(a) t=70 (b) t=90 (c) t=124

Fig 3.2 Wave Front Diagram at Three Different Times During the Incident Phase of the Dynamic Event

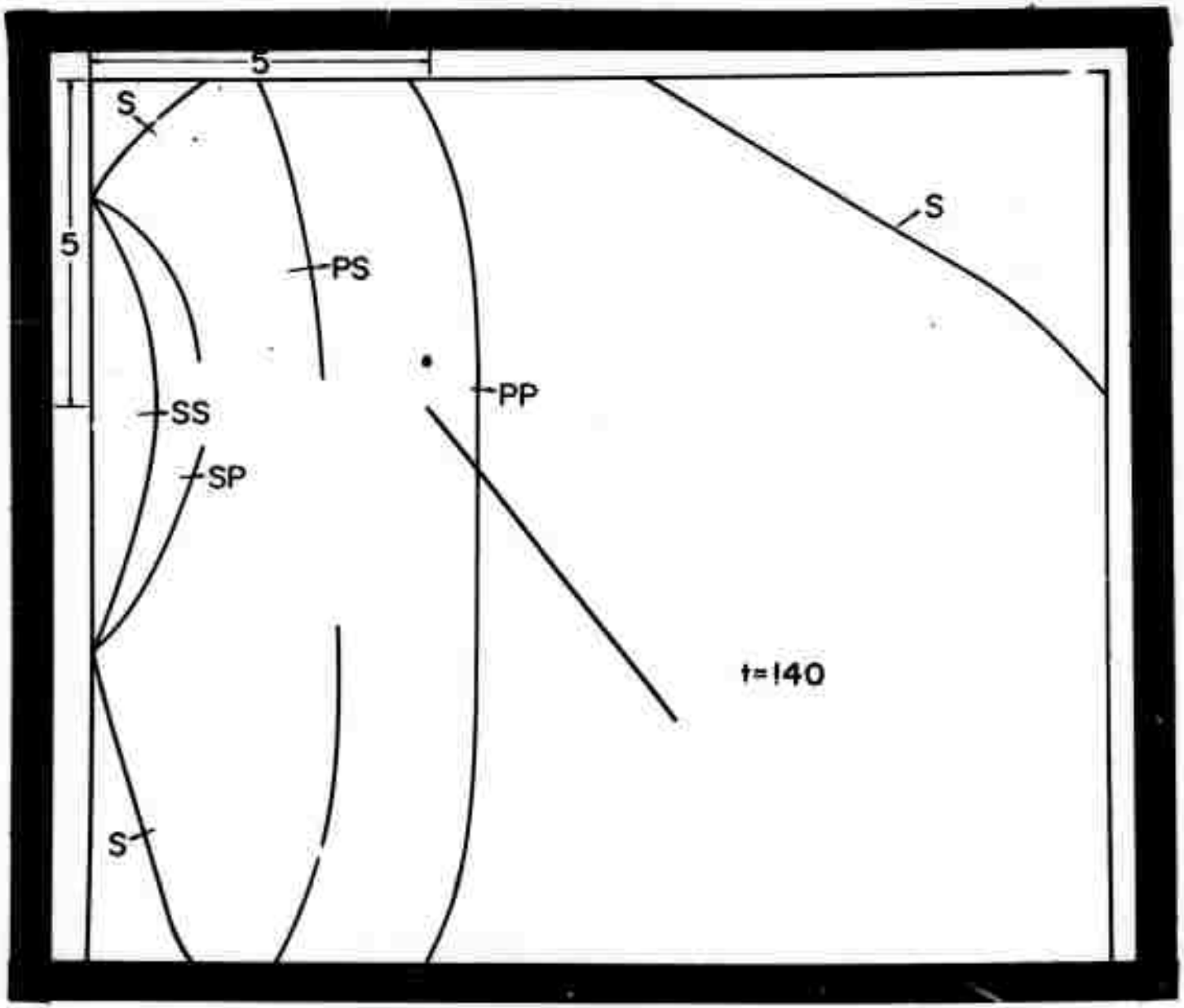

Fig. 3.3 Wave Front Diagram During the Reflection Process

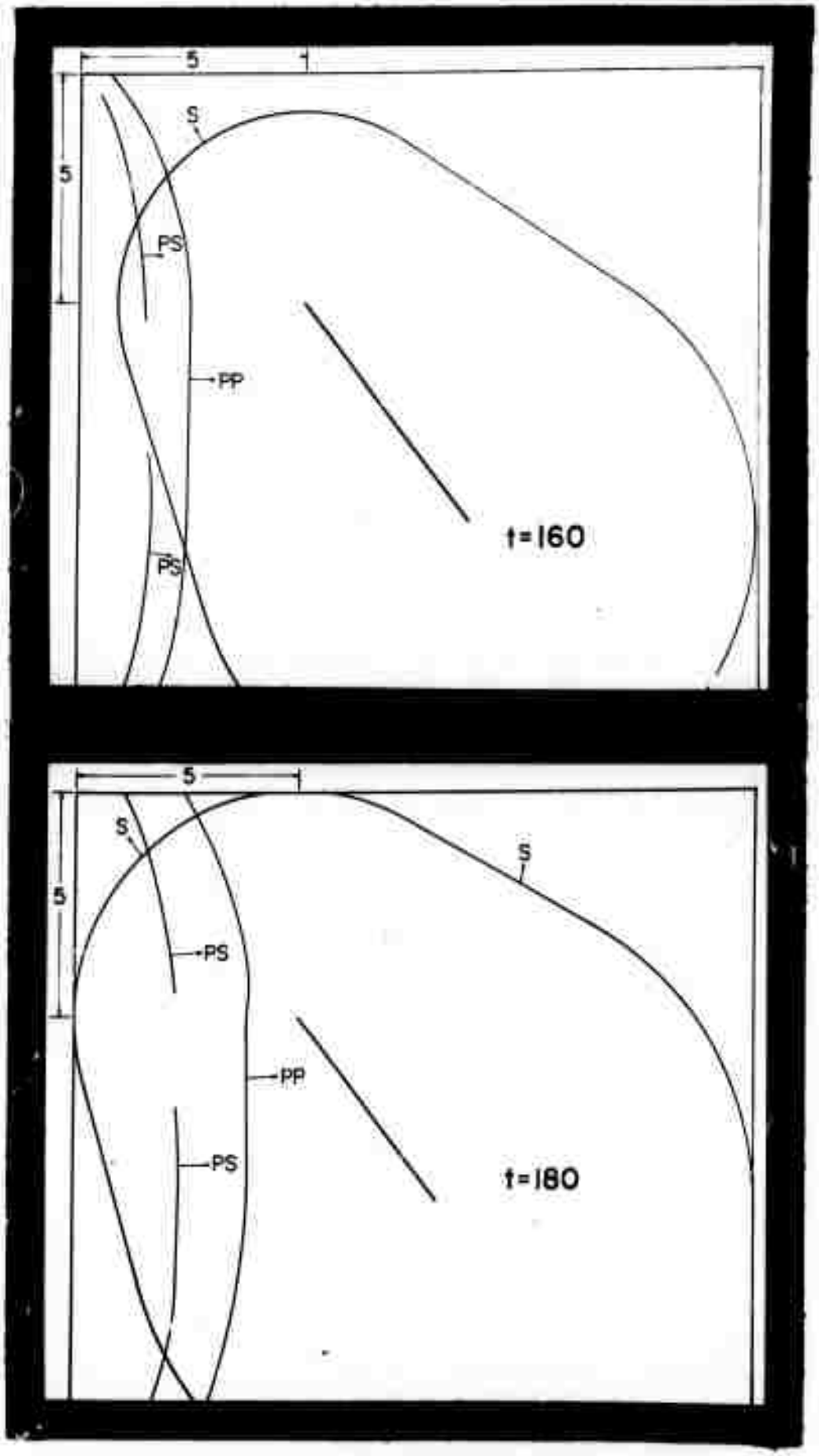

Fig. 3.4 Wave Front Diagrams During the Interaction Phase

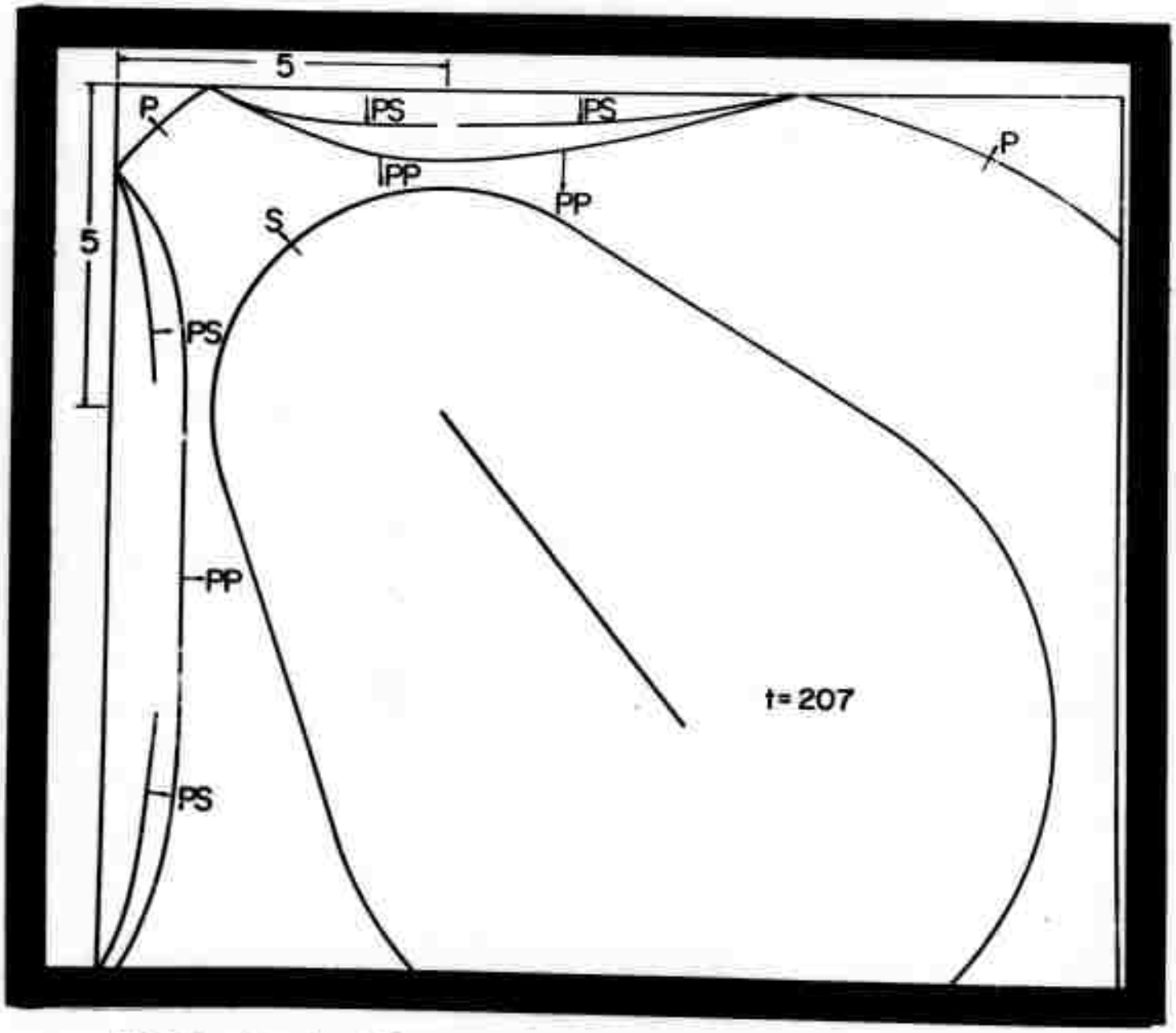

Fig 3.5 Wave Front Diagrams Representing the Final Reflection of the S Wave

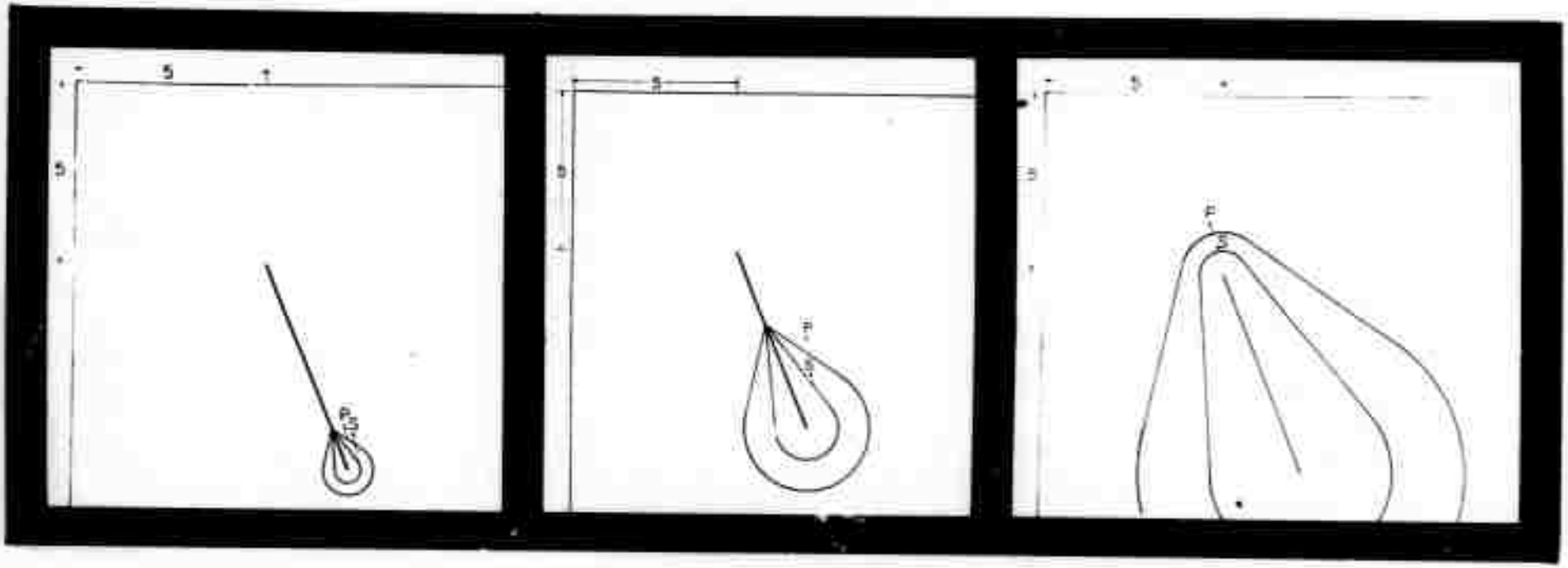

(a) t=10 (b) t=30 (c) t=52

Fig 3.6 Wave Front Diagrams During Detonation Period

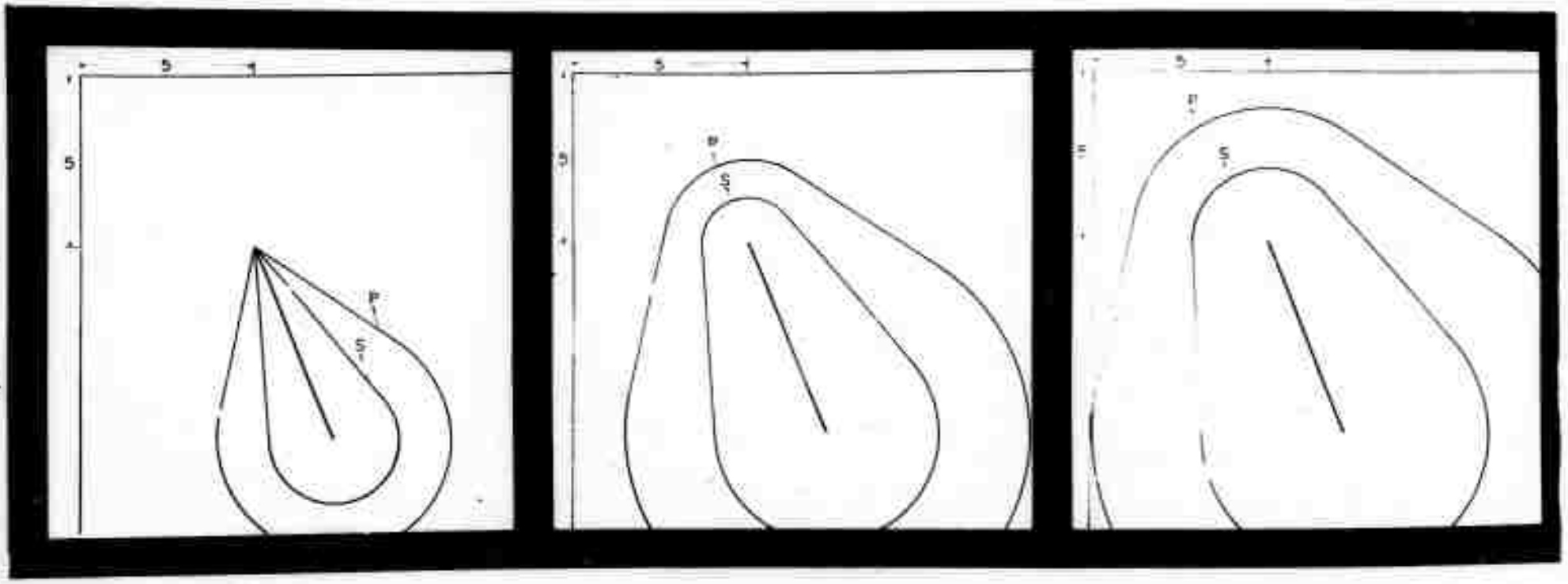

(a) t=70 (b) t=90 (c) t=110

Fig 3.7 Wave Front Diagrams for Incident Wave Propagation Period

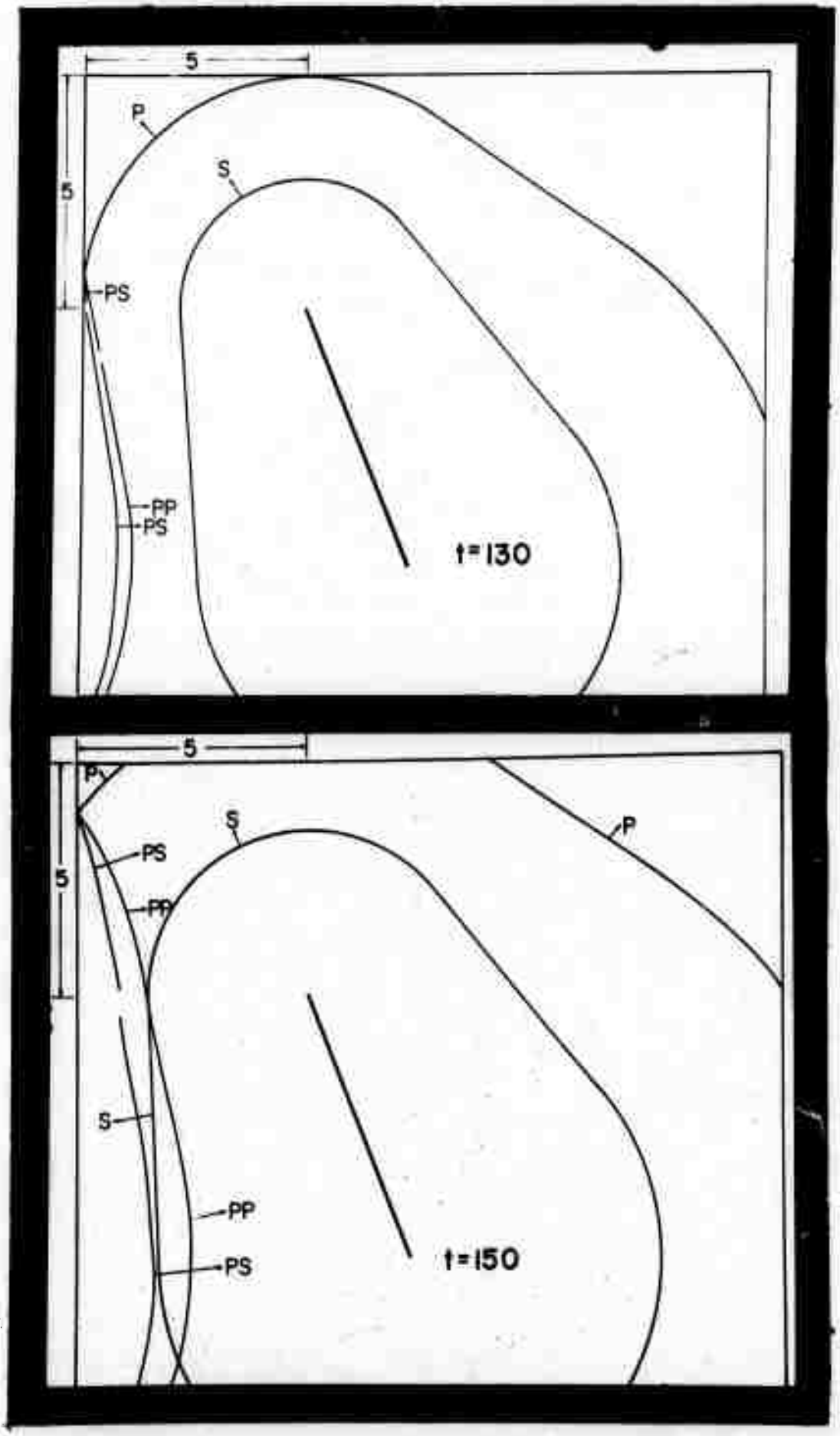

Fig 3.8 Wave Front Diagrams Associated with the Reflecting P Wave and the Interaction of the PP and PS Waves with the Incident S Wave

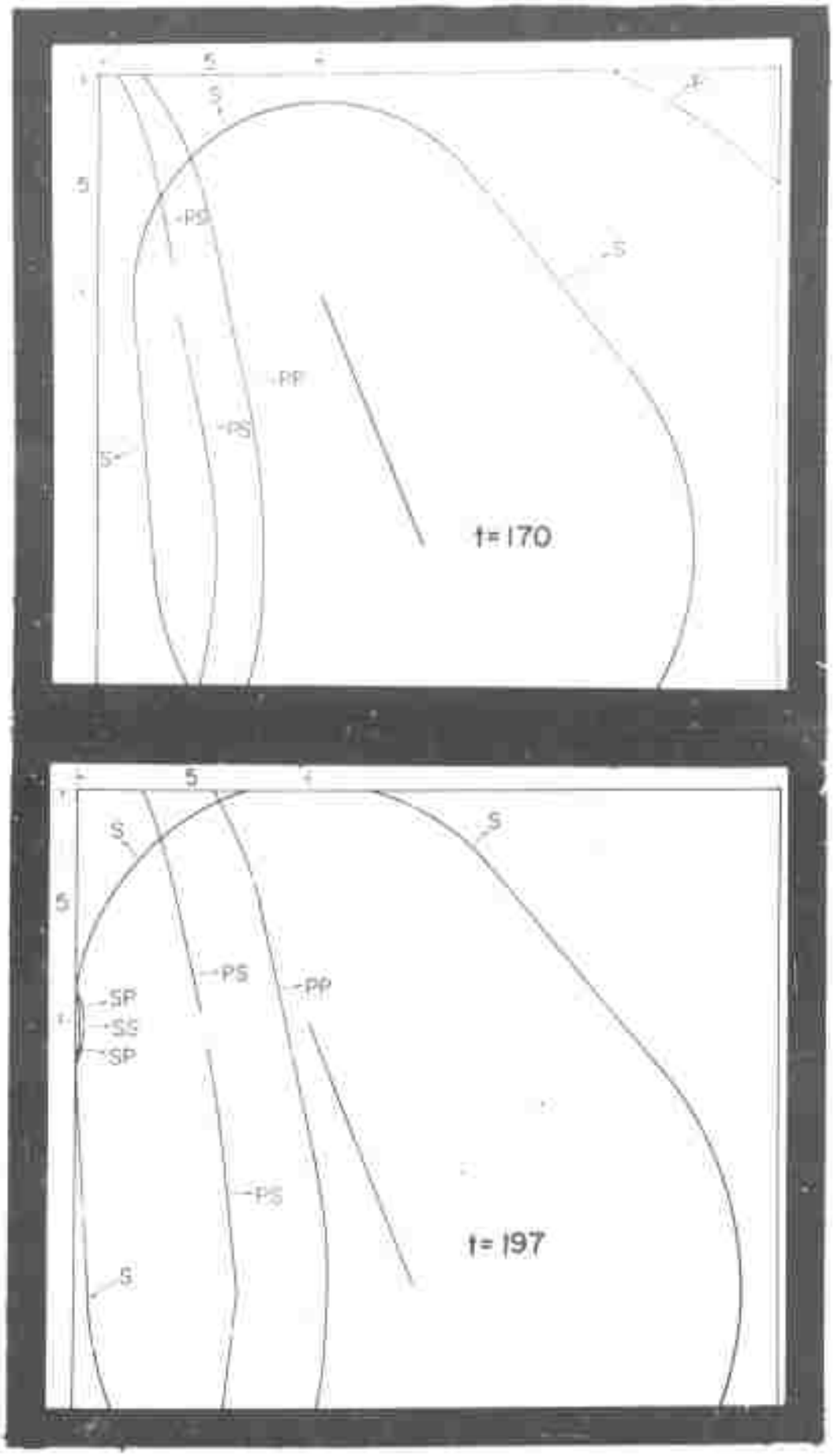

Fig. 3.9 Wave Front Diagrams for the Final Stage of Interaction and the Initiation of the S Wave Reflection

Fig. 4.1 A Typical Fringe Pattern Representing the P Wave During the Incident Phase of the Dynamic Event

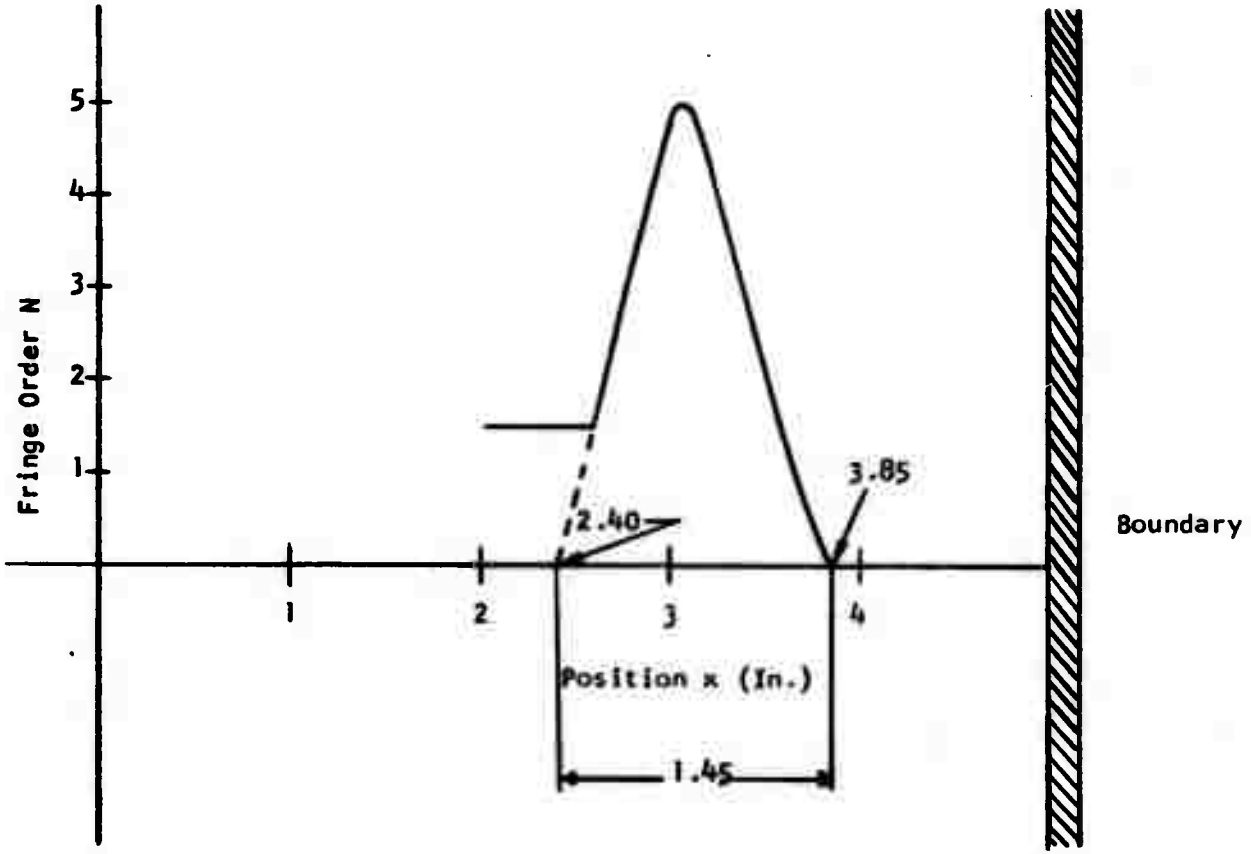

Fig. 4.2 Fringe Order - Position Profile Showing Wave Length

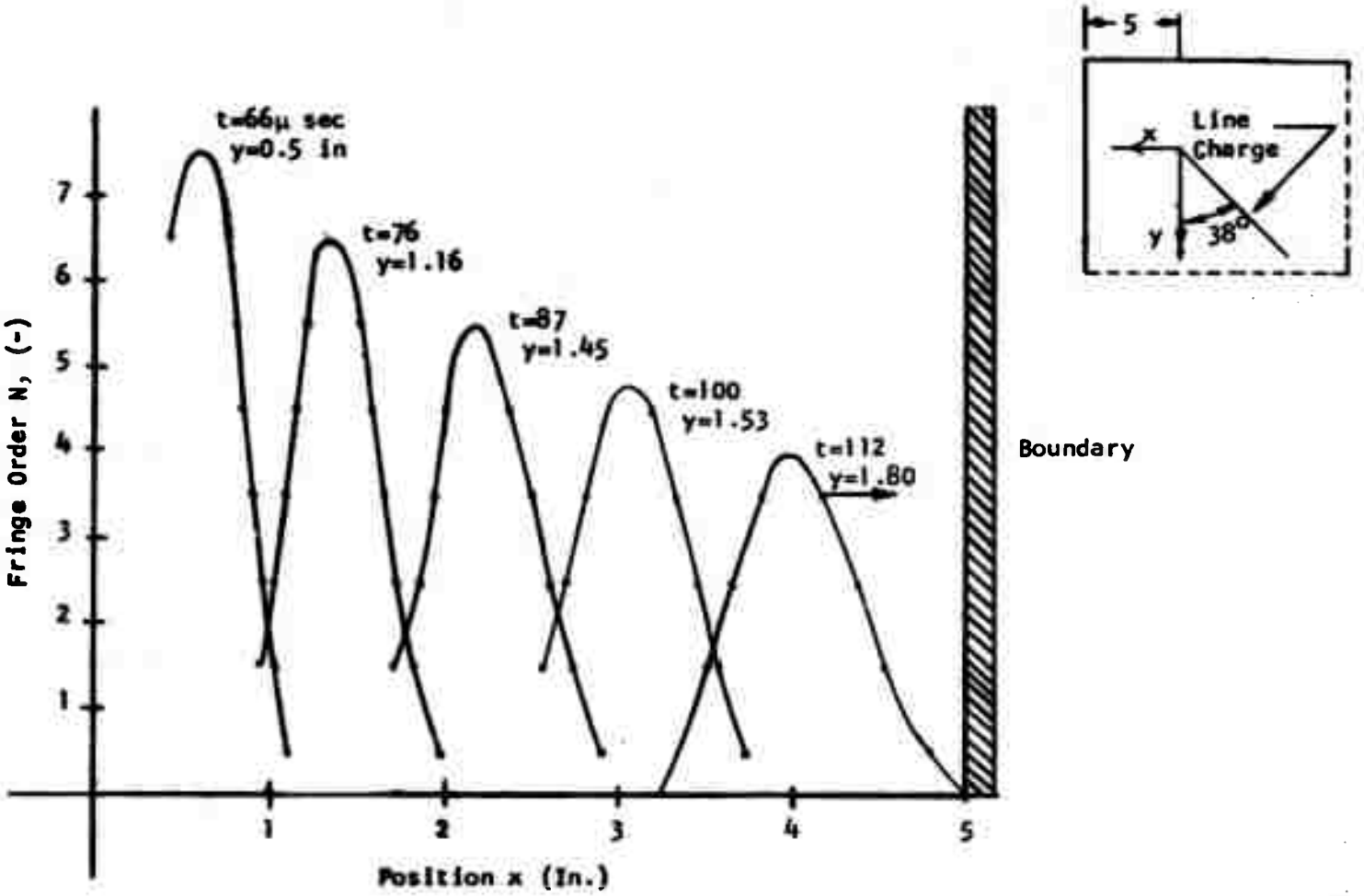

Fig. 4.3 Fringe Order as a Function of Position for the Incident P Wave

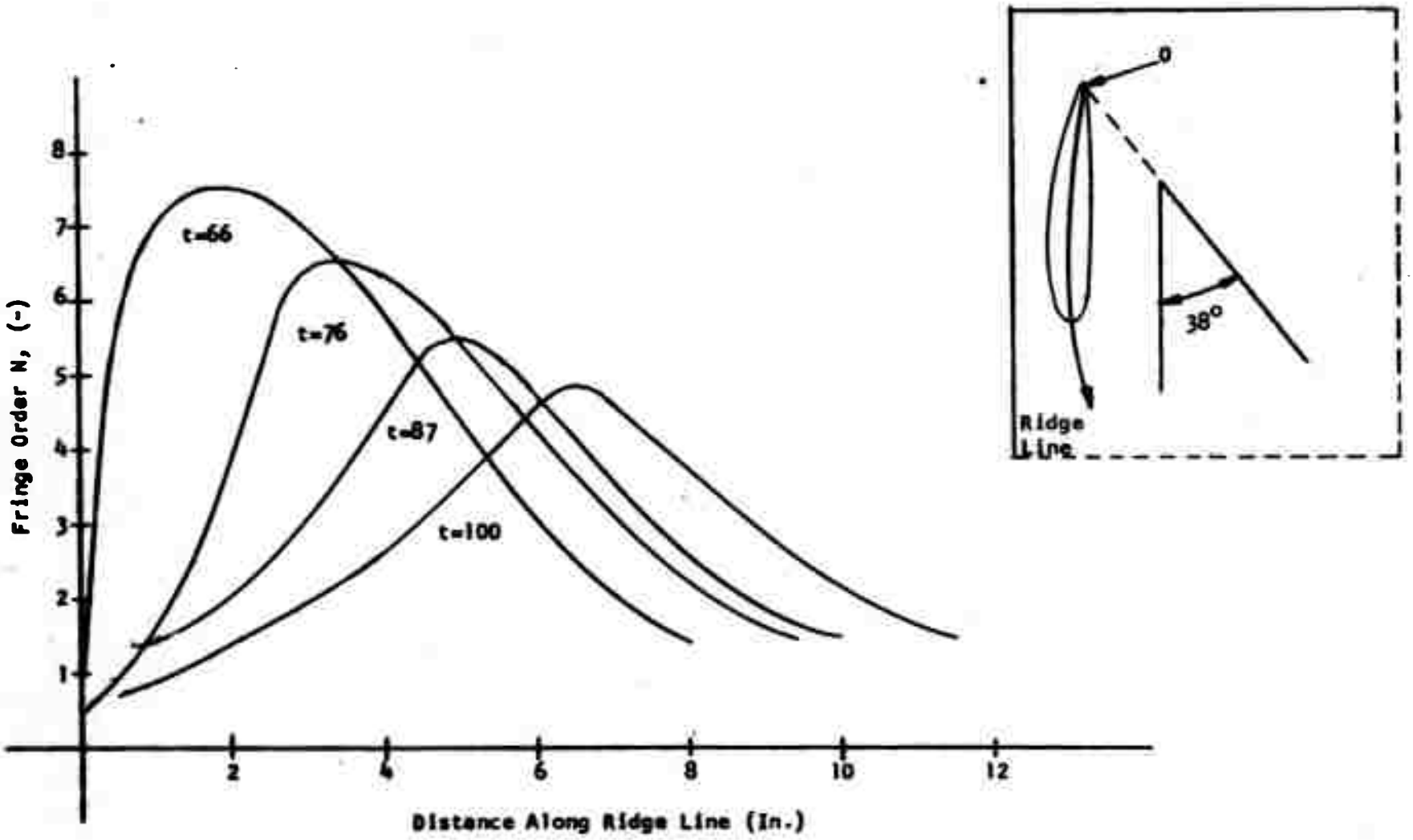

Fig. 4.4 Fringe Order as a Function of Position Along the Ridge Line of the P Wave

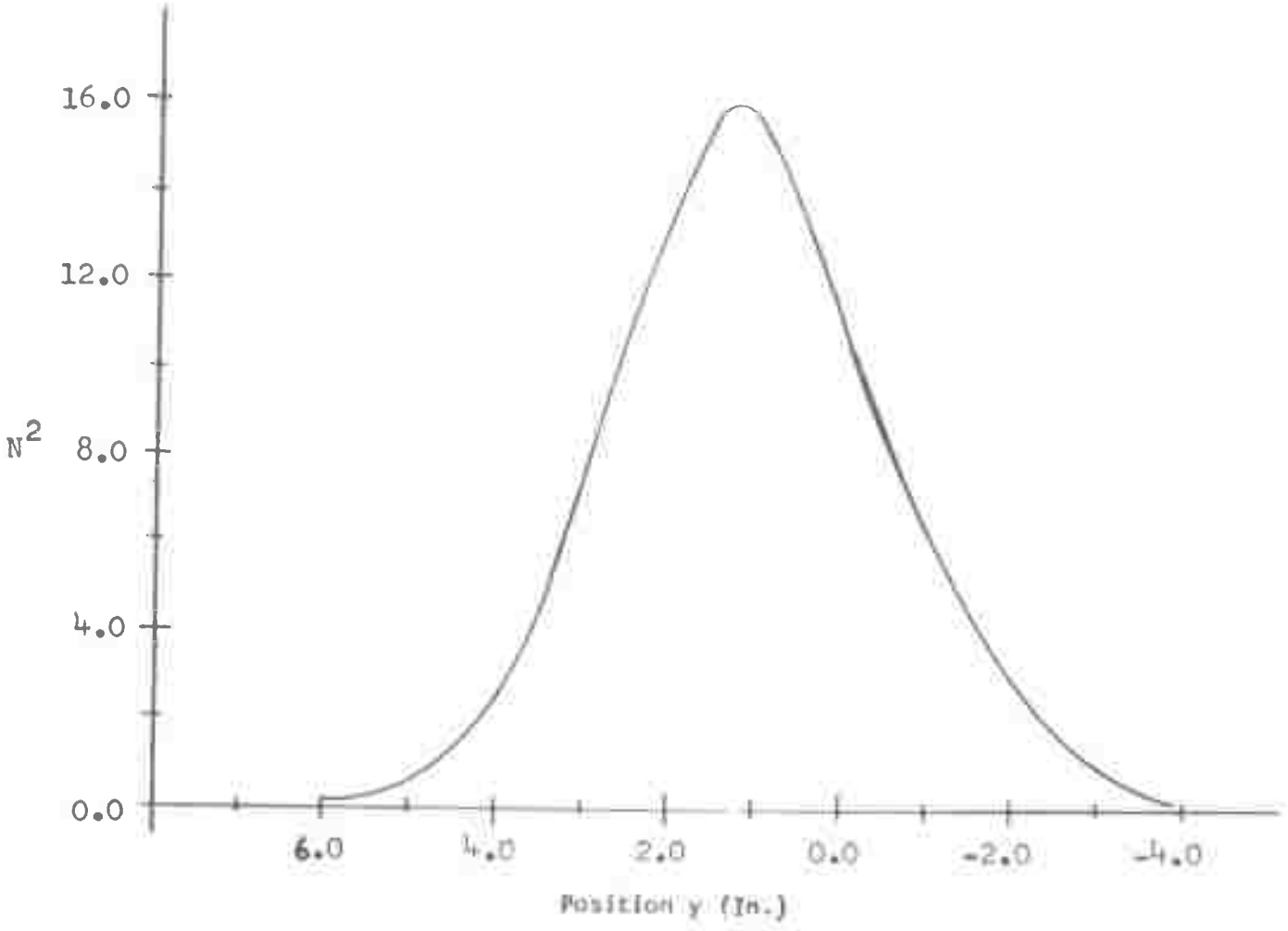

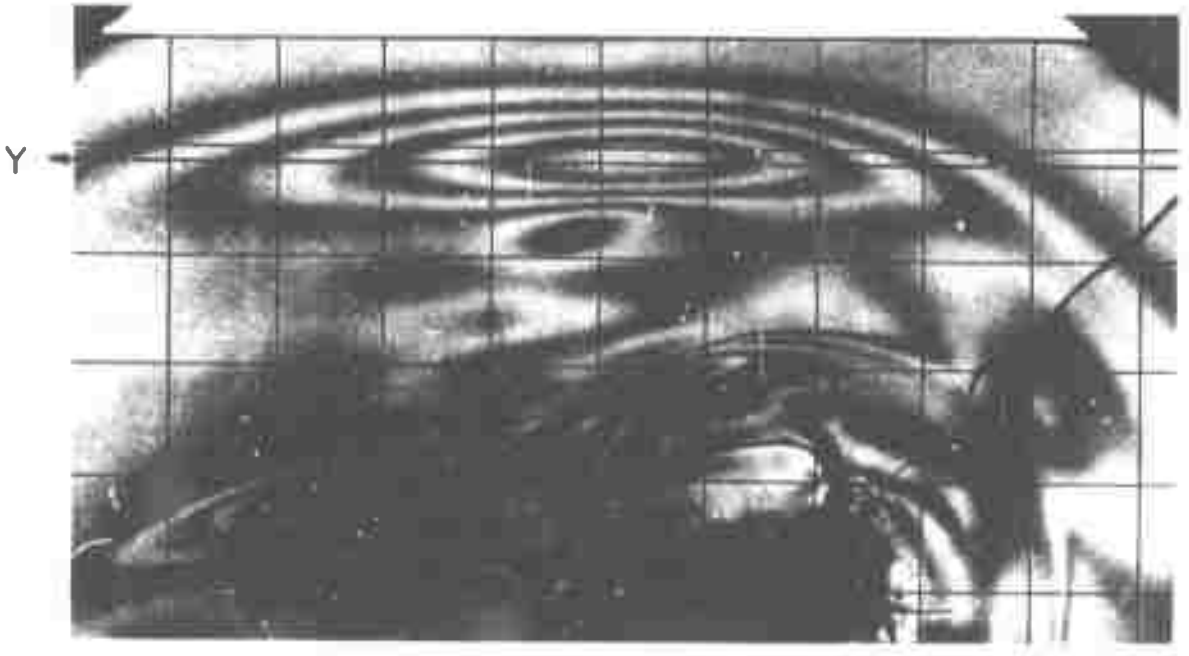

Fig. 4.5 Peak Energy Distribution as a Function of Position in the Incident P Wave.

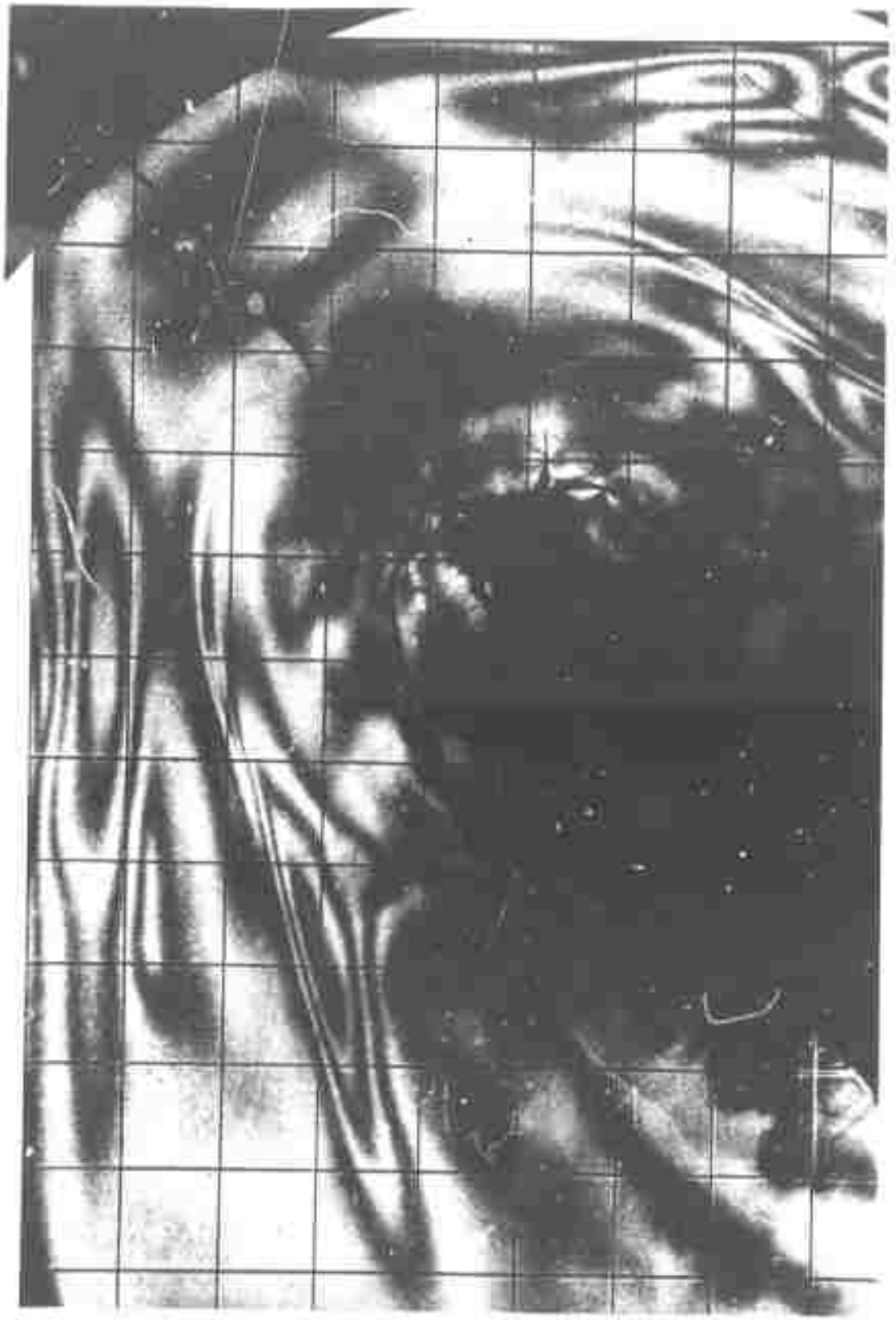

Fig 4.6 Fringe pattern showing the incident S wave prior to interaction with the reflected PP and PS waves

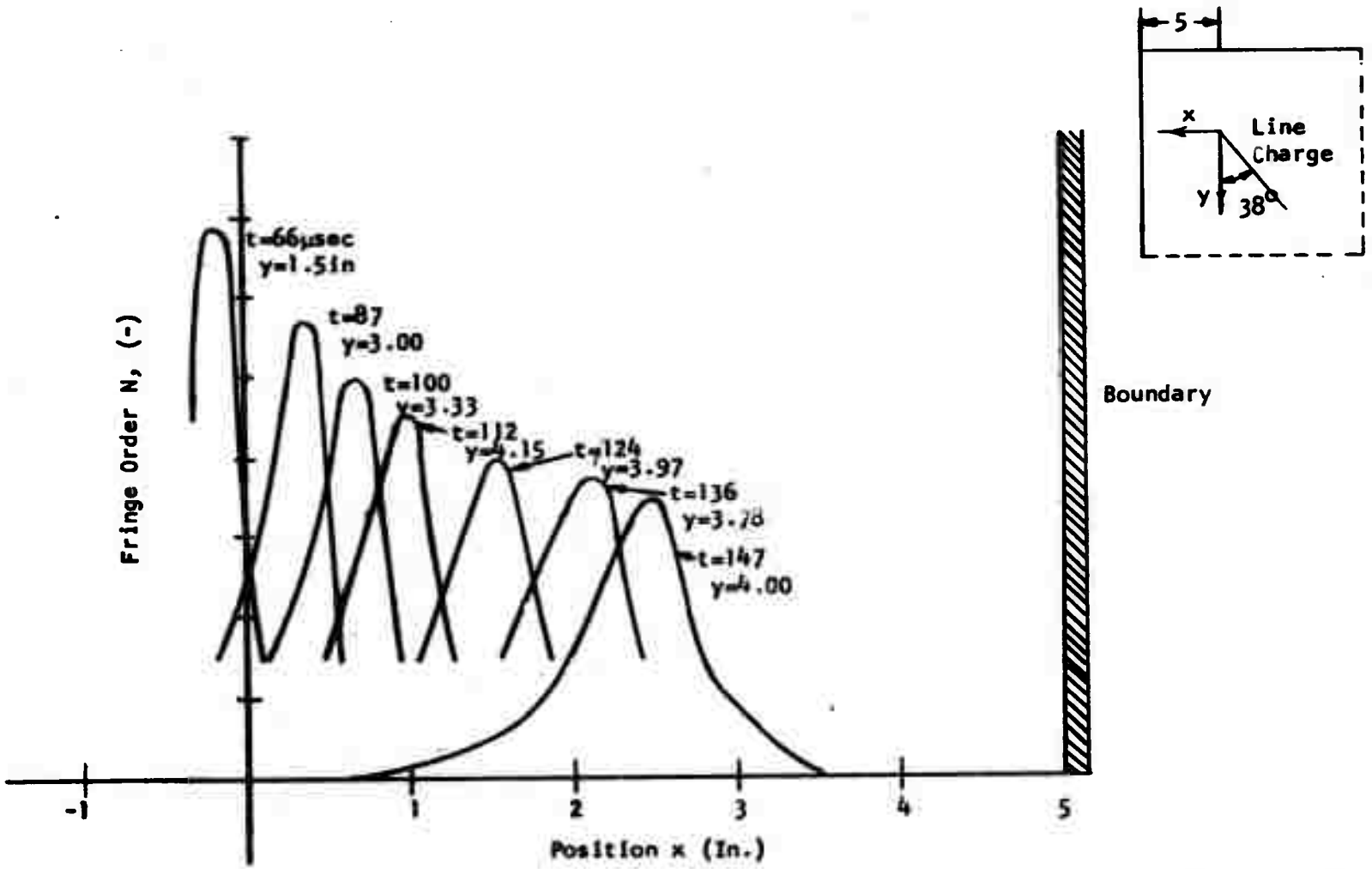

Fig. 4.7 Fringe Order as a Function of Position for the Incident S Wave

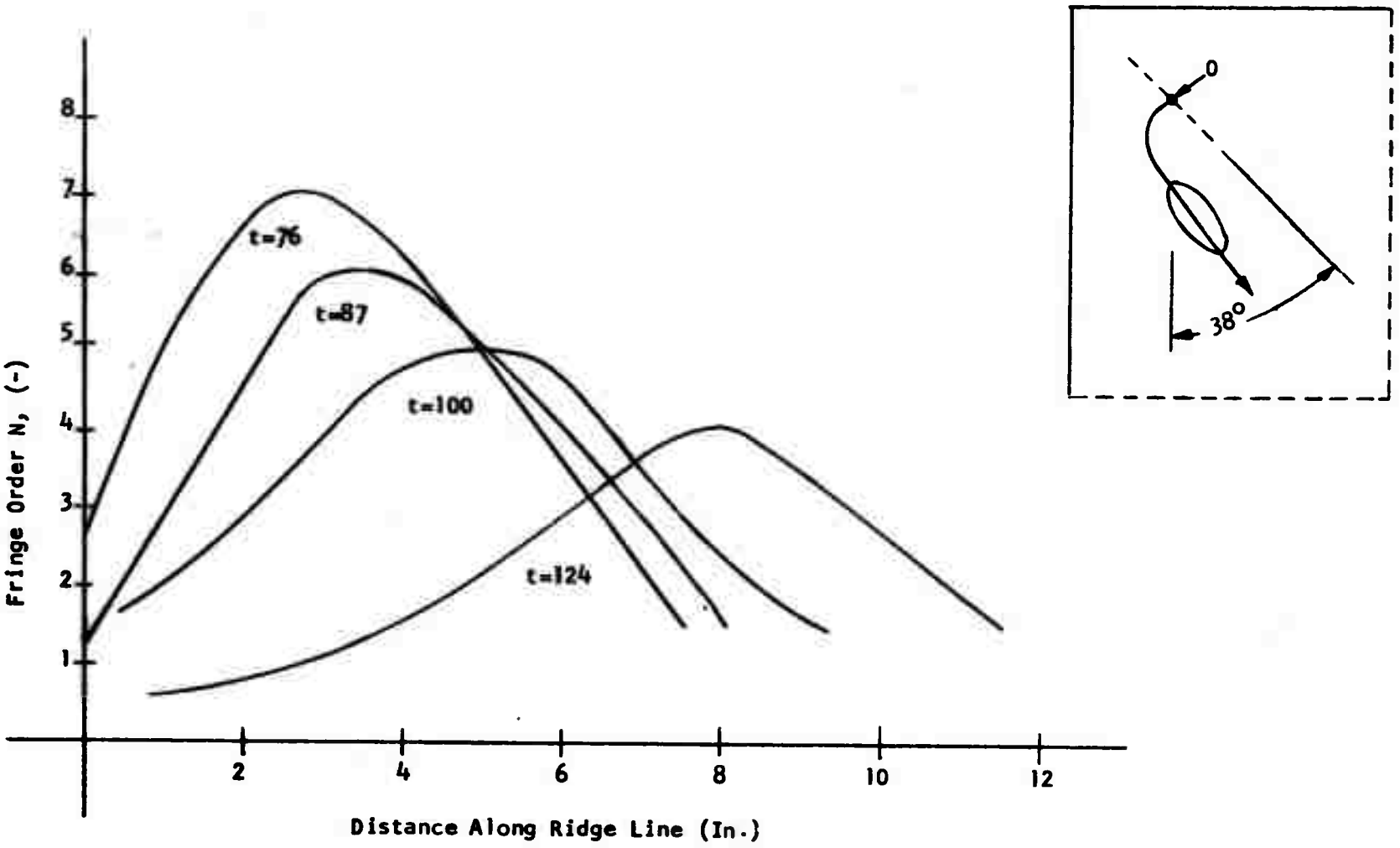

Fig. 4.8 Fringe Order as a Function of Position along the Ridge Line of the S Wave

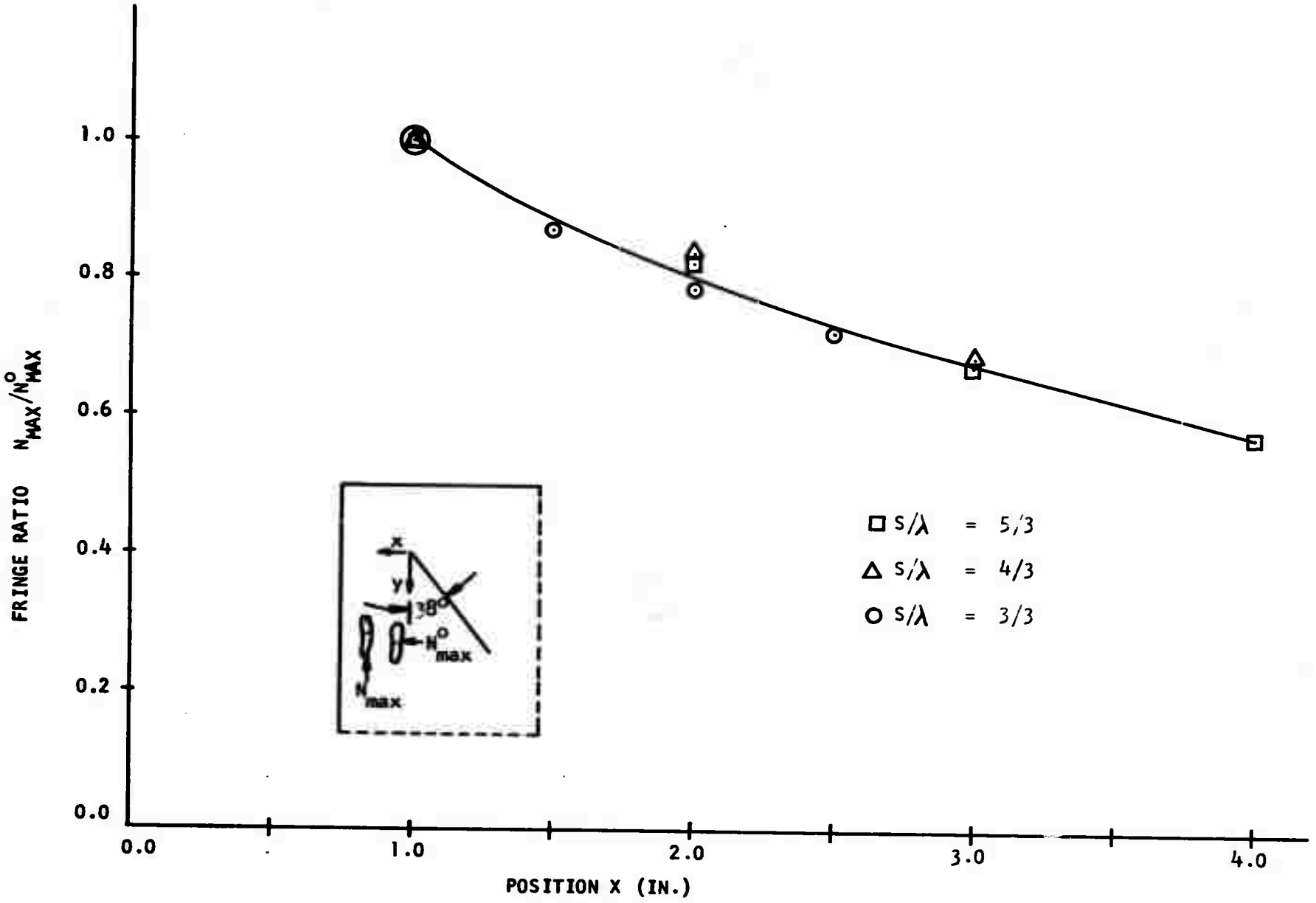

Fig. 4.9 Normalized Fringe Order as a Function of Position Showing the Attenuation of the P Wave

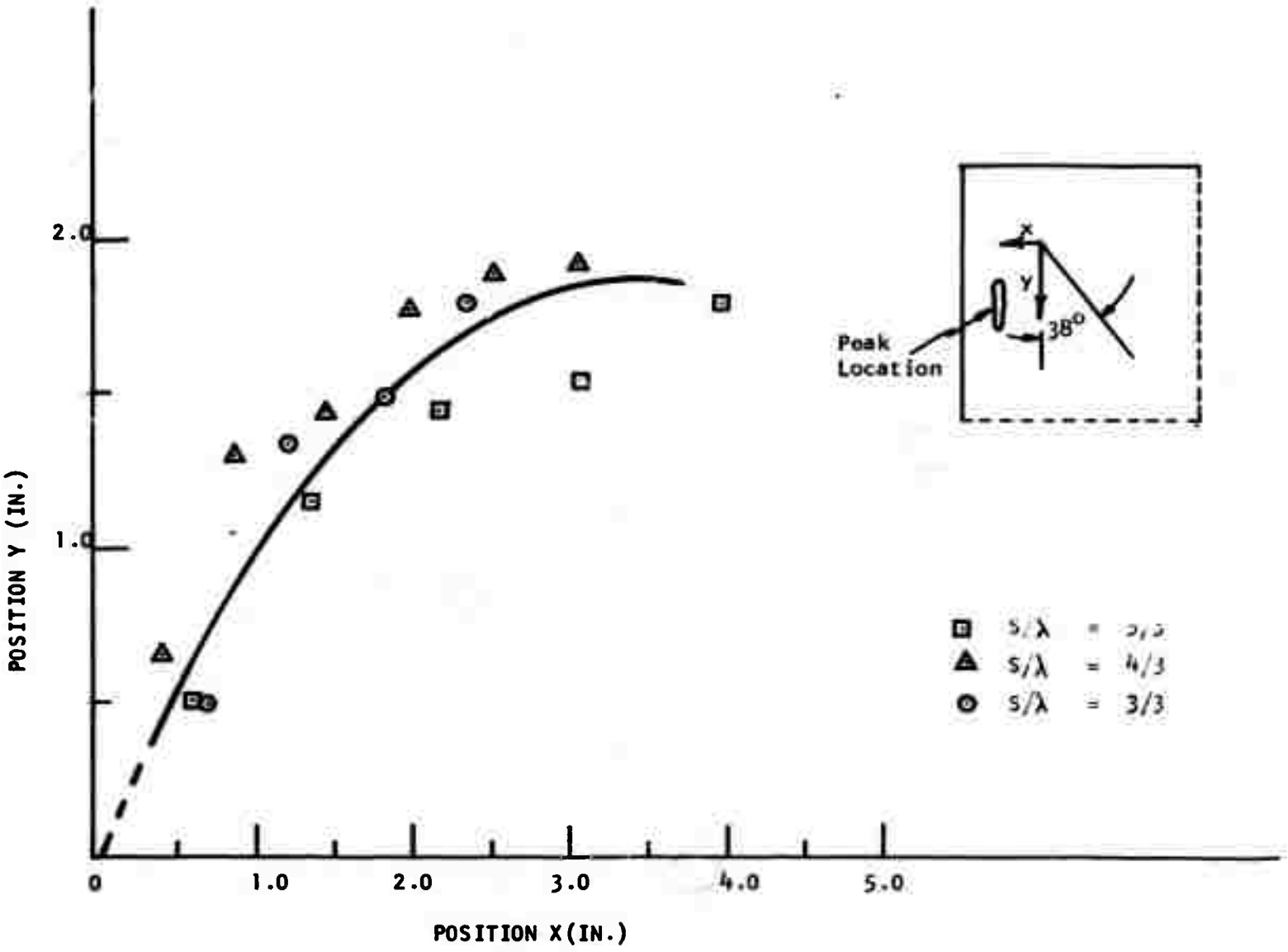

Fig. 4.10 Position of N_{MAX} in Incident P Wave

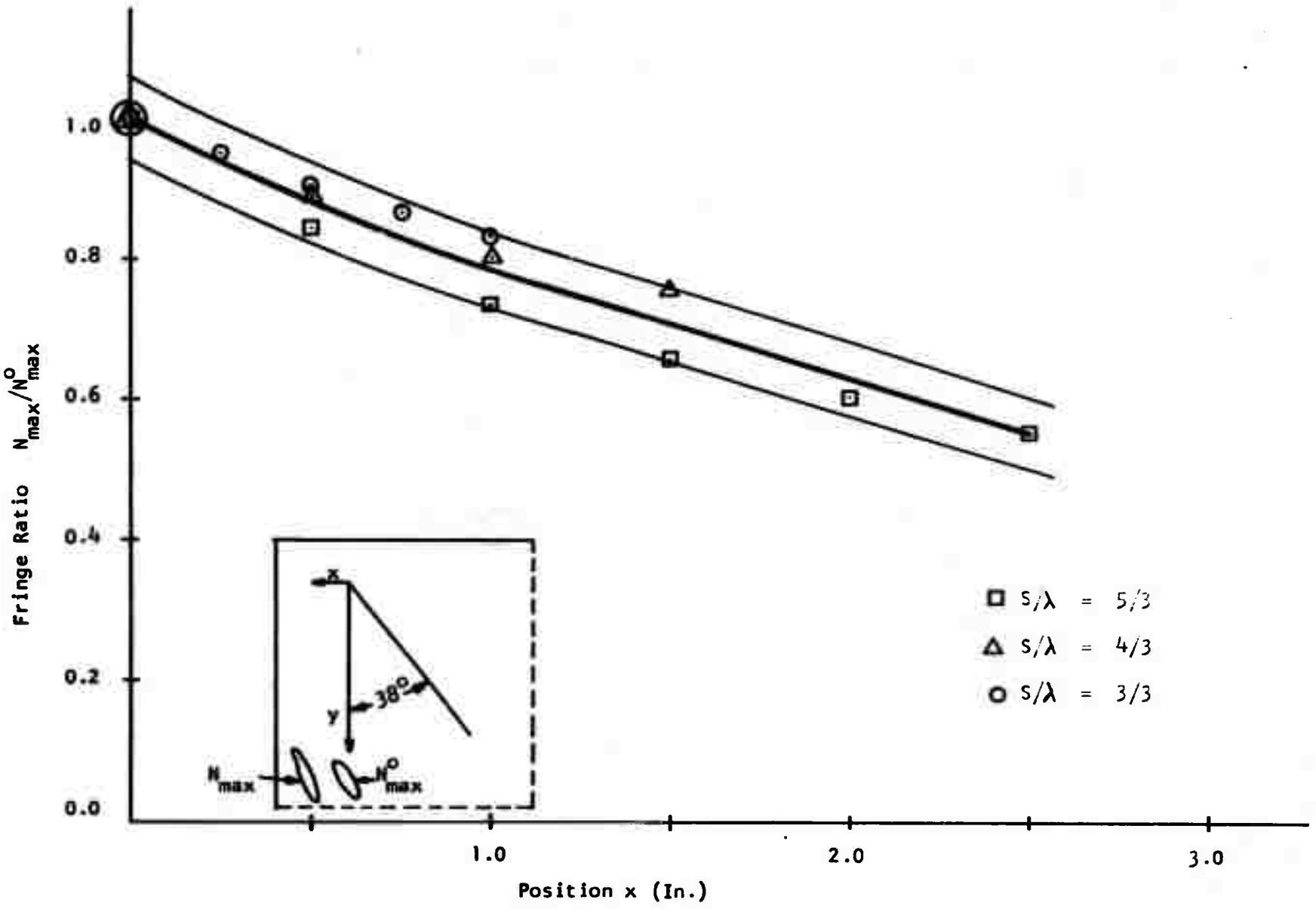

Fig. 4.11 Normalized Fringe Order as a Function of Position Showing Attenuation of the S Wave

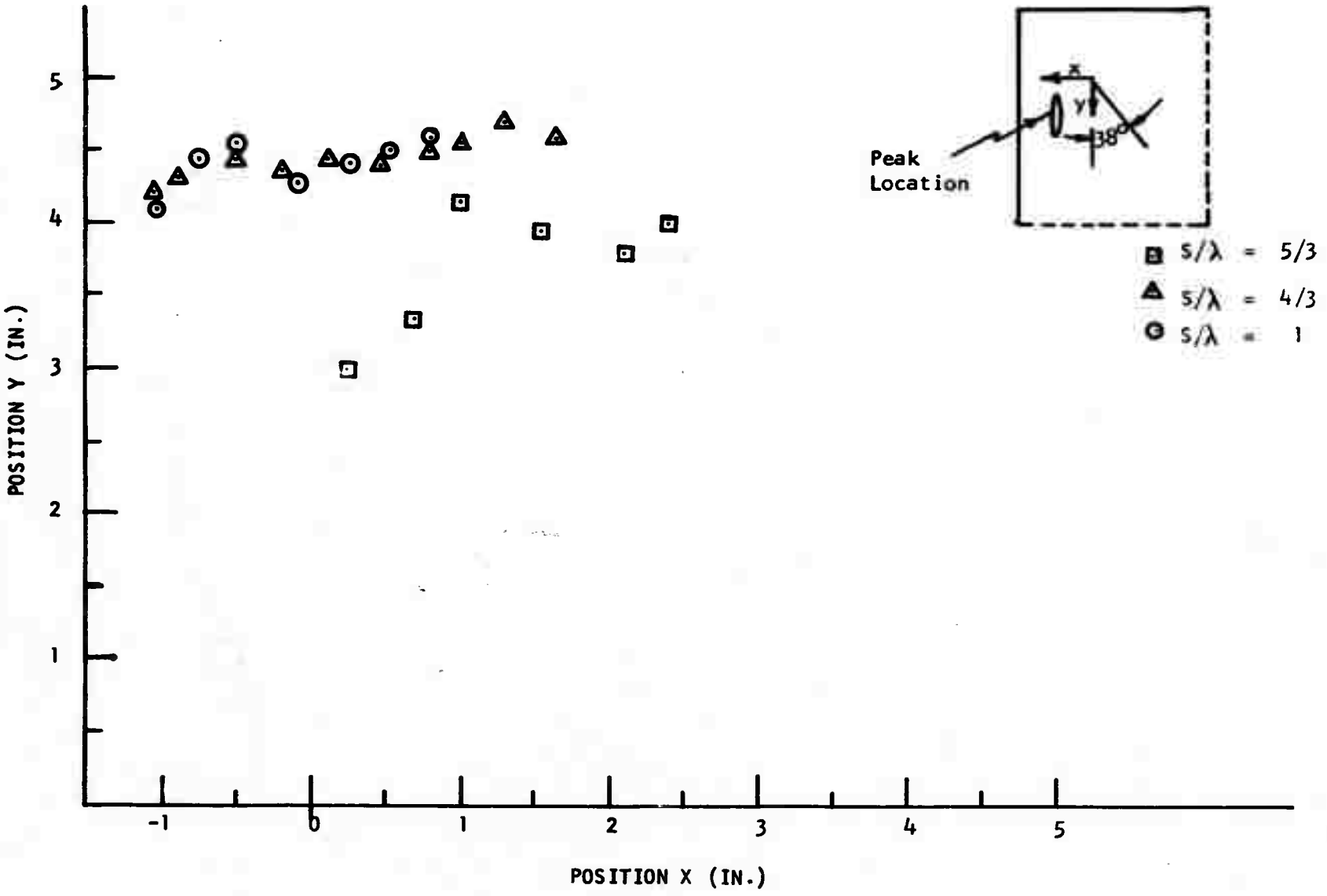

Fig. 4.12 Position of N_{max} in the Incident S Wave

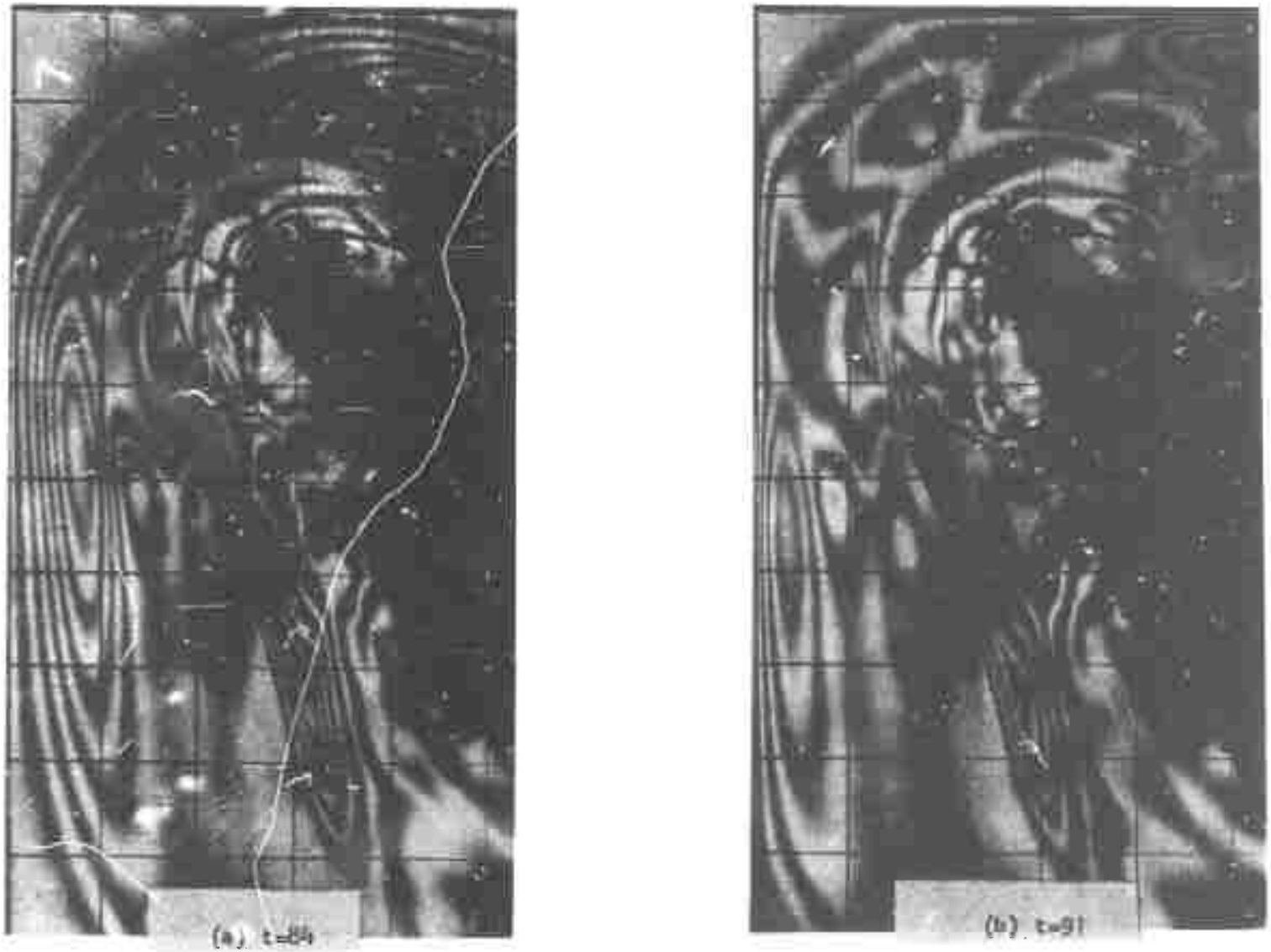

Fig. 4.13 Fringe Patterns Depicting Early Portion of Reflection Phase

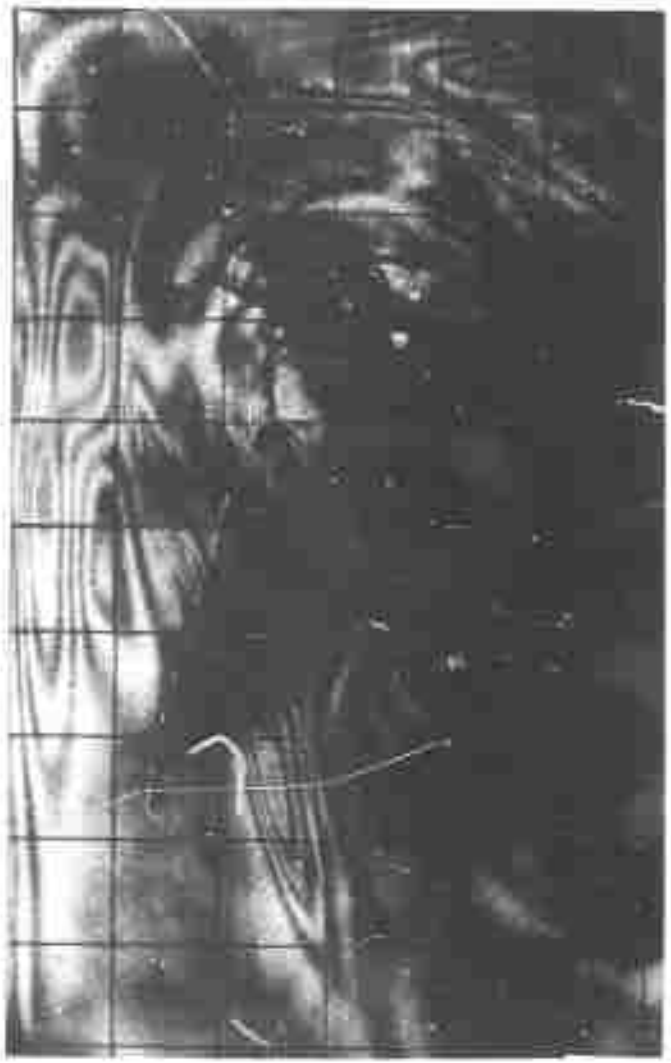

(a) t= 99

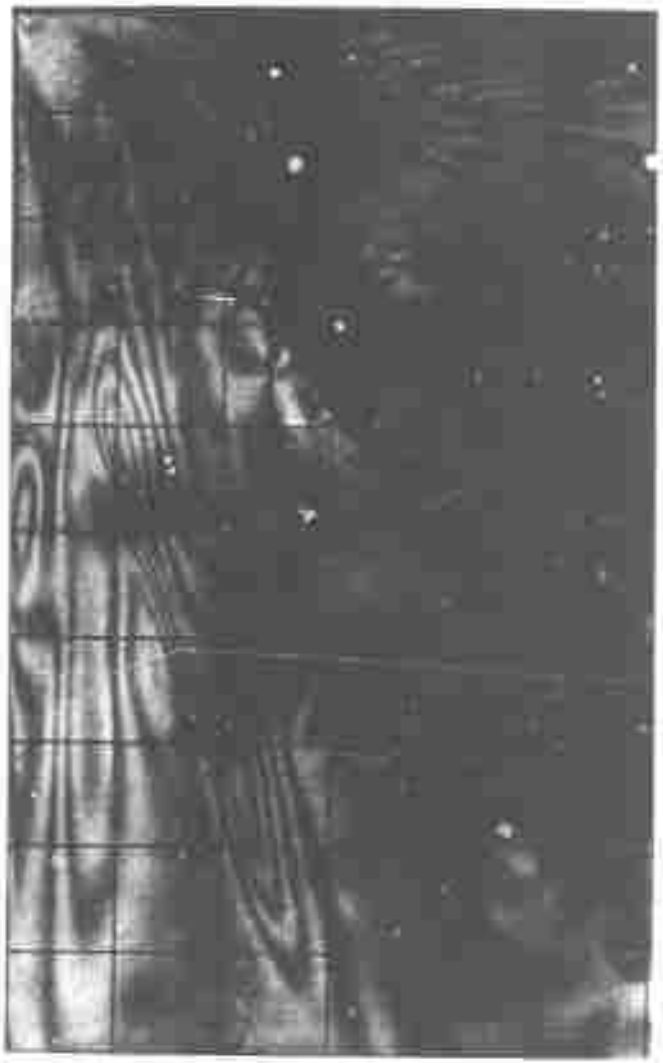

(b) t= 106

Fig. 4.14 Fringe Patterns Illustrating Late Portion of the Reflection Phase

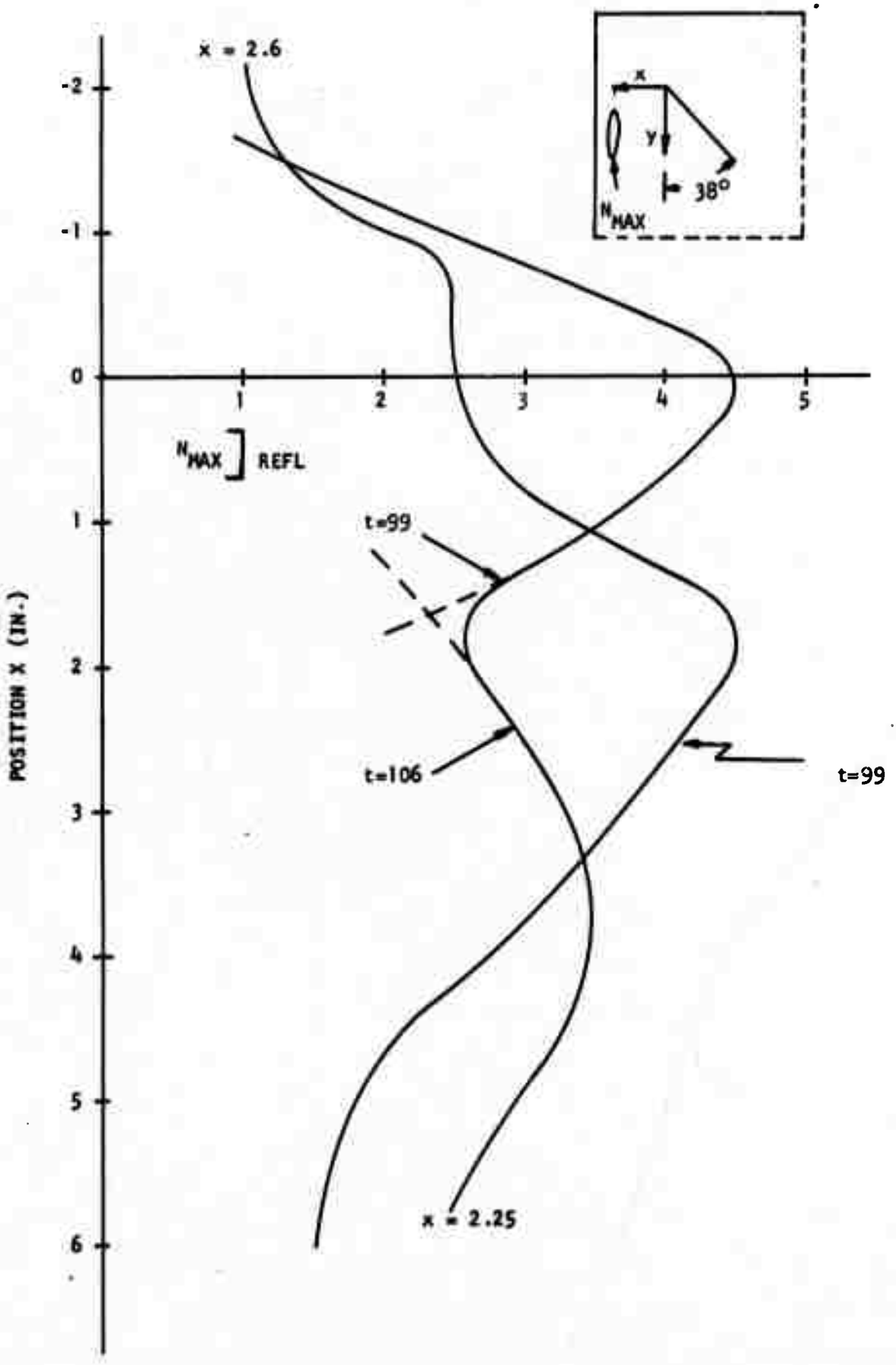

Fig. 4.15 Maximum Fringe Order Associated with Reflected PP and PS Waves

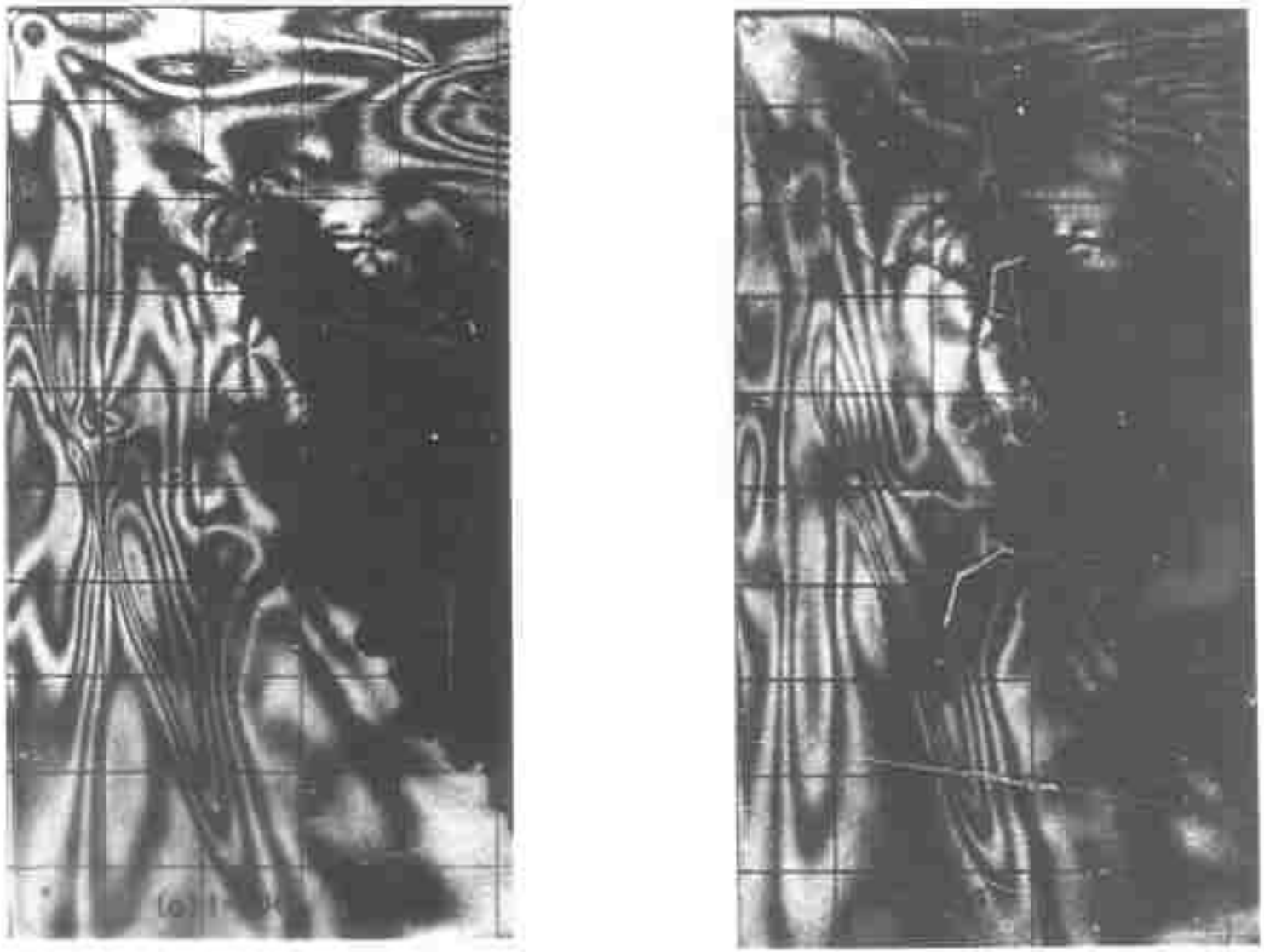

Fig. 4.16 Fringe Patterns Showing the Features of Interaction of the Reflected PP and PS Waves with the Incident S Waves

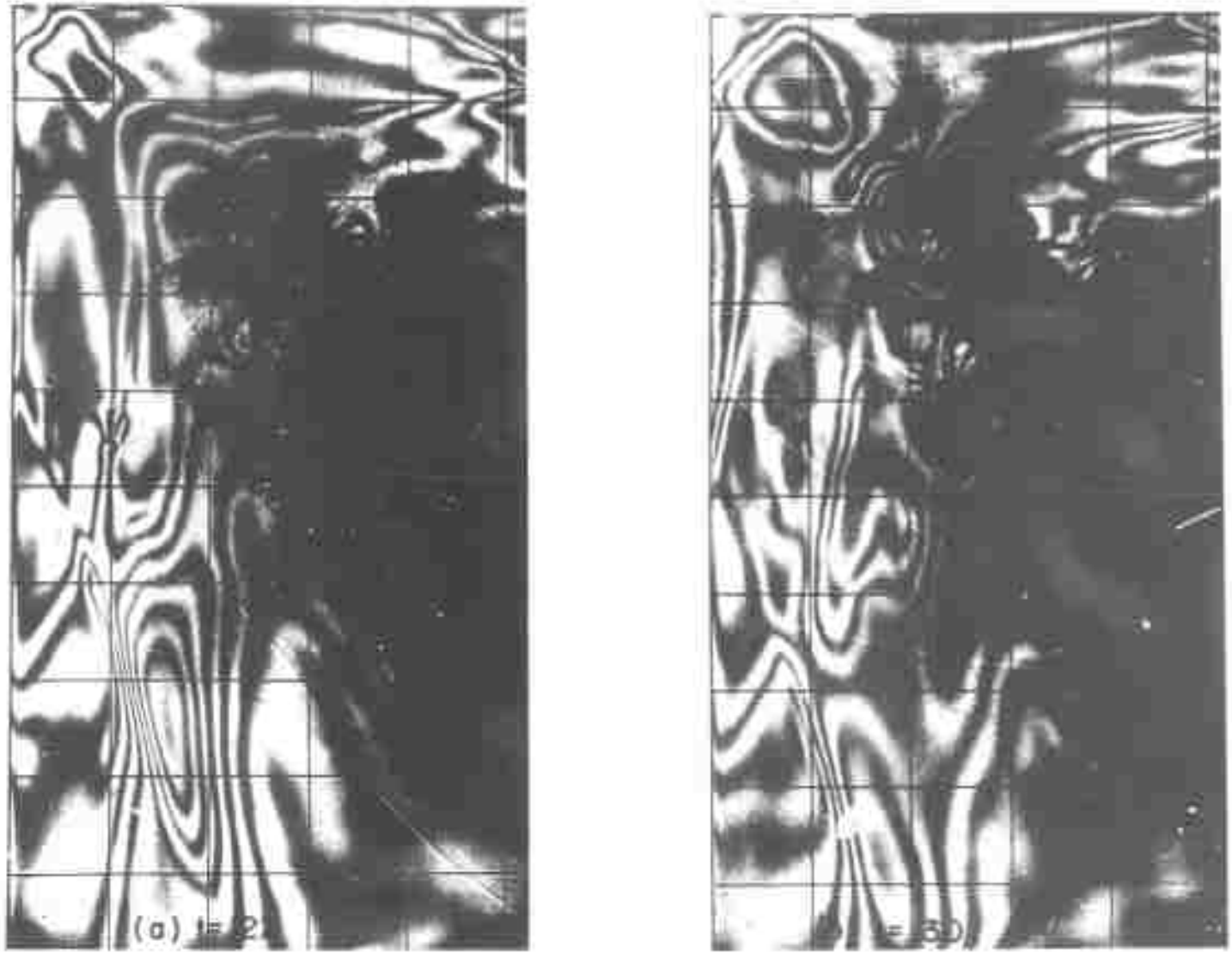

Fig. 4.17 Fringe Patterns Showing the Final Stage of the Interaction Process

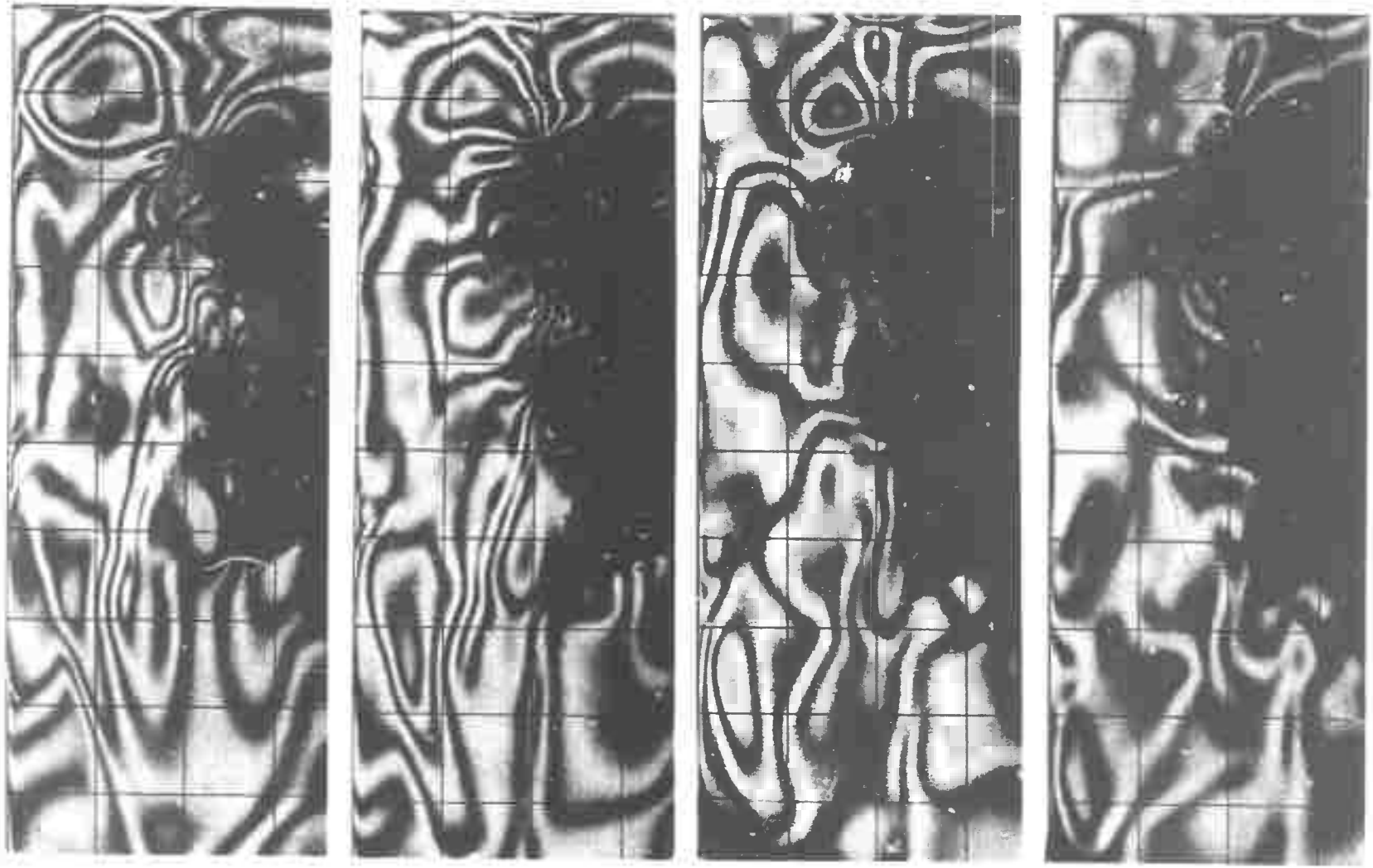

Fig. 4.18 Fringe Patterns Showing Reflection of S Wave from Lower Portion of the Vertical Boundary

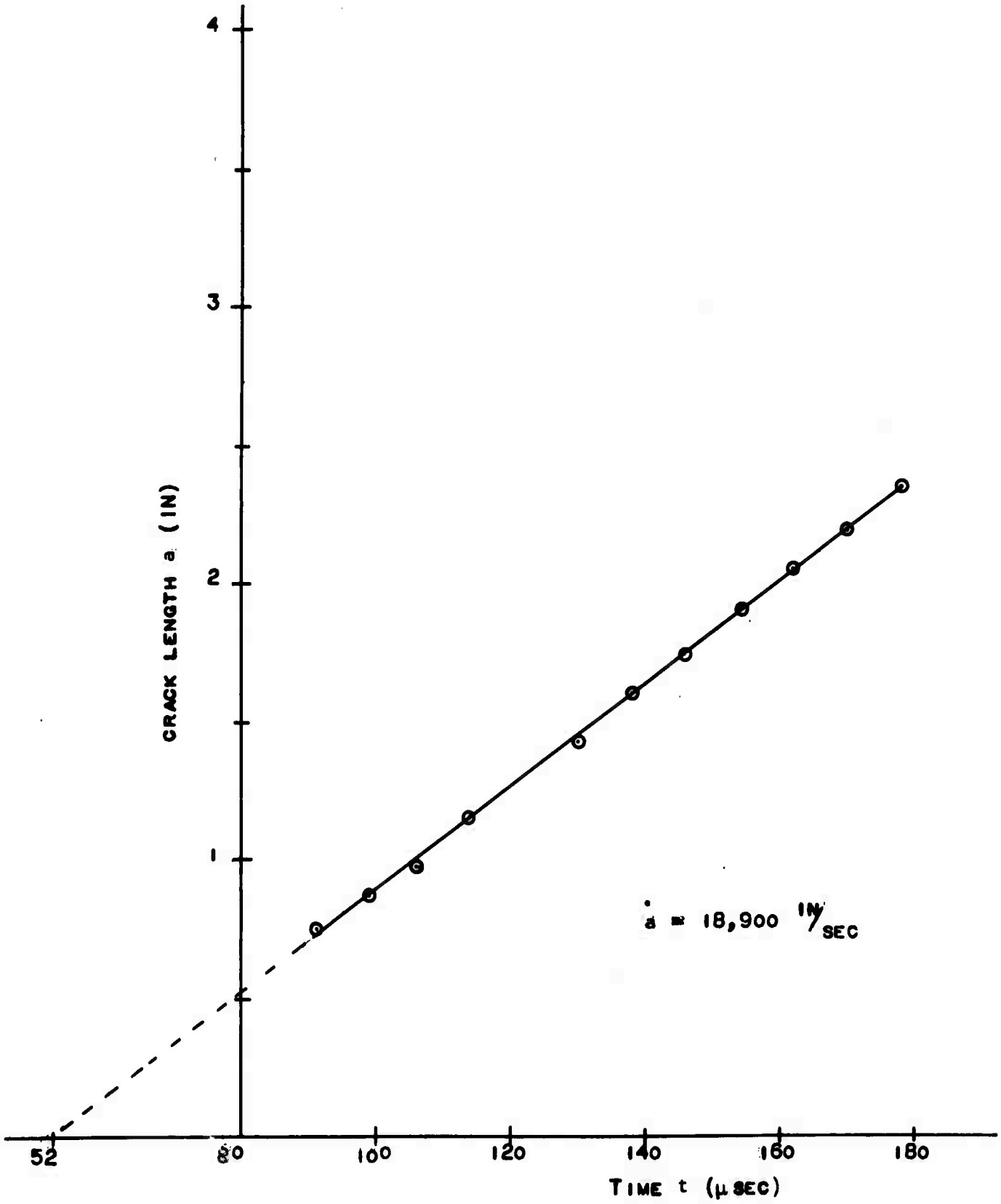

Fig. 4.19 Crack Length as a Function of Time

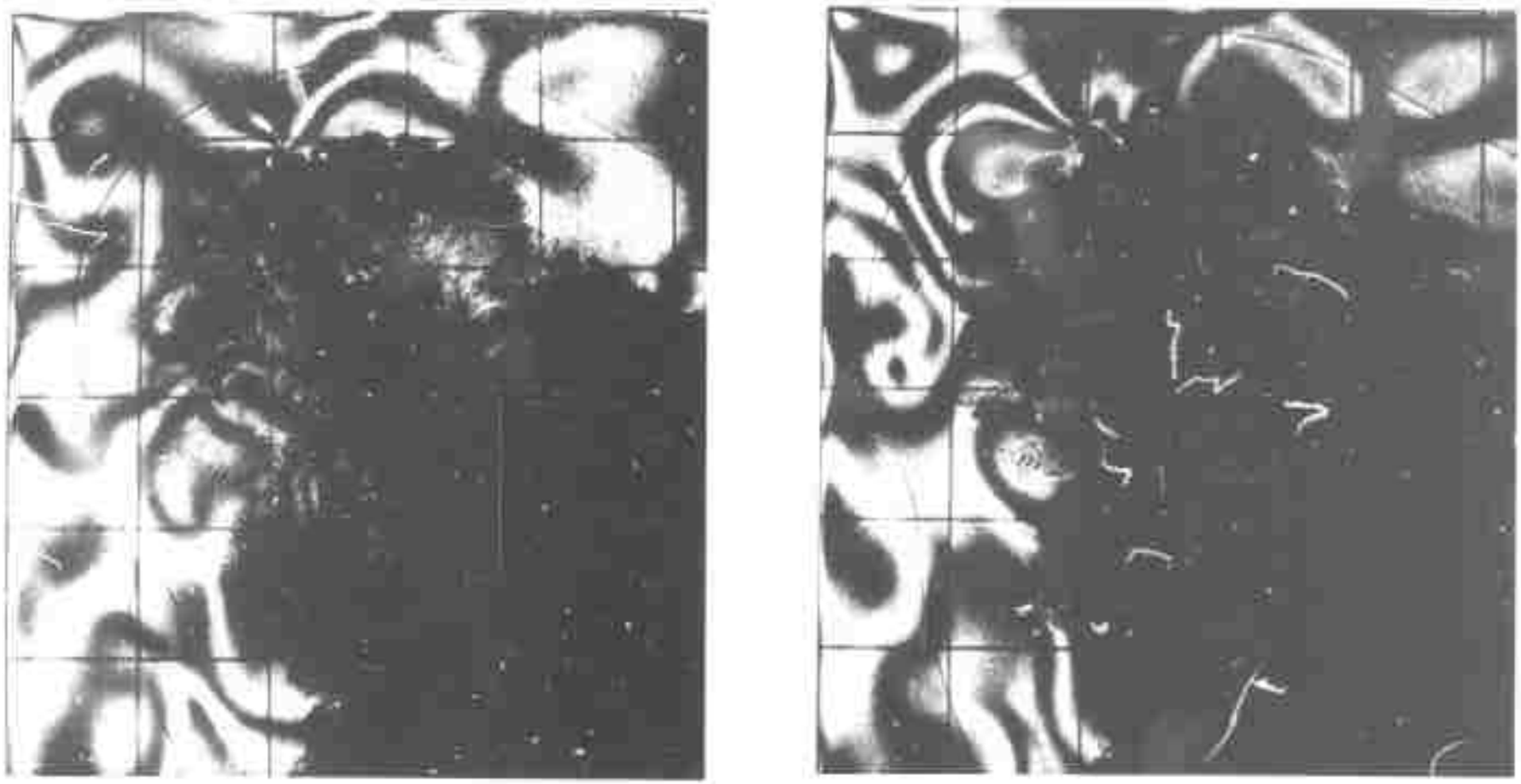

(a) t=170

(b) t=178

Fig. 4.20 Crack Propagation in Low Order Fringe (Stress) Fields

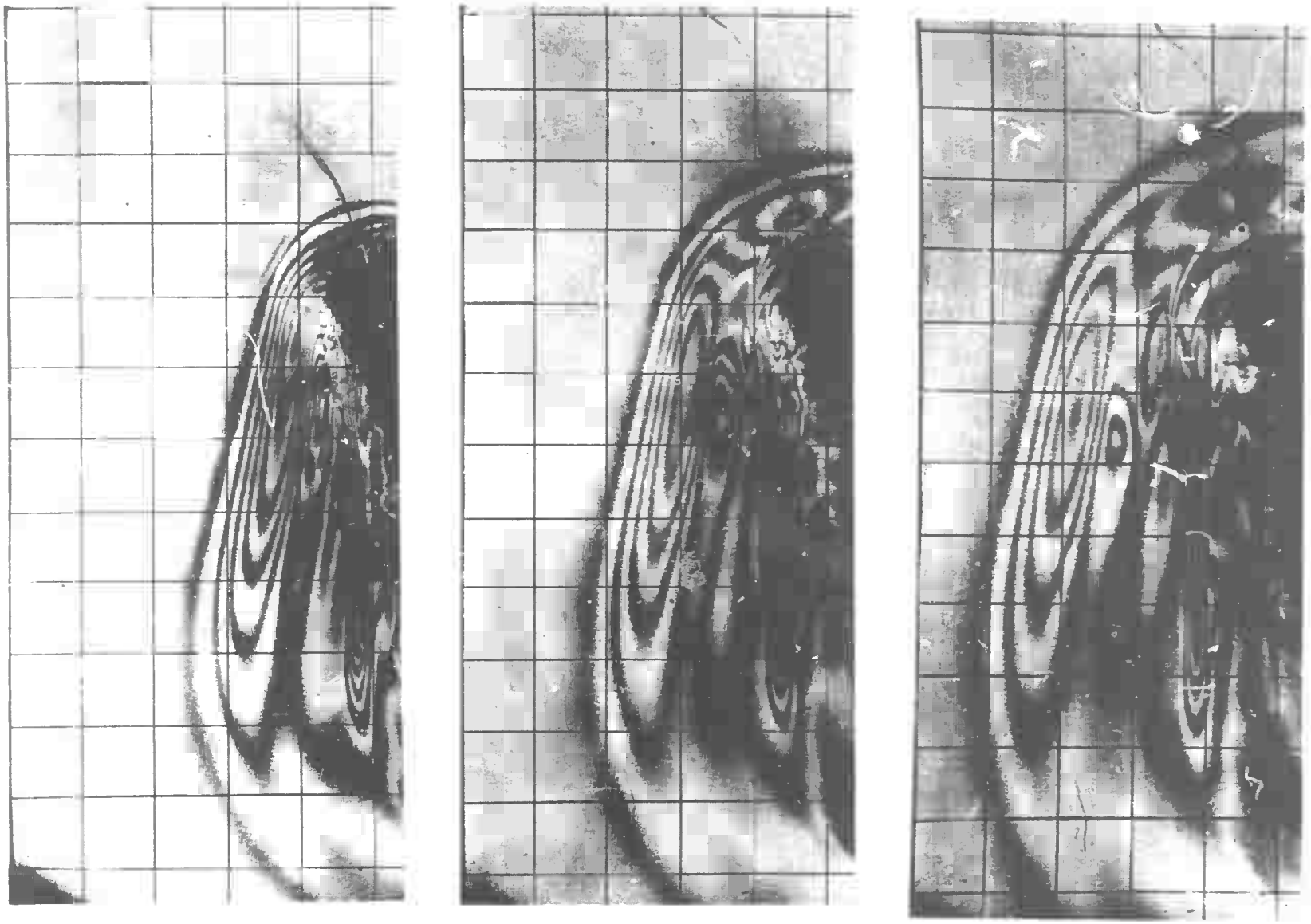

(a) t=67 (b) t=77 (c) t=87

Fig. 4.21 Incident P Wave Propagation - S Wave Model ω = 22 degrees.

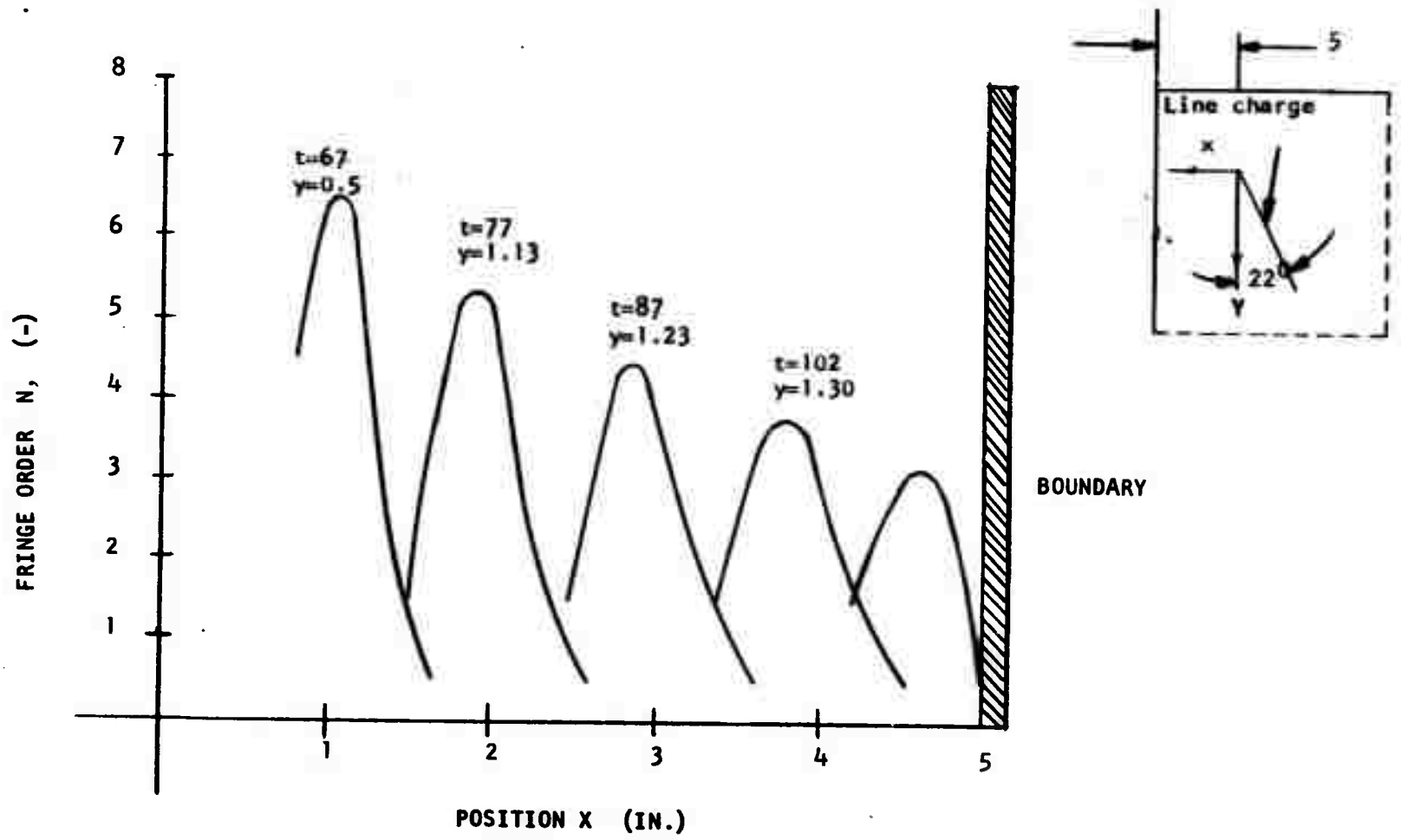

Fig. 4.22 Fringe Order - Position Profiles for P Wave Propagation in the S Wave 22 Degree Model

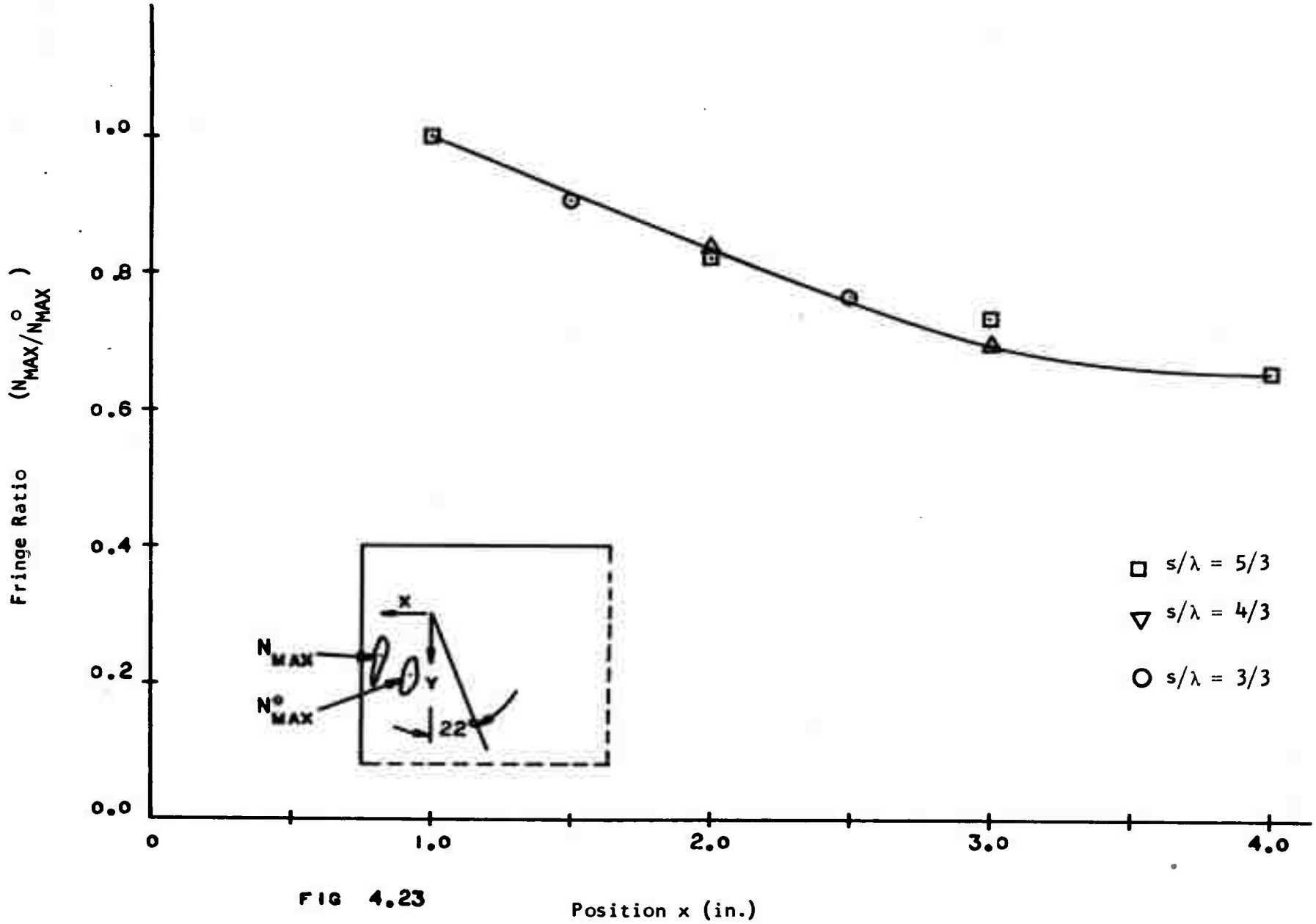

FIG 4.23

Fig. 4.23 Normalized Fringe Order as a Function of Position Showing the Attenuation of the P Wave

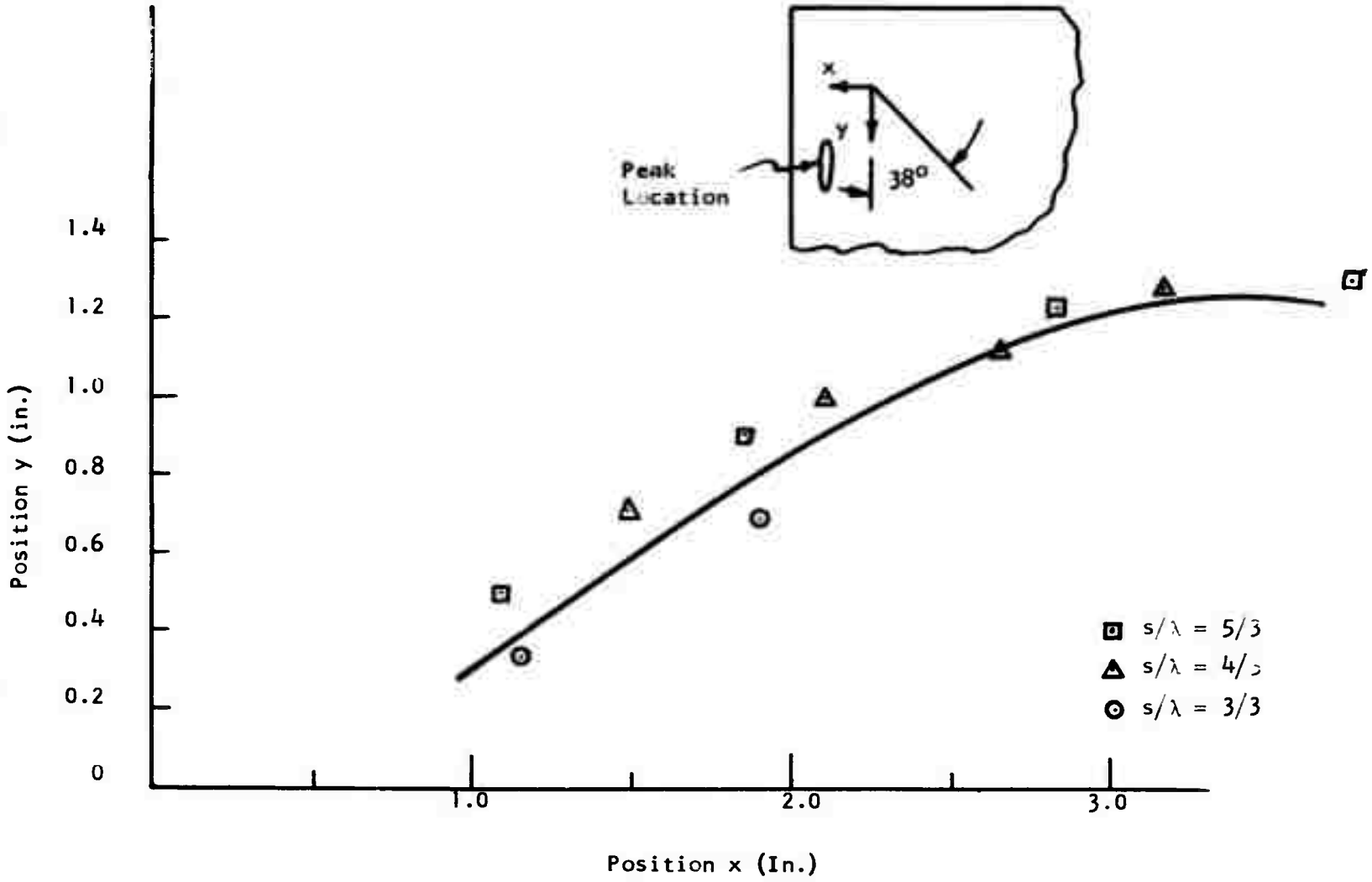

Fig. 4.24 Position of N_{MAX} Associated with the Incident P Wave

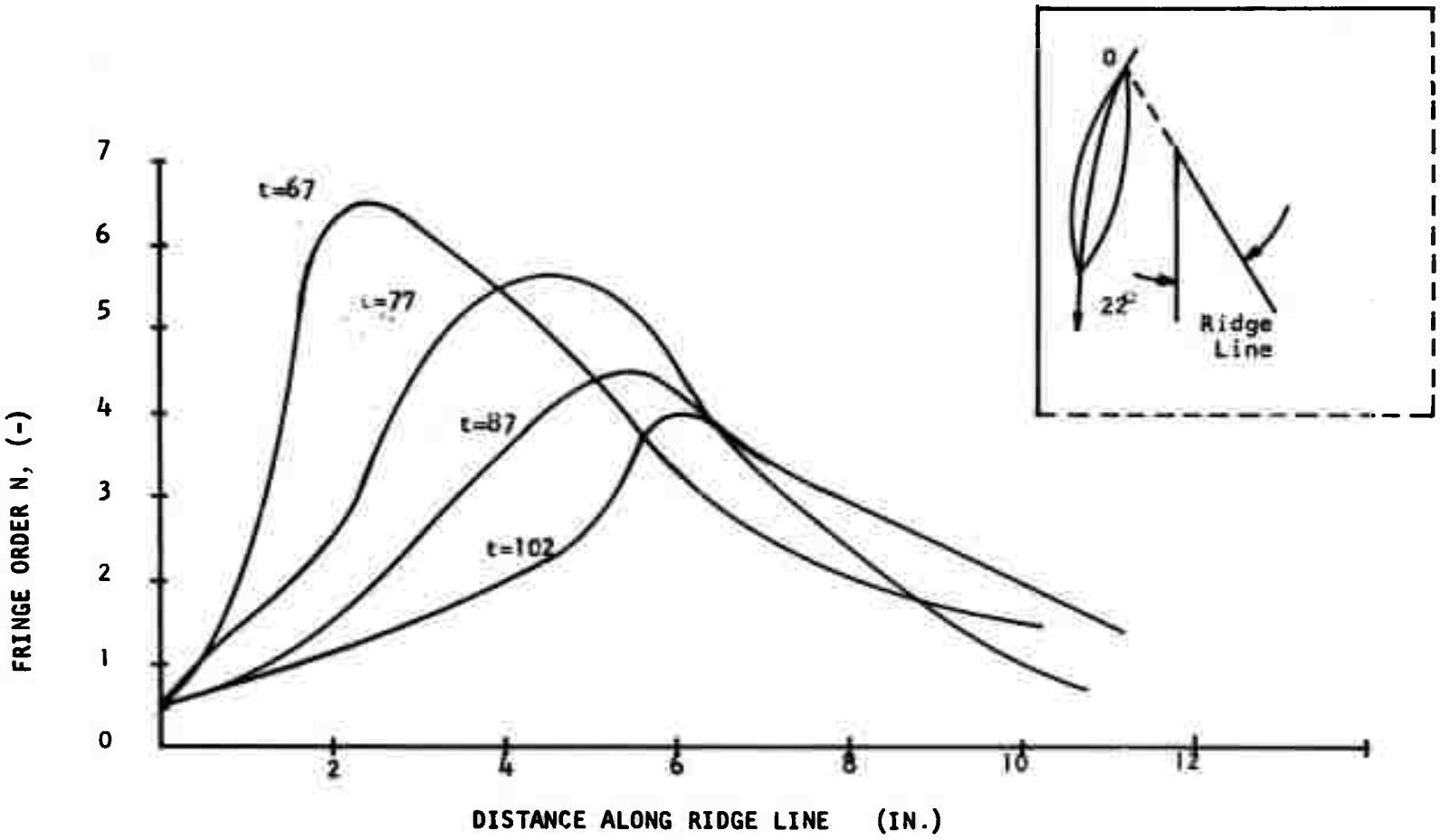

Fig. 4.25 Fringe Order as a Function of Position along the Ridge Line of the P Wave

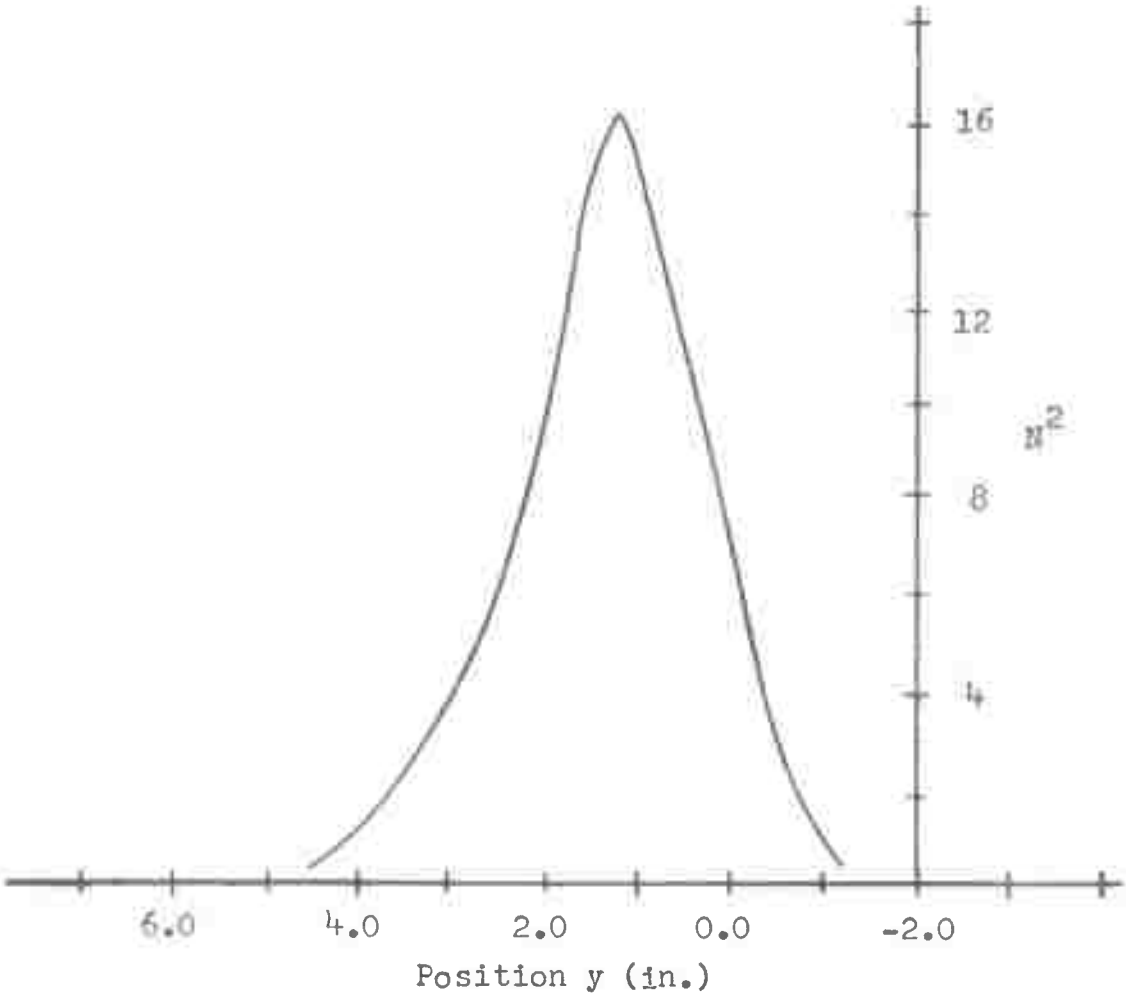

Fig. 4.26 Energy Distr.bution as a Function of Position for the Incident P Wave

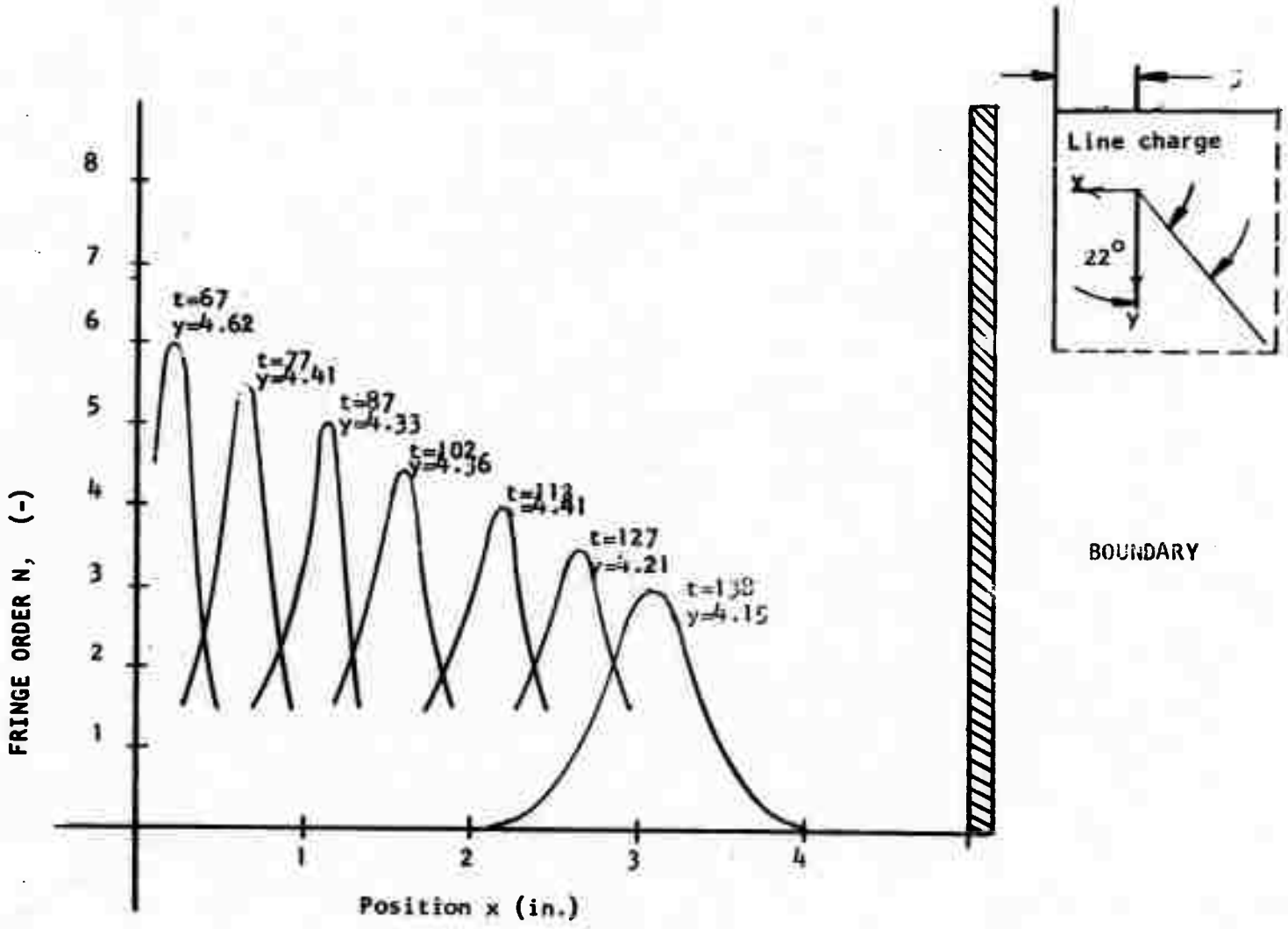

Fig. 4.27 Fringe Order as a Function of Position for the Incident S Wave

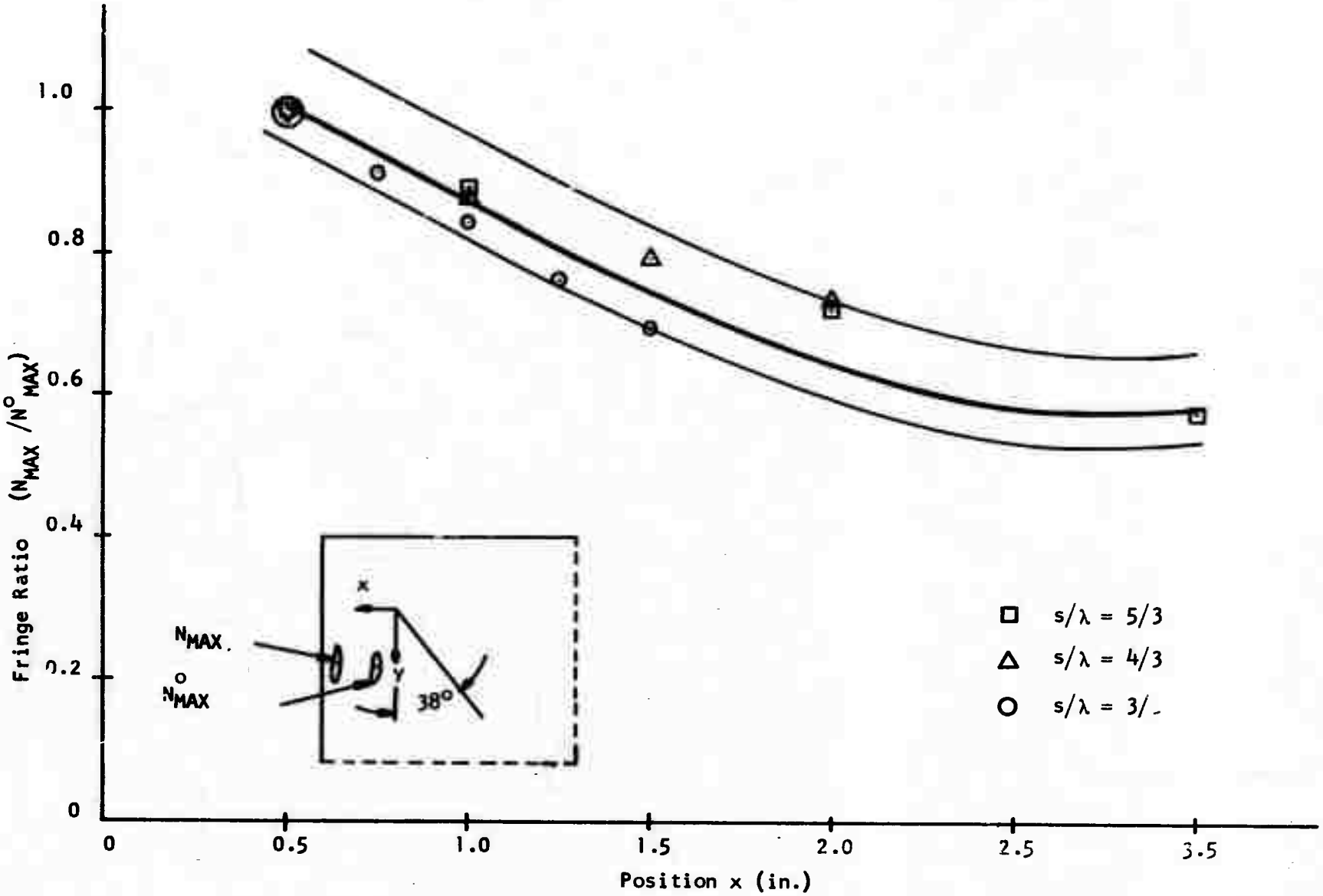

Fig. 4.28 Normalized Fringe Order as a Function of Position Showing the Attenuation of the S Wave

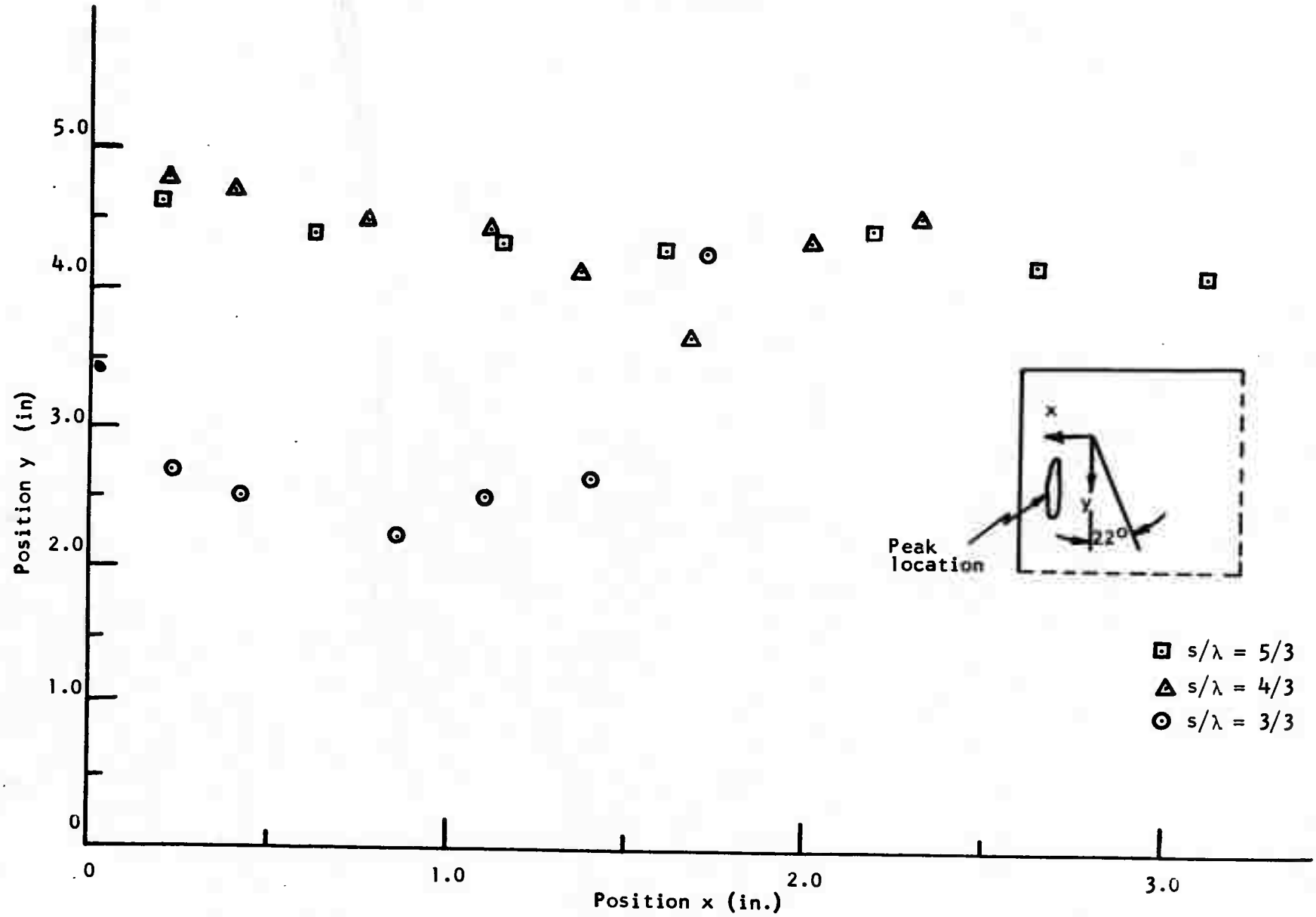

Fig. 4.29 Position of N_{MAX} in Incident Shear Wave

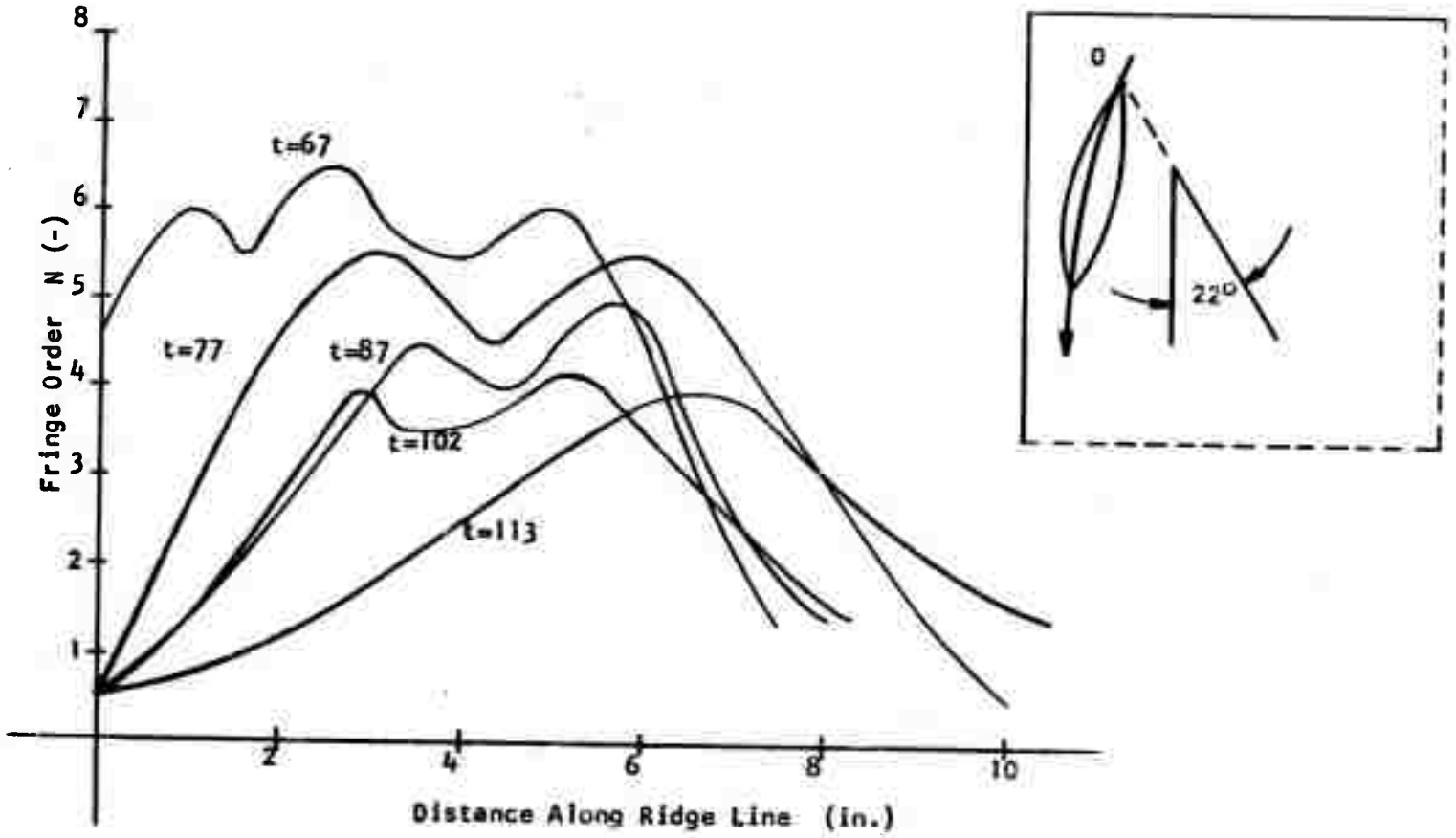

Fig. 4.30 Fringe Order as a Function of Position along the Ridge Line of the Incident S Wave

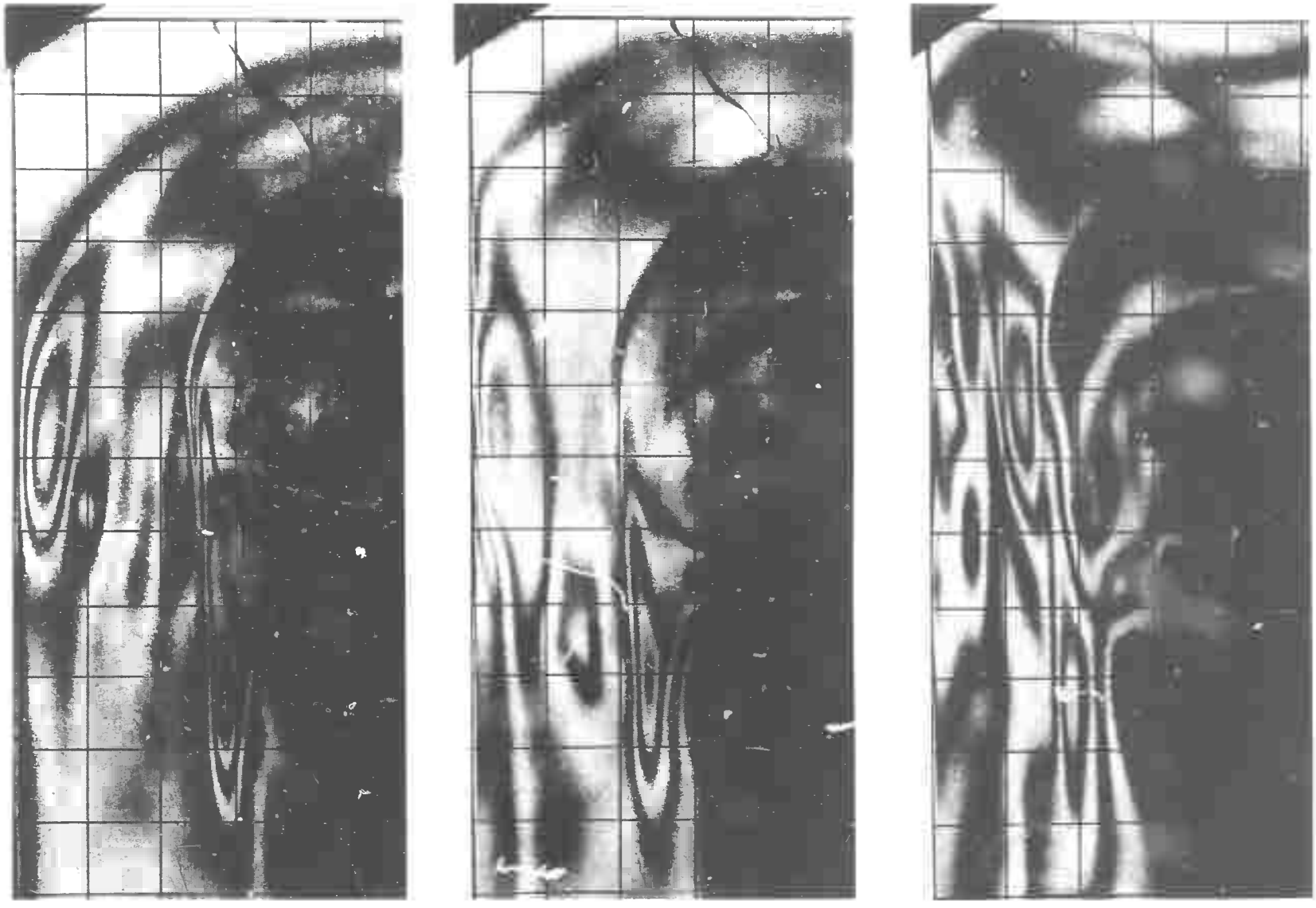

(a) t=113 (b) t =127 (c) t=138

Fig. 4.31 Fringe Patterns Showing Reflection of Incident P Wave

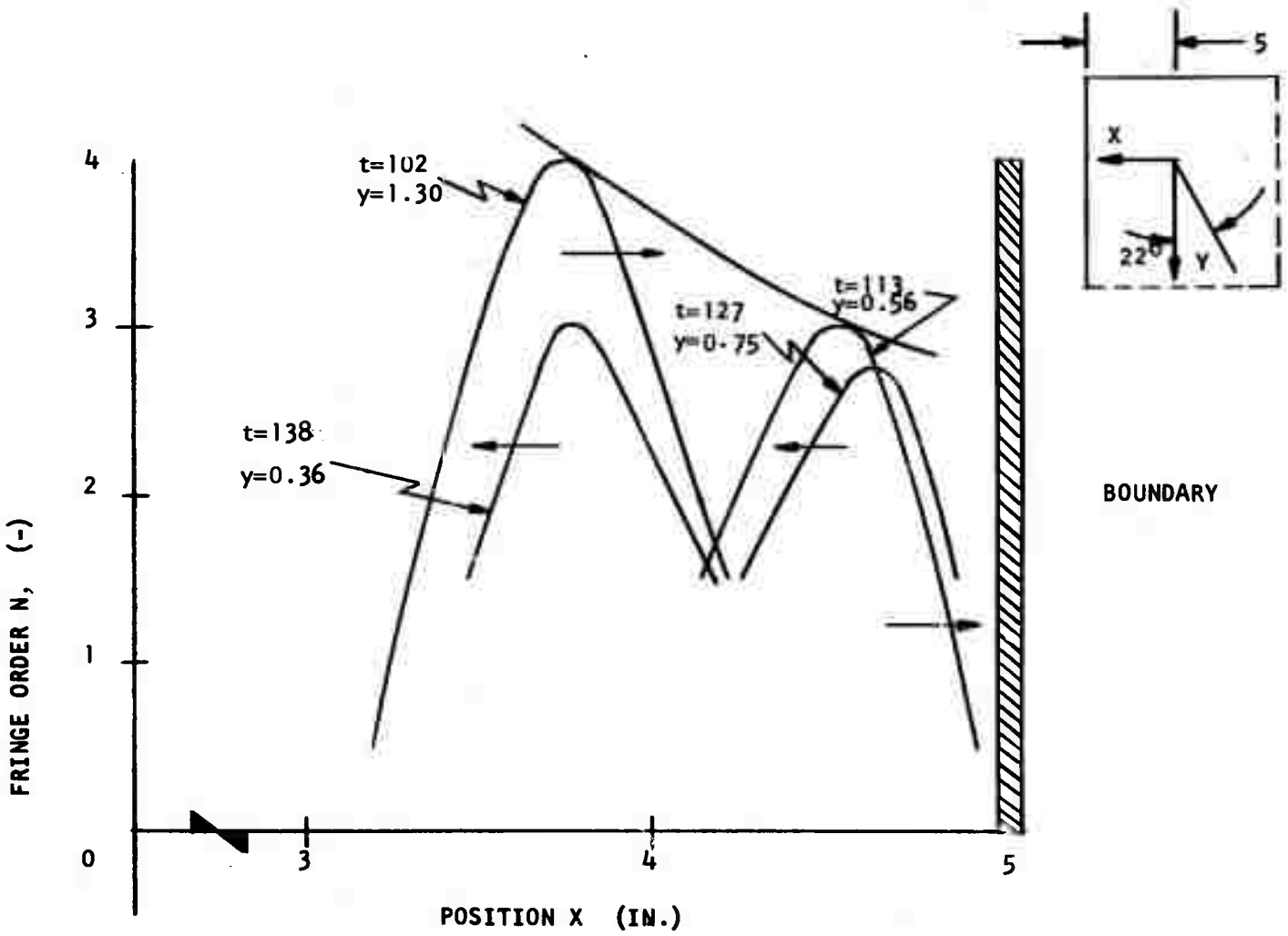

Fig. 4.32 Fringe Profiles Before and After Reflection of the P Wave

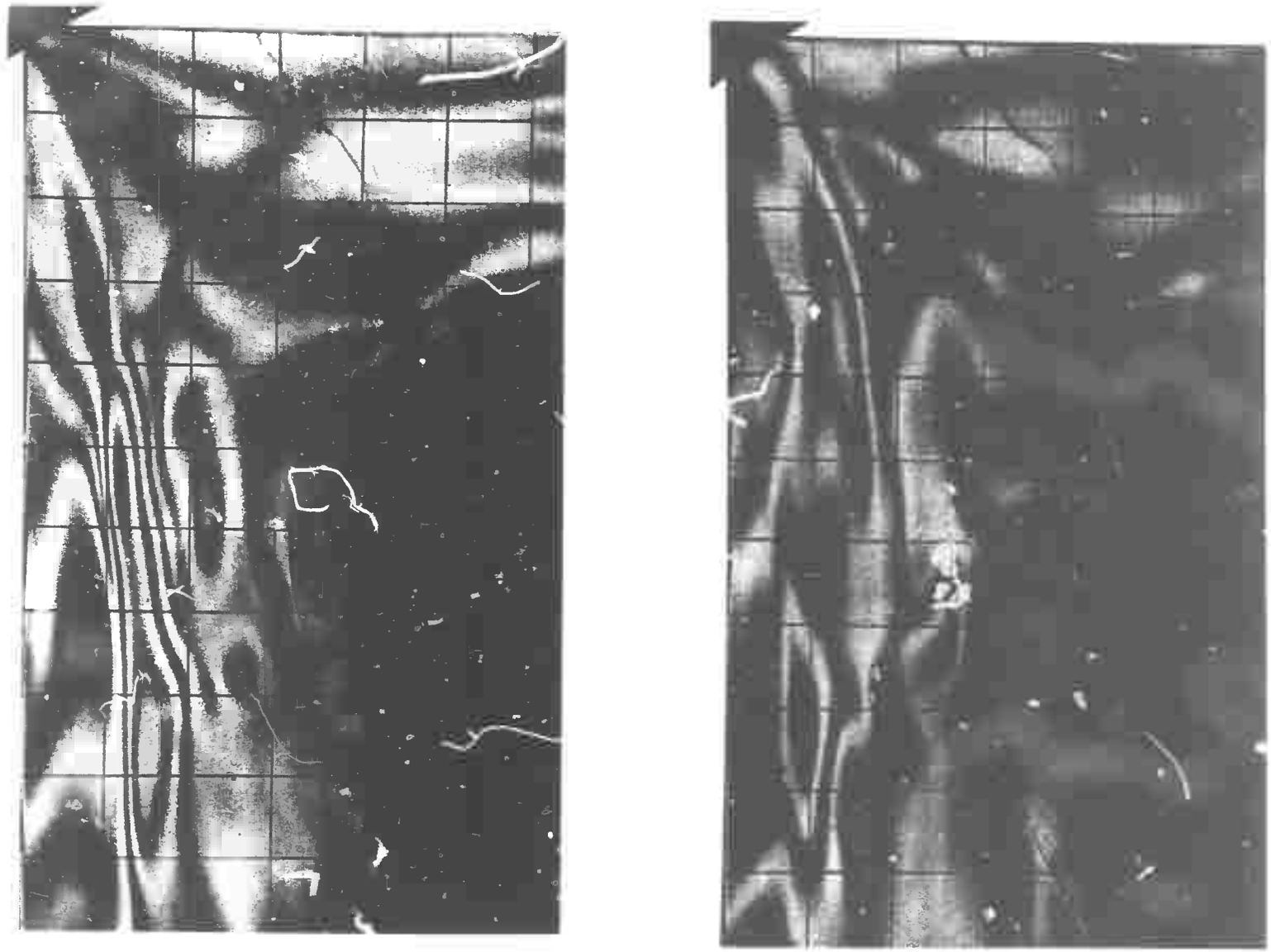

(a) t=150 (b) t=163

Fig. 4.33 Fringe Patterns Illustrating Interaction of the Reflected PP and PS Waves with the Incident S Wave

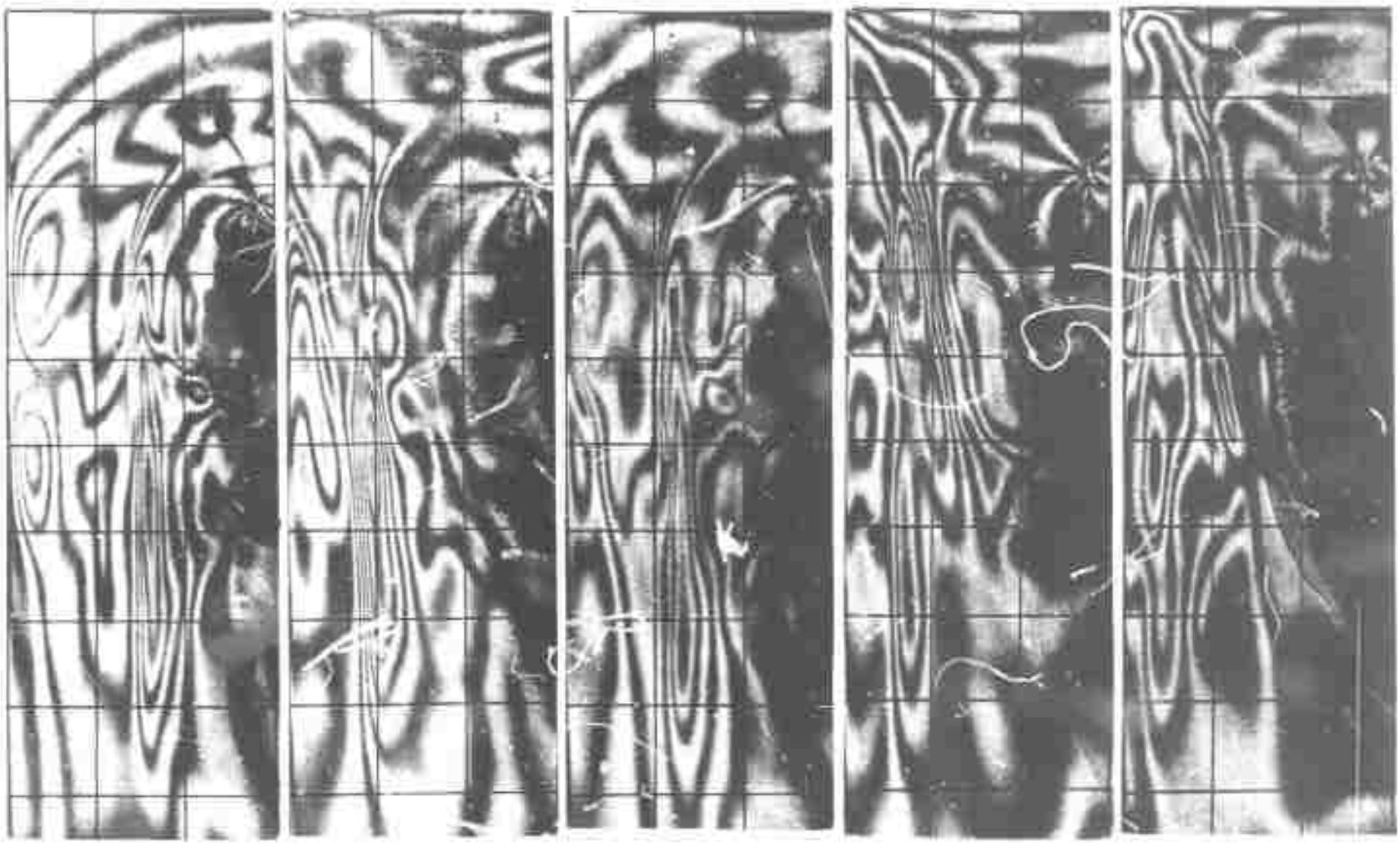

(a) t=78 (b) t=86 (c) t=94 (d) t=101 (e) t=109

Fig. 4.34 Fringe Patterns Showing Interaction and Then S wave Reflection

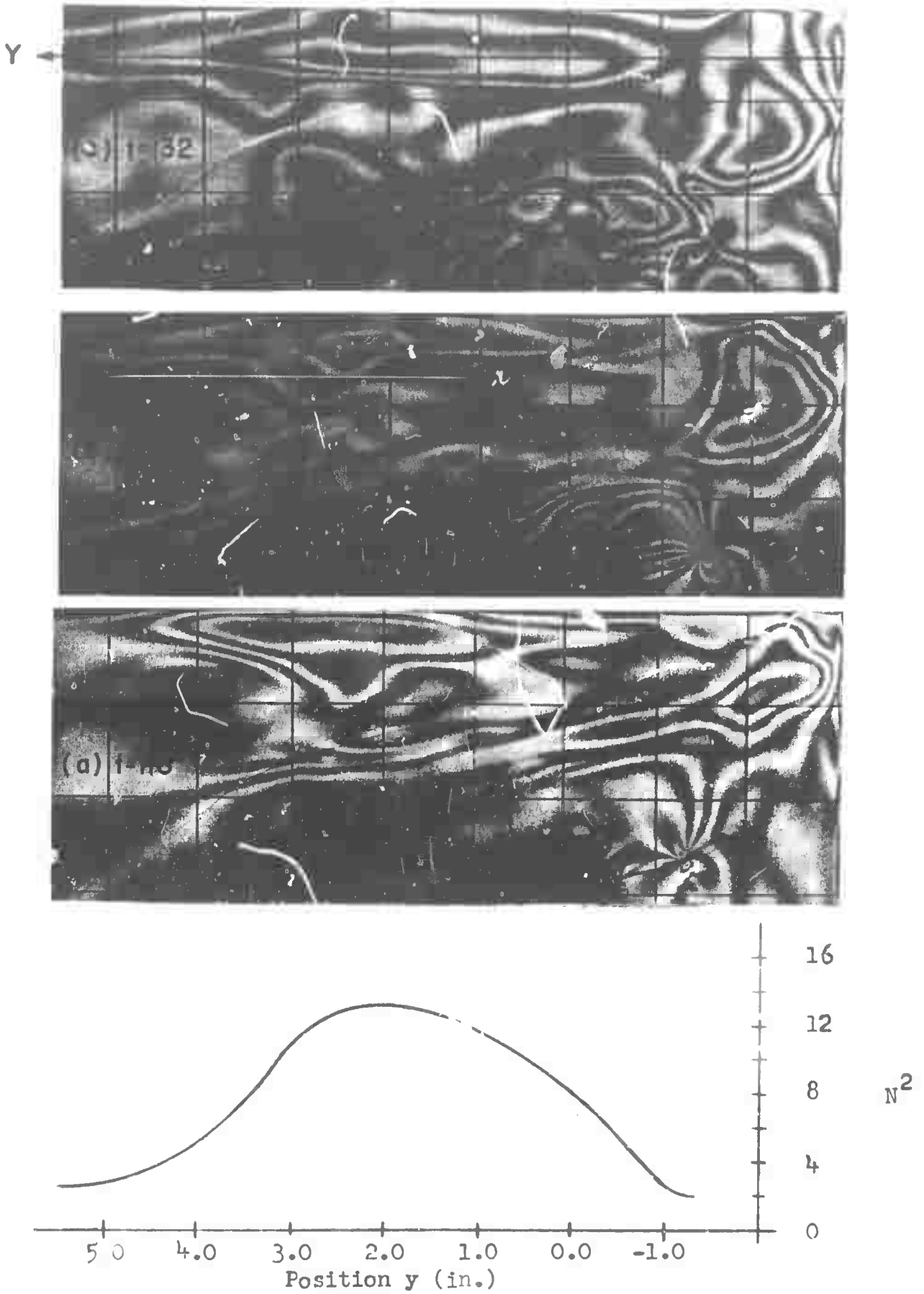

Fig. 4.35 Energy Distribution in Reflected Shear Wave

t= 164

Fig. 4.36 Crack Propagation in Low Stressed Regions

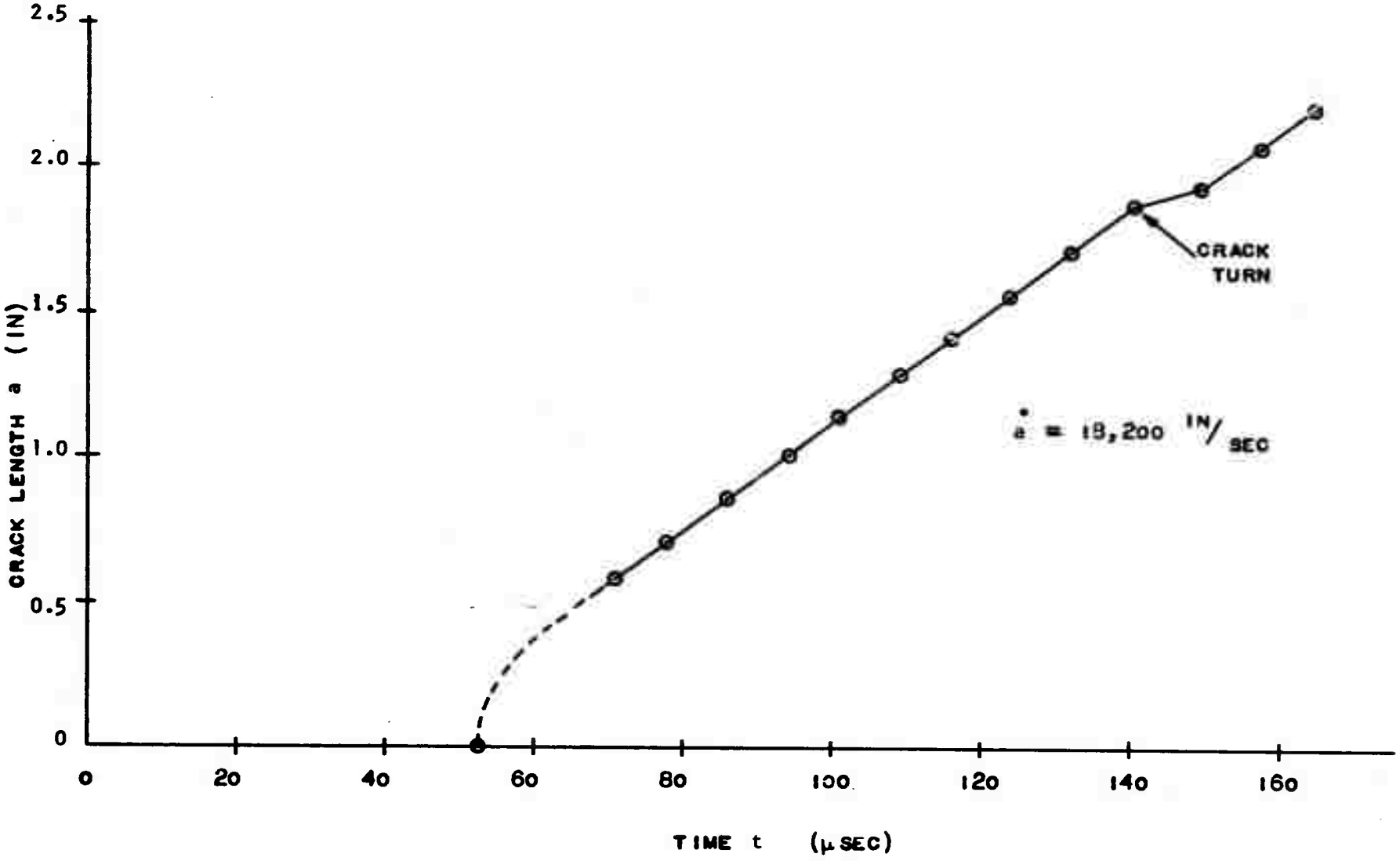

Fig. 4.37 Crack Propagation in Low Stressed Regions

APPENDIX A

A complete Set of Fringe Patterns for the Six Dynamic Experiments

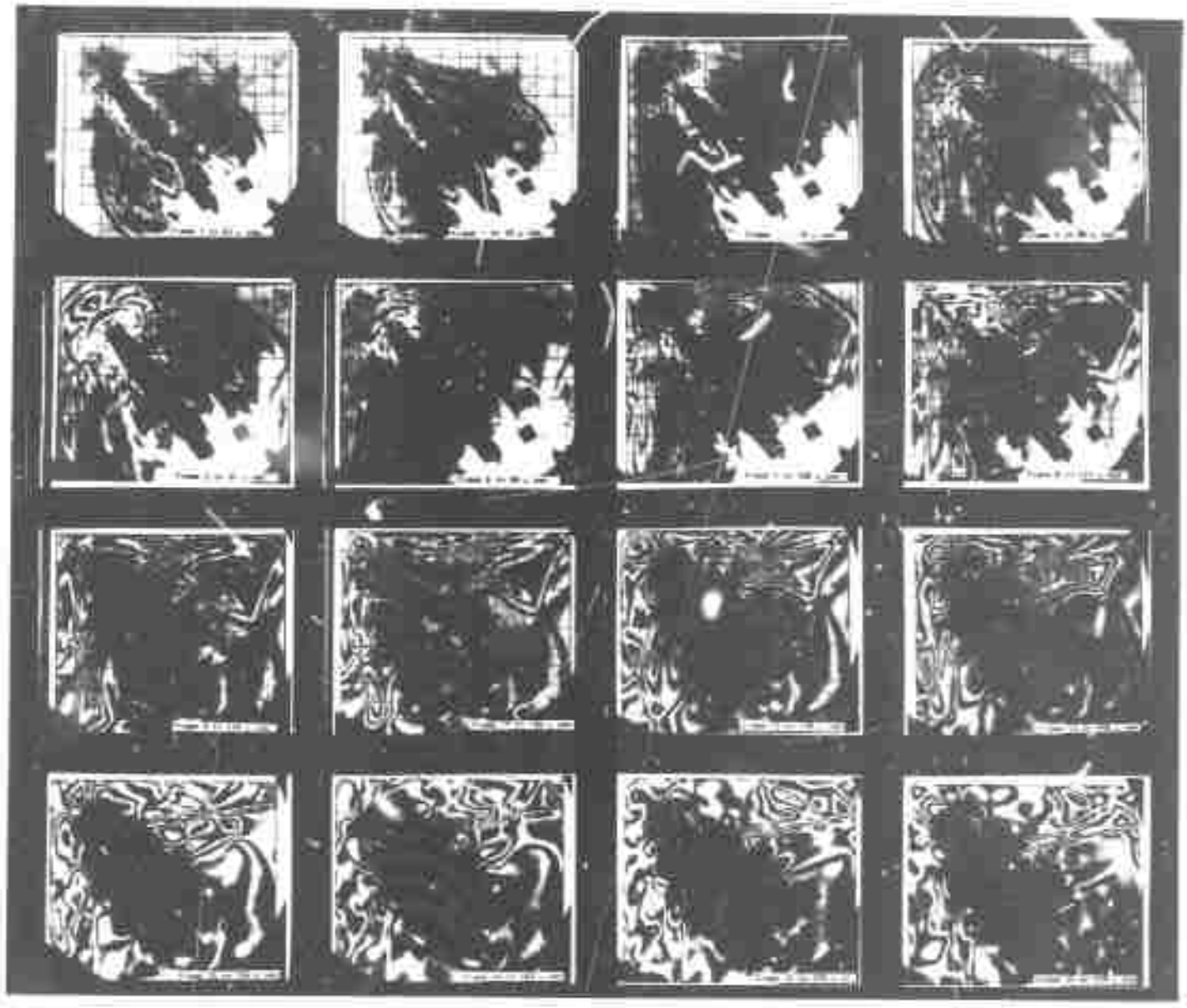

Fig A.1 Complete Set of Data Obtained for the 38^{o} Model with $s/\lambda = 1$

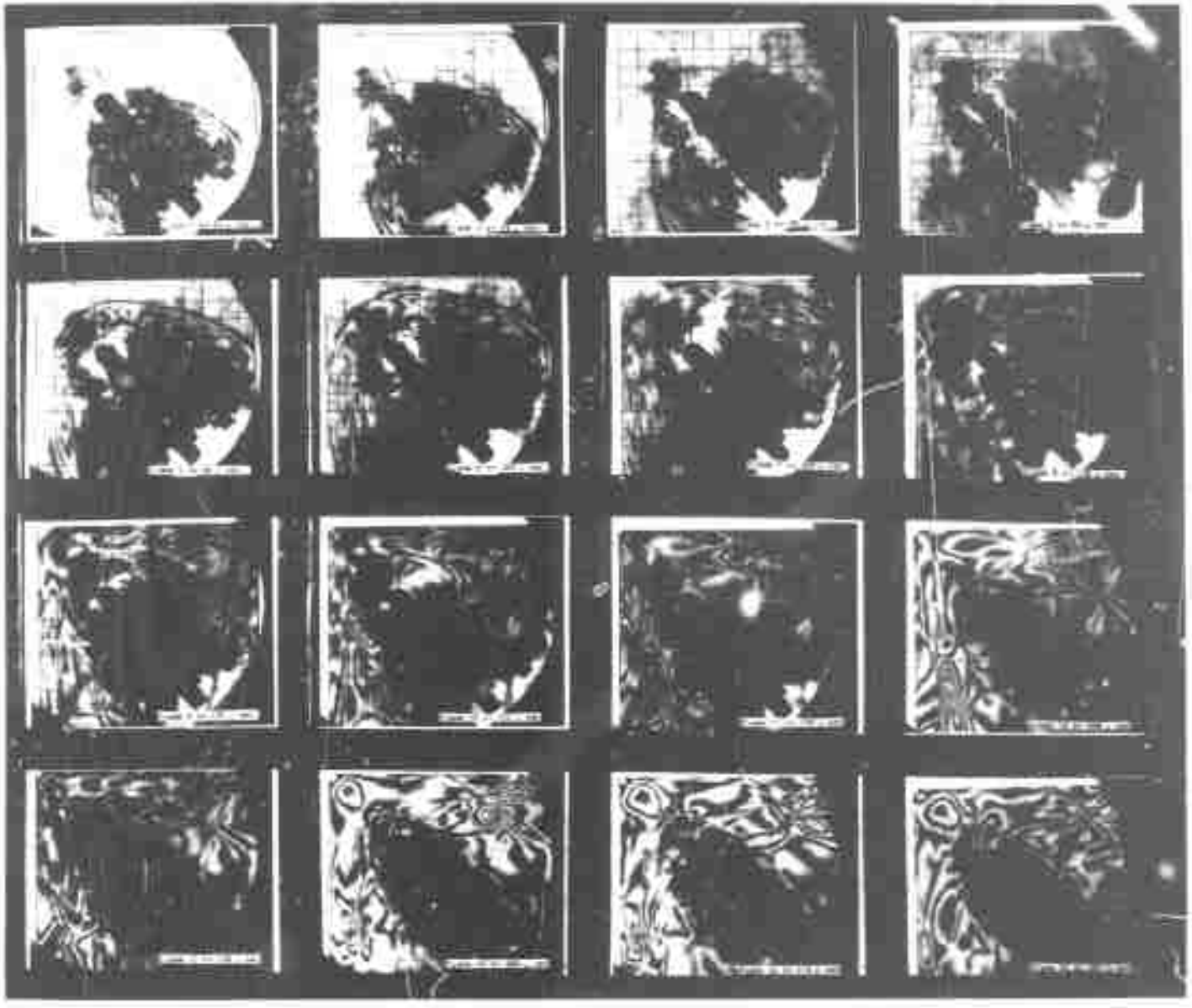

Fig A.2 Complete Set of Data Obtained for the 38° Model with $s/\lambda = 4/3$

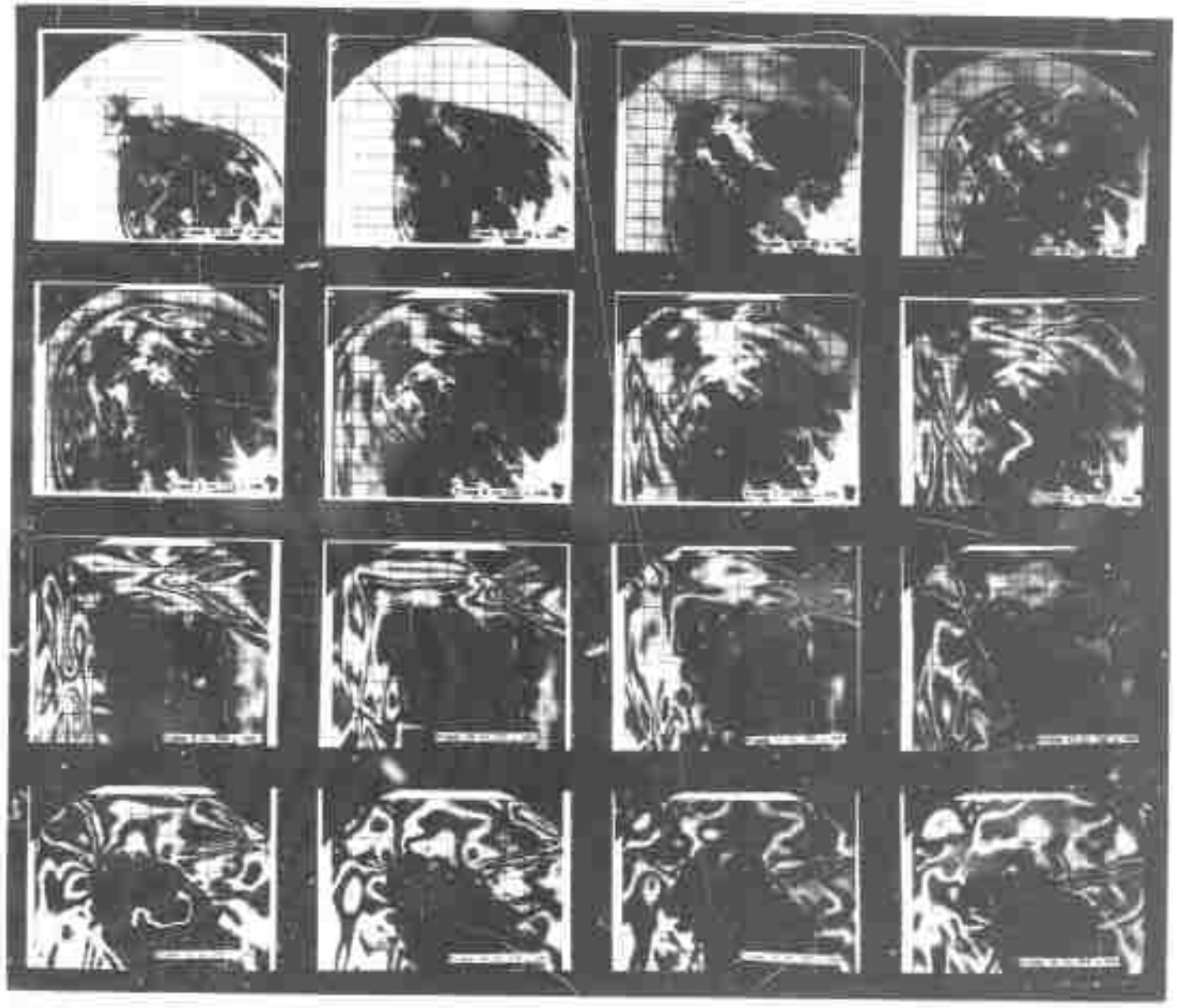

Fig A.3 Complete Set of Data Obtained for the 38^{o} Model with $s/\lambda = 5/3$

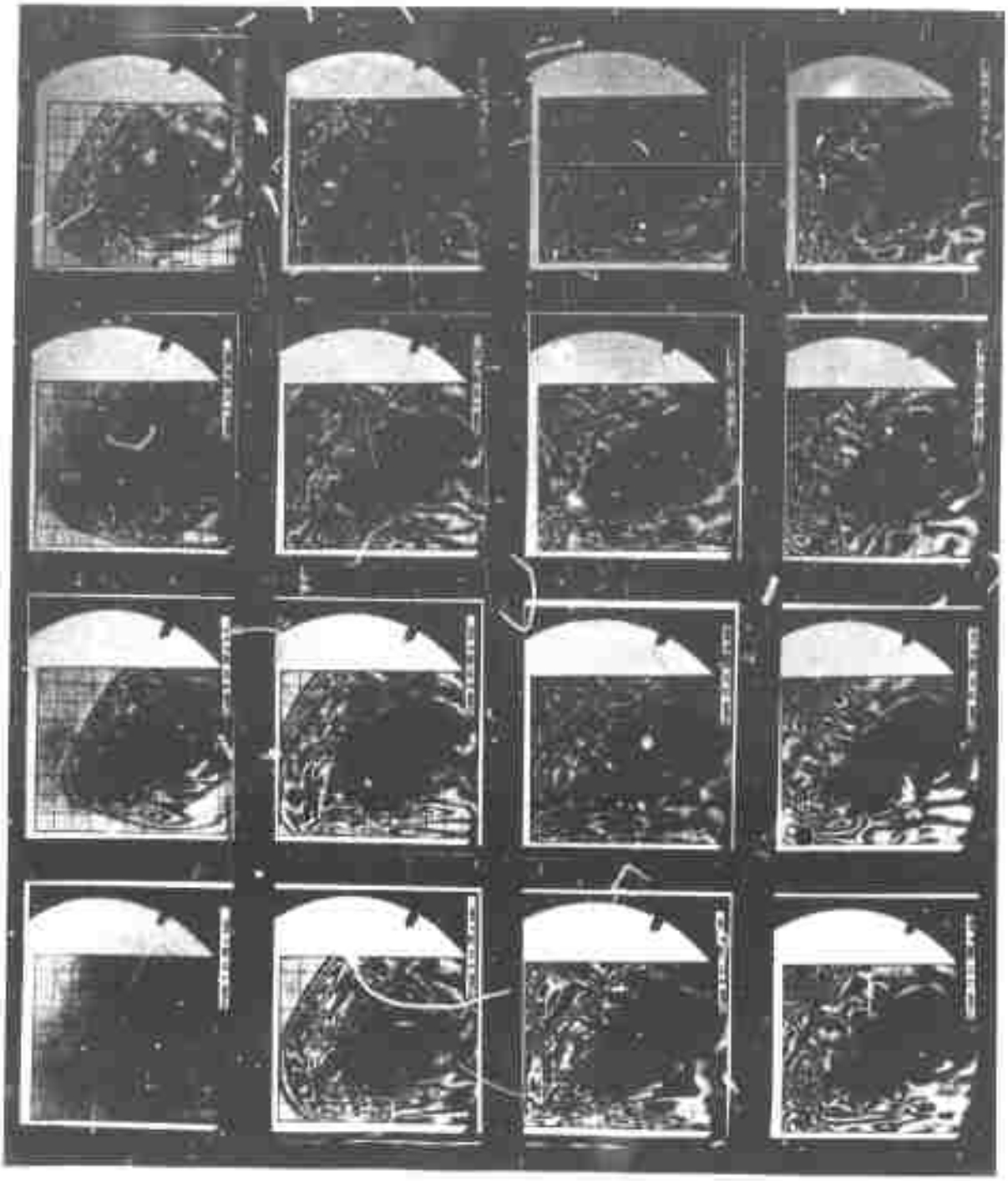

Fig A.4 Complete Set of Data Obtained for the 22^{o} Model with $s/\lambda = 1$

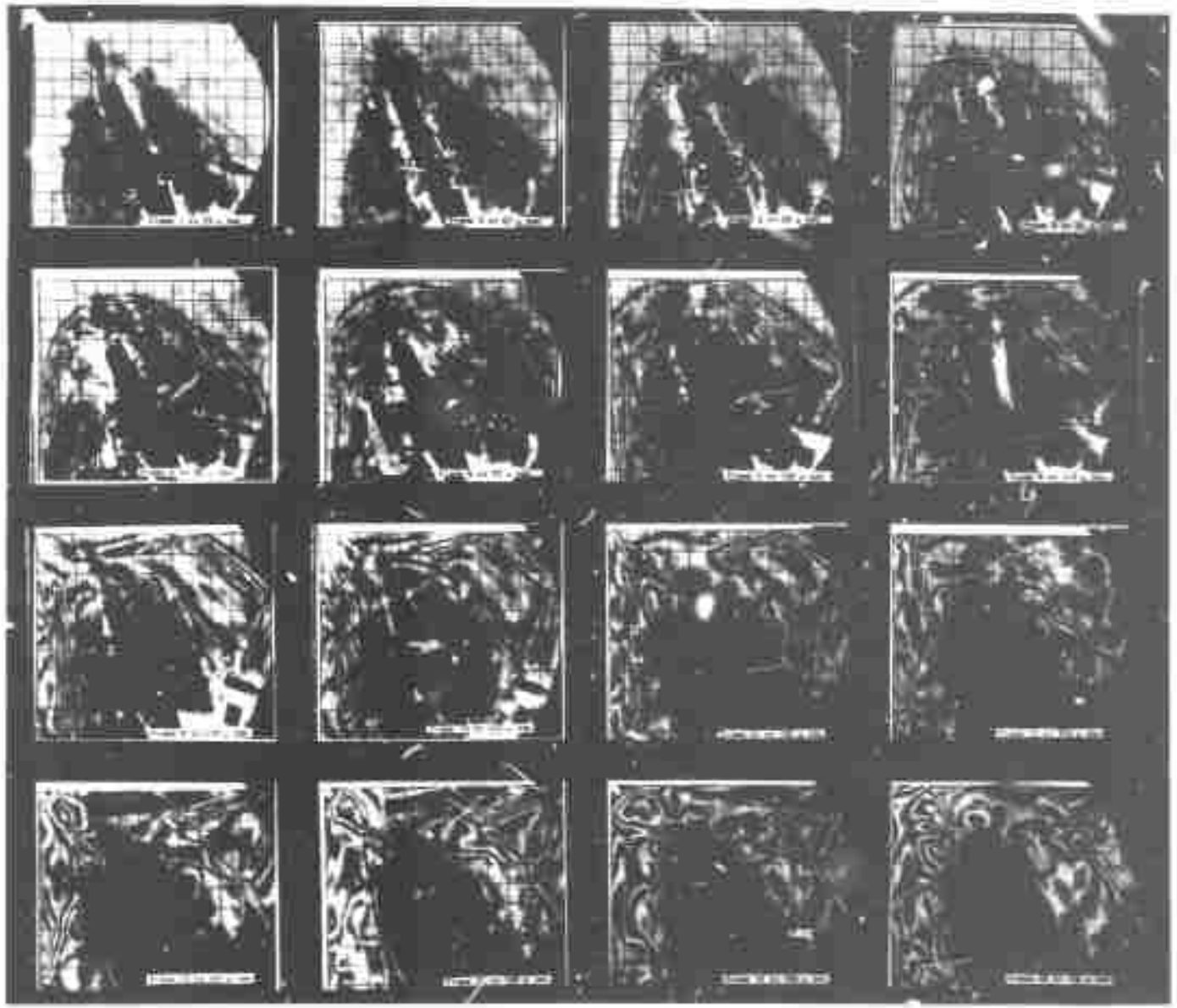

Fig A.5 Complete Set of Data Obtained for the 22° Model with $s/\lambda = 4/3$

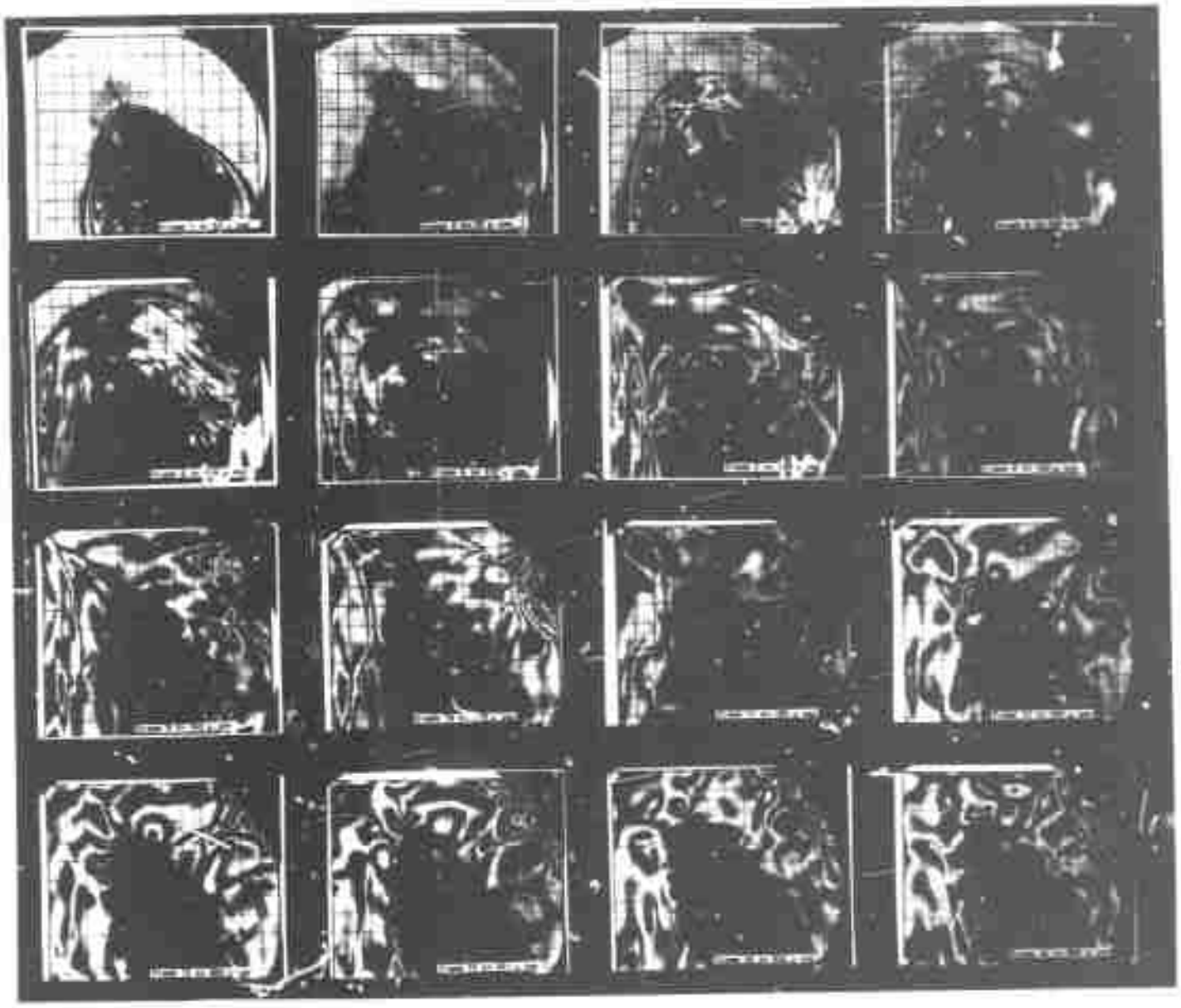

Fig A.6 Complete Set of Data Obtained for the 22° Model with $s/\lambda = 5/3$